University of Reading

MIMO Channel Capacity using Covariance Matrix and Configuration Selection for Switched Parasitic Antennas

Paramvir Kaur Pal

University of Reading

UK

Thesis submitted for the degree of Doctor of Philosophy

September-2018

Declaration

I confirm that this is my own work and the use of all material from other sources has been properly and fully acknowledged.

Paramvir Kaur Pal

In the loving memory of my dear friend Harneet Arora...

Acknowledgments

I would like to take this opportunity to express my deepest appreciation and gratitude to my supervisor Professor Simon Sherratt for endless support and all the beneficial discussions. It has been a great pleasure and privilege to work with him and benefit from his rich knowledge and experience. His constant support and guidance during my research have been priceless that made this thesis possible.

I would also like to express my gratitude to Professor Fu-Chun Zheng, particularly in the early stage of my research and for providing me the opportunity to pursue PhD in University of Reading.

Last but not the least, I do not have words to thank my husband Sajal, for his kind heart and believing in me in every step of the way. He took care of all the little things, and made sure that I had the time, space and resources to work hard with an open mind. My deepest thanks to our lovely kids, Arnab and Anushka for accompanying me in this challenging and stimulating experience with all ups and downs. I would like to thank them for being very supportive, patient, understanding and sacrificing to help me accomplish this work.

Finally, my sincerest thanks to our parents for their endless love and encouragement throughout the PhD.

Abstract

Multiple-Input Multiple-Output (MIMO) is considered a promising technology to increase the channel capacity and link reliability for future wireless communication systems. The benefits of MIMO can be obtained by placing the antenna terminals far apart to provide uncorrelated signals at the receiver. Reducing the inter-element spacing between the antenna terminals causes signal correlation and mutual coupling that degrade the system performance. However, implementation of MIMO technology is not possible when considering low-cost, battery operated portable devices with limited physical space constraint.

The key idea of this thesis is focused on the performance of MIMO with switched parasitic antennas (SPA), in which parasitic elements are switched between terminated impedance loads. MIMO-SPA exploits the pattern diversity by changing the mutual coupling between the antenna array elements. It exploits the electromagnetic field to a greater extent and provides different radiation patterns. The switching operation of parasitic elements changes the current distribution on the antenna array elements and alters the radiation patterns. With the availability of multiple channel realizations, it is possible to select the optimal pattern configuration for a particular propagation environment.

The research work in this thesis consists of three parts: The first part of the thesis focuses on the design and analysis of MIMO-SPA, including the channel characteristics and antenna properties. MIMO-SPA consists of active elements connected to RF hardware and surrounded with a number of parasitic elements terminated with

controllable loads. The use of parasitic elements exploits the pattern diversity by changing the electromagnetic mutual coupling between the antenna elements. The parasitic element switches between reflector and director states by controlling the terminated loads electronically. The second part of this thesis shows the performance of MIMO-SPA in terms of channel capacity for different loading configurations. Simulation results prove that the proposed MIMO-SPA approach provides comparable results to conventional MIMO systems with reduced size and hardware complexity. The channel capacity further improves using a modified covariance matrix with the incremental antenna selection technique (IAST) and the water-pouring algorithm (WPA) technique. The improved covariance matrix with the optimal power allocation shows significant improvement over uniformly distributing the power among all the transmit antennas.

The MIMO-SPA system is capable of operating under multiple radiation patterns with multiple channel realizations. This additional degree of freedom (DoF) comes with an overhead of attaining channel state information (CSI) of all the pattern configurations. This channel knowledge should be sent back to the transmitter through a limited feedback link. Lastly, the third part of the thesis proposes a novel selection method using condition number to select optimal pattern configuration. A condition number indicates the multipath richness present in the channel. This channel quality information can be sent back to the transmitter with a low-rate feedback link. The condition number suggests how much SNR is required by the system for proper transmission.

Table of Contents

List of Figures

List of Tables

List of Abbreviations

Table 1: List of Abbreviations

Abbrev.	**Meaning**
3GPP	3rd Generation Partnership Project
AoA	Angle of Arrival
AoD	Angle of Departure
A/D	Analog-to-Digital
AS	Antenna Selection
AST	Antenna Selection Technique
AWGN	Additive White Gaussian Noise
BER	Bit Error Rate
BLAST	Bell Laboratories Layered Space-Time
BS	Base Station
BSA	Beam Switching Antenna
CCI	Channel Covariance Information
CDF	Cumulative Distribution Function
CEM	Computational Electromagnetic
CMI	Channel Mean Information
CN	Condition Number
CQI	Channel Quality Indicator
CSI	Channel State Information
CSIR	Channel State Information at the Receiver

Table 1 – continued from previous page

Abbrev.	Meaning
CSIT	Channel State Information at the Transmitter
DoF	Degree of Freedom
D/A	Digital-to-Analog
DC	Direct Current
DL	Down Link
DSA	Decremental Selection Algorithm
EMF	Electro Motive Force
ESPAR	Electronically Steerable Parasitic Array Radiator / Receptor
EVD	Eigen Value Decomposition
EVS	Eigen Value Spread
FDD	Frequency Division Duplexing
FET	Field-Effect Transistors
IAST	Increment Antenna Selection Technique
i.i.d.	Independent and Identically Distributed
ISA	Incremental Selection Algorithm
ISM	Industrial Scientific and Medical
LNA	Low Noise Amplifier
LTE	Long Term Evolution
MEMS	Micro-Electromechanical Systems
MISO	Multi-Input Single-Output
MIMO	Multi-Input Multi-Output
ML	Maximum-Likelihood
MMSE	Minimum-Mean Square Error
MoM	Method of Moments
OC	Open Circuit
OFDM	Orthogonal Frequency Division Multiplexing
PA	Power Amplifier
PCB	Printed Circuit Board

Table 1 – continued from previous page

Abbrev.	Meaning
PDSCH	Physical Downlink Shared Channel
PE	Parasitic Elements
PIFA	Planar Inverted-F Antennas
PIN	Positive Intrinsic Negative
PMI	Precoding Matrix Indicator
QPSK	Quadrature Phase Shift Keying
QoS	Quality of Service
RF	Radio Frequency
RI	Rank Indicator
RL	Return Loss
SC	Short Circuit
SISO	Single Input Single Output
SIMO	Single Input Multiple Output
SINR	Signal-to-Interference Noise Ratio
SM	Spatial Multiplexing
SNR	Signal-to-Noise Ratio
SPA	Switched Parasitic Antennas
STBC	Space-Time Block Code
SV	Singular Value
SVD	Singular Value Decomposition
TDD	Time Division Duplexing
TDMA	Time Division Multiple Accessing
UT	User Terminal
WiMAX	Worldwide Interoperability for Microwave Access
WPA	Water Pouring Algorithm
ZF	Zero-Forcing

Notations and Symbols

In this PhD thesis, a small letter describes a vector and a bold capital letter describes a matrix of the specified size. Moreover, the following notations and symbols are used:

Table 2: Notations and Symbols

Symbol	**Meaning**
$(\cdot)^*$	Conjugate operator
$(\cdot)^T$	Transpose operator
$(\cdot)^H$	Conjuage transpose (Hermitian) operator
$(\cdot)^{-1}$	Inversion operator
$\mathbb{E}$	Mean value operator
λ_{max}	The maximum eigenvalue of a square matrix
λ_{min}	The minimum eigenvalue of a square matrix
I_R	An identity matrix of size R
j	Imaginary unit
$\mathbb{C}$	The set of complex numbers
$det(\cdot)$	Determinant of a matrix
$diag(\cdot)$	A (square) diagonal matrix with the elements of the enclosed vector laid across the main diagonal of the matrix
(ϑ, θ)	Elevation angles
(φ, ϕ)	Azimuth angles
Ω	Solid angle
λ	Free-space carrier wavelength
κ	Condition number

Chapter 1

Introduction

Multiple-Input Multiple-Output (MIMO) systems have emerged as an innovative technology in wireless communication systems due to their ability to provide higher data rates and better link coverage. MIMO systems offer benefits in reliable transmission, higher channel capacity and link quality in rich multipath propagation environments [1–3]. The important feature of MIMO systems is to turning the multipath propagation into a benefit for the system. If the propagation channel in MIMO systems is in deep fade, the link reliability can be enhanced by using different diversity techniques. On the other hand, if the propagation channel is not in deep fade, the transmission data can be divided independently to sub-channels by using spatial multiplexing (SM) techniques for higher data rates. Thus, MIMO systems effectively take advantage of random fading [4] [5] to deliver reliable data and delay spread [2] [6] of multipath propagation to multiply data transfer rates. The channel capacity of MIMO systems grows linearly with the number of antennas used at the transmitter and the receiver side. MIMO provides all these benefits without requiring any additional bandwidth and transmission power.

1.1 Motivation

Most of the MIMO benefits can be exploited with the large separation between the antenna array terminals at both ends of the communication link. Placing multiple antennas with large separation in handset or portable wireless devices where the space is main constraint puts challenges on the MIMO systems. Insufficient spacing between antenna elements causes high correlation between the MIMO sub-channels, and degrades the system performance. Due to strict size constraints in portable devices, placing the multiple antennas far from each other, to obtain uncorrelated channels is quite impossible.

To overcome above limitations, switched parasitic antenna (SPA) is one of the promising solution to improve the MIMO system performance, especially in the environments where it is difficult to obtain enough spatial decorrelation. Compared to conventional MIMO systems that have fixed radiation characteristics, MIMO-SPA exploits the pattern diversity and provides the multiple channel realizations. The parasitic elements sample the electromagnetic field in greater extent and provide different radiation patterns. Instead of using all the active elements to increase the data rate, more information can be recovered from the parasitic elements by changing the controllable loads. The parasitic element exploits the pattern diversity by changing the electromagnetic mutual coupling between the antenna array elements [7].

In MIMO-SPA, less number of active elements are fed by RF source and parasitic elements are terminated with the controllable loads. The parasitic element requires only a simple control circuitry instead of an expensive RF-chain. It reduces the hardware cost and circuit power consumption in MIMO-SPA system. In addition, SPA system employs mutual coupling between active and parasitic elements to achieve desired radiation patterns. Thus, inter-element spacing is desired to be smaller in MIMO-SPA, compared to conventional MIMO systems. Therefore, a MIMO-SPA

needs less volume, suited to a small portable terminal where the physical space is the primary constraint.

The benefits of MIMO-SPAs can be further exploited when the transmitter knows the channel. The receiver can send this information back to the transmitter. The feedback mechanism can be more rigorously designed and is more feasible in practice if the dynamic behavior of the eigenvalues is known statistically. The covariance feedback represents the eigen-value spread (EVS) and can be sent back to the transmitter.The power allocation can be distributed with an improved covariance matrix by using the incremental antenna selection technique (IAST) with water-pouring algorithm (WPA). With the improved covariance matrix, the channel capacity also improves in MIMO-SPA systems.

When CSI is available at the transmitter, it also demands high bandwidth feedback channels [8]. To overcome the feedback overhead, this thesis also introduces a MIMO channel quality metric which can be used to improve the MIMO-SPA link performance. A condition number (CN) indicates the channel quality, and is related to the EVS of the channel matrix.

MIMO-SPA shows the potential of simultaneously addressing both the size and multiple RF hardware challenges of conventional MIMO techniques. Therefore, using this type of antenna in future wireless communication systems can enhance their performance by adding an additional degree of freedom which can be obtained by changing the antenna characteristics according to the propagation channels.

1.2 Research Question

The main objective of this research is to investigate the system characteristics of MIMO-SPA with various radiation pattern configurations. Proposed MIMO-SPA an-

tenna system includes few active antennas surrounded with multiple parasitic antennas exploiting the pattern diversity by controlling the impedance loads.

In particular, this thesis examines the performance improvement with MIMO-SPA compared to the conventional MIMO made of active elements only. MIMO-SPA provides number of channel realizations with the different radiation pattern configurations. The system performance in terms of channel capacity needs to be inspected across these different channel realizations. The MIMO channel capacity also depends on the covariance matrix in terms of correlation in the propagation channel. It also aims to find out the correlation in different propagation environments with different covariance matrices. This study aims to analyze the improved covariance matrix by using IAST and WPA in different MIMO-SPA structures.

The system performance need to be examined with computer simulations in two-by-two (2×2) and four-by-four (4×4) MIMO systems using parasitic antenna elements. The switching of the parasitic elements between *on* and *off* states provides the finite number of pattern configurations. This additional degree of freedom (DoF) comes with an overhead to acquire information about all the radiation pattern configurations. The objective is to select the optimal pattern configuration based on the MIMO channel quality metric.

1.3 Methodology

The Monte Carlo simulations conducted in this thesis can be represented by the flowchart as shown in Figure 1.1:

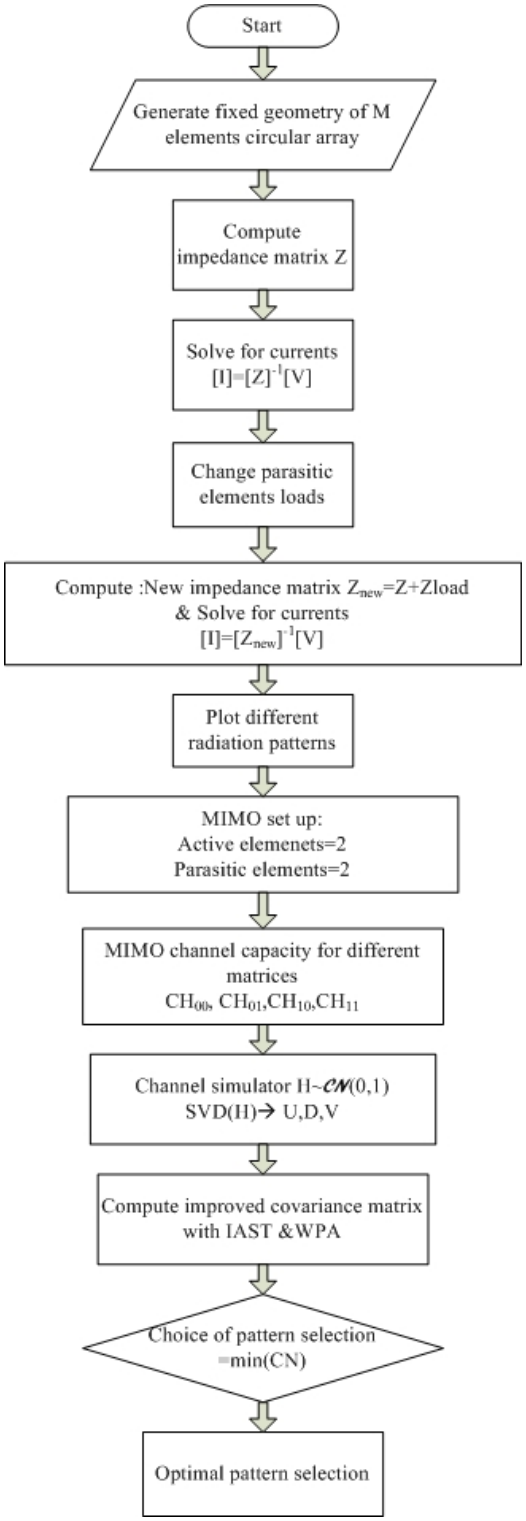

Figure 1.1: Flowchart of the simulation.

1.4 Contributions

Some of the results presented in this thesis have been published in ETRI Journal [9]: "MIMO Channel Capacity and Configuration Selection for Switched Parasitic Antennas", which is included in the Appendix-A.

The main contributions of this thesis can be summarized as follows:

- Induced electro motive force (EMF) method: MIMO-SPA exploits pattern diversity, where antennas are designed to radiate with different radiation patterns to create uncorrelated channels across different array elements. In this thesis, generation of these radiation patterns are investigated by using induced EMF method.

- MIMO-SPA channel capacity with improved covariance matrix: Performance evaluation of MIMO-SPA in terms of channel capacity with improved covariance matrix for different parasitic antenna geometries. Moreover, though MIMO channel capacity has been improved with the covariance matrix in the conventional MIMO systems, the current literature has not proposed this method for MIMO systems using parasitic elements.

- Pattern configuration selection: A novel selection metric has been introduced for MIMO using parasitic antennas that allows selection of the best pattern configuration at the receiver end. The selection parameter can also be sent back to the transmitter to reduce feedback overhead in future MIMO wireless communication systems.

The proposed model in this thesis considers the advantages of SPAs for use in small user terminal (UT) devices. SPAs provide the different pattern configurations which improve the system performance as compared to conventional antenna array ap-

proaches. The MIMO-SPA receiver model with a smaller number of active elements provides spatial multiplexing gain and the number of parasitic elements exploits the pattern diversity. The power allocation in the covariance matrix also shows improvement in MIMO-SPAs. At the receiver terminal, the CN selects the best pattern configuration and can be sent back to the transmitter with less feedback overhead.

1.5 Organization of Thesis

The overall structure of the thesis takes the form of seven chapters as follows:

–*Chapter 2*: This chapter gives a brief overview of MIMO systems and reconfigurable antennas. The chapter is divided into two sections. In the first section, it starts with a brief introduction of the MIMO communication system model with the requirement of precoding techniques at the transmitter side. Overviews of MIMO channel metrics and different channel models are also presented. The concept of antenna selection in MIMO systems with selection algorithms are also summarized. The basic antenna array theories with the parameters that influence the MIMO performance are also discussed. Reconfigurable MIMO systems using pattern diversity provided by electronically steerable parasitic array radiator (ESPAR) and SPA are also reviewed. In the second section, previous contributions in terms of related work are discussed.

–*Chapter 3*: This chapter introduces the basics of parasitic arrays used in MIMO systems. Then network presentation of antenna array and antenna modelling with Z-parameters are revisited. The SPA system description shows an experimental setup for compact MIMO-receiver using various parasitic elements. Finally, different radiation patterns with different MIMO-SPA geometry are examined.

–*Chapter 4*: This chapter investigates the channel capacity in MIMO systems using SPAs. A MIMO system model with impedance matrices is developed using the Z-

parameter to show the effect of parasitic elements at both link ends. Then the effect of the parasitic elements on the channel capacity is examined mathematically. The MIMO channel capacity analysis with different pattern configurations is analyzed with MATLAB simulations. Finally, the system improvement with covariance matrices is examined and tightness of the bounds is also given.

–*Chapter 5*: This chapter proposes a novel method that allows selection of the antenna configuration at the receiver without any extra power consumption. The optimal selection of the MIMO-SPA pattern configuration is based on the channel condition number. Analysis of the condition number has been studied and its effect on the channel capacity for MIMO-SPA has been investigated in detail.

–*Chapter 6*: This chapter discusses the main contributions of this work to the area of MIMO systems by using SPA . This chapter concludes the thesis and presents a critique of the findings.

–*Chapter 7*: Finally, this chapter suggests topics for future work. Further areas of work are proposed in antenna design solutions to exploit the benefits of MIMO-SPAs for next generation wireless communication systems.

Chapter 2

Background Study and Related Work

2.1 Overview of MIMO Communication Systems

MIMO systems have become a most attractive technique because of their potential to provide several benefits in wireless communication applications. They provide the significant enhancement in terms of quality of service (QoS) and system performance in comparison to conventional smart antenna systems [4] [10–12]. By deploying multiple numbers of antennas at both ends of a wireless communication system, they provides better link reliability through diversity techniques. They can also increase data rates by transmitting the multiple data streams through spatial multiplexing techniques. Due to the potential benefits of MIMO systems in recent years, further research has been done in both the academic and industrial fields [13] [14].

MIMO technology offers three gains: diversity gain, spatial multiplexing gain and beamforming (array gain) [15] [16] as shown in Figure 2.1.

- Diversity gain: The diversity techniques intend to send and receive the information through multiple transmit and receive antennas respectively. By taking the advantage of multipath fading, it improves the link reliability and QoS.

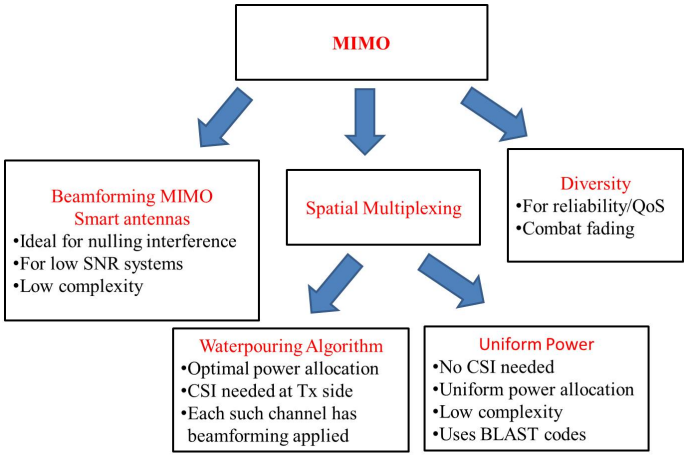

Figure 2.1: MIMO basic types

- Spatial Multiplexing gain: This technique allows to increase the capacity by transmitting independent data streams simultaneously in parallel to multiple transmit antennas and achieves the higher transmission speed.

- Beamforming (Array gain): Beamforming can be defined as a technique that matches the transmit and receive signals to the propagation channel. It increases signal power at the receiver due to the coherent combining of signals from multiple antennas at the receiver or at the transmitter or at both sides [17]. With the SVD, both transmitter and receiver can form a beam and can match to the propagation channel. The beamforming gain is a function of the maximum singular value of the channel. Beamforming steer the antenna beam in a certain physical direction.

2.1.1 MIMO System Model

A single-user MIMO system consists of M_t transmit and N_r receive antennas as shown in Figure 2.2. The channel can be represented with matrix $\mathbf{H}$ with $M_t \times N_r$ dimensions.

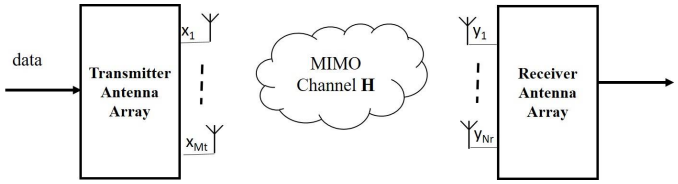

Figure 2.2: $M_t \times N_r$ MIMO system.

The received signal vector $\mathbf{y}$ can be written as [18]:

$$\mathbf{y} = \sqrt{\frac{\mathsf{E}_x}{M_t}}\mathbf{H}\mathbf{x} + \mathbf{n} \tag{2.1}$$

where $\mathbf{x} = [x_1, x_2, ..., x_{M_t}]^T \in \mathbb{C}^M$ represents the complex-baseband transmitted symbol vector and $\mathbf{y} = [y_1, y_2, ..., y_{N_r}]^T \in \mathbb{C}^N$ is the received vector related through an $M_t \times N_r$ channel matrix $\mathbf{H}$. A receiver noise vector $\mathbf{n} = [n_1, n_2, ..., n_{N_r}]^T \in \mathbb{C}^N$ is a spatially white, zero-mean, circularly symmetric complex Gaussian noise vector, normalized so that $\mathbb{E}\{nn^H\} = \mathbf{I}_{N_r}$. The total average energy of the transmitted signal is denoted by E_x.

In a flat-fading channel, MIMO channel matrix $\mathbf{H}$ is represented by random complex fading coefficients, where h_{ij} represents the channel gain from transmit antenna j to the receive antenna i.

2.1.2 MIMO Precoding

In MIMO systems, the output at the receiver is the mixture of multiple transmitted signals. The main difficulty in MIMO channels is the separation of the data streams at the receiver which are sent in parallel from the multiple transmit antennas. This problem can be solved by using a precoder with knowledge of the CSI at the transmitter side, as shown in Figure 2.3.

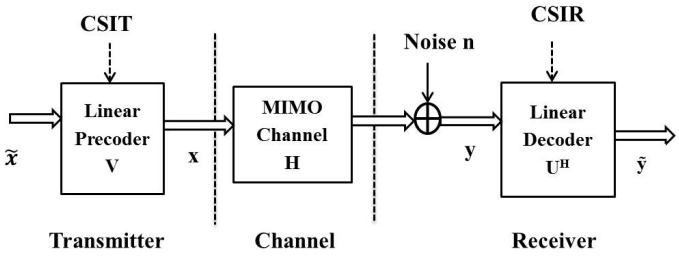

Figure 2.3: A single-user MIMO system with linear precoding/decoding.

In time division duplex (TDD) systems, the uplink and downlink uses the same frequencies and the transmitter can have channel knowledge through the reciprocity principle. In frequency division duplex (FDD) systems, both links are not reciprocal and this information can be estimated at the receiver with channel estimation techniques. This information needs to be sent back to the transmitter via low-rate feedback channels.

If CSI is available at the transmitter, the transmitted symbols can be partially separated by means of a precoder at the transmitter and can be received by using a decoder at the receiver. With CSI at the transmitter side, the Singular Value Decomposition (SVD) [19] model can be performed as shown in Figure 2.3. The transmitted signal is pre-processed with $\mathbf{V}$ on the transmitter side and a received signal is post-processed with $\mathbf{U}^H$ on the receiver side.

If SVD is performed on the matrix $\mathbf{H}$, then it degenerates to:

$$\mathbf{H} = \mathbf{U}\mathbf{D}\mathbf{V}^H \tag{2.2}$$

where $\mathbf{U}$ and $\mathbf{V}$ are unitary matrices in $(N_r \times N_r)$-dimension and in $(M_t \times M_t)$-dimension, respectively. Matrix $\mathbf{V}^H$ is the conjugate transpose of the matrix $\mathbf{V}$. It is noticed that $\mathbf{V}^H\mathbf{V} = \mathbf{U}^H\mathbf{U} = 1$. The matrix $\mathbf{D}$ is a rectangular matrix, whose diagonal elements are non-negative real numbers and off-diagonal elements are zero. The diagonal entries of matrix $\mathbf{D}$ are the singular values of the channel matrix $\mathbf{H}$, $\sigma_1 \geqslant \sigma_2 \geqslant ... \geqslant \sigma_{rank}$, where $rank = min(M_t, N_r)$. The squared singular values are also known as the eigen-values of $\mathbf{H}\mathbf{H}^H$: ${\sigma_i}^2(\mathbf{H}) = \lambda_i(\mathbf{H}\mathbf{H}^H)$. The SVD model decomposes the MIMO channel into independent parallel channels. The number of positive singular values represent the possible number of independent sub-channels formed in MIMO systems as shown in Figure 2.4. These independent channels $\lambda_1, \lambda_2, ...\lambda_{rank}$ are also known as eigenmodes [20] [21]. Thus, it is possible to send different streams of data through the same number of independent channels as the number of eigenvalues of $\mathbf{H}$, this process is known as Spatial Multiplexing (SM).

The eigenvalues represent the gains of the individual links as shown in Figure 2.4. The channel capacity can be improved if the transmission power is adaptively allocated over the eigenmodes by using the WPA. Similarly, the data rate can also be optimized by applying adaptive modulation schemes to the eigenmodes [22] [23]. In the adaptive systems, the eigenvalues can be adjusted according to the propagation channel status to boost the overall performance. This process requires precoder with CSI at the transmitter and decoder at the receiver to decode the output signal.

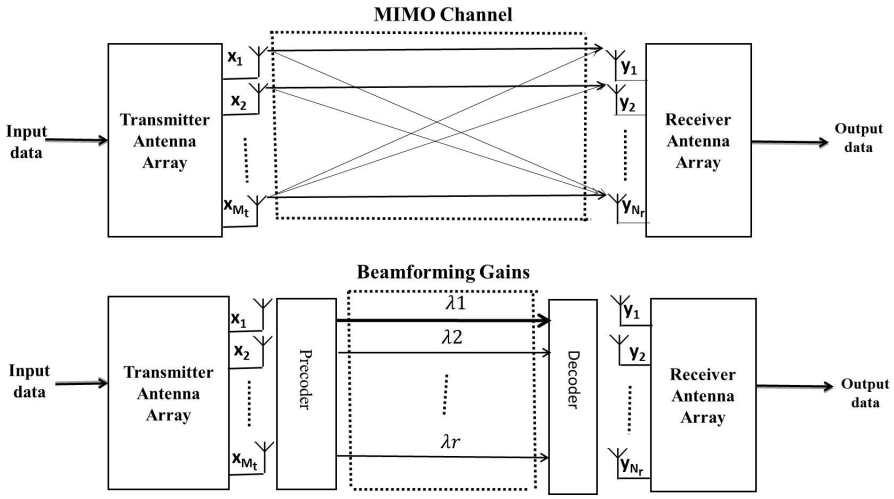

Figure 2.4: Eigenbeamforming transmission schematic.

2.2 MIMO Channel Capacity

The channel capacity of a communication system can be defined as the maximum transmission rate for which a reliable communication is possible [17] in the system. It is an important metric in closed-loop MIMO schemes that adapts the transmission rate by adapting the channel quality information [24].

2.2.1 When CSI is Known to the Transmitter Side

When multiple antennas are present at both the link ends, the SVD decomposition, gives the maximum number of data streams that can be transmitted simultaneously. It can make the MIMO channel equivalent to virtual single-input single-output (SISO) links and the MIMO channel capacity can be achieved by summation of all the SISO links capacities.

By using SVD, the output signal at the receiver (2.1) as given in [18] [25] can be

formulated as follows:

$$\tilde{\mathbf{y}} = \sqrt{\frac{\mathsf{E_x}}{M_t}}\mathbf{U}^H\mathbf{H}\mathbf{V}\tilde{\mathbf{x}} + \tilde{\mathbf{n}} \tag{2.3}$$

By using (2.2),(2.3) can be written as:

$$\tilde{\mathbf{y}} = \sqrt{\frac{\mathsf{E_x}}{M_t}}\mathbf{D}\tilde{\mathbf{x}} + \tilde{\mathbf{n}} \tag{2.4}$$

With SVD, the output is divided into r virtual SISO channels, the output across one channel is,

$$\tilde{y_i} = \sqrt{\frac{\mathsf{E}_s}{M_t}}\sqrt{\lambda_i}\tilde{x_i} + \tilde{n_i}, \qquad i = 1, 2, ..., r. \tag{2.5}$$

The transmit power for the ith transmit antenna can be written as $\gamma_i = E\{|x_i|^2\}$. With the energy of the transmitted signal $\mathsf{E_x}$ and the power spectral density of the noise N_0, the capacity of the ith virtual SISO channel can be written as:

$$C_i(\gamma_i) = log_2\left(1 + \frac{\mathsf{E_x}\gamma_i}{M_t N_0}\lambda_i\right), \qquad i = 1, 2, ..., r. \tag{2.6}$$

The total available power at the transmitter is limited to the total number of transmit antennas:

$$E\{\mathbf{x}^H\mathbf{x}\} = \sum_{i=1}^{M_t} E\left\{|x_i|^2\right\} = M_t \tag{2.7}$$

As discussed earlier, with SVD, the channel capacity of MIMO is the sum of the capacities of the virtual SISO links and can be written as:

$$\mathbf{C} = \sum_{i=1}^{r} C_i(\gamma_i) = E\left\{\sum_{i=1}^{r} log_2\left(1 + \frac{\mathsf{E_x}\gamma_i}{M_t N_0}\lambda_i\right)\right\} \tag{2.8}$$

The total power constraint as in (2.7) must be satisfied and the capacity can be

maximized with the proper power allocation:

$$\mathbf{C} = E\left\{ \max_{\sum_{i=1}^{r}\gamma_i = M_t} \sum_{i=1}^{r} log_2\left(1 + \frac{\mathsf{E_x}\gamma_i}{M_t N_0}\lambda_i\right)\right\} \tag{2.9}$$

subject to $\sum_{i=1}^{r}\gamma_i = M_t$. The optimization problem in (2.9) can be solved with some threshold P as:

$$\begin{aligned} \gamma_i^{opt} &= \left(P - \frac{M_t \mathsf{N_0}}{\mathsf{E}_x\lambda_i}\right)^+, \quad i = 1, 2, ..., r. \\ \sum_{i=1}^{r}\gamma_i^{opt} &= M_t \end{aligned} \tag{2.10}$$

where P is a constant and $(z)^+$ is defined as:

$$(z)^+ = \begin{cases} z & \text{if} \quad z \geq 0 \\ 0 & \text{for} \quad z < 0 \end{cases} \tag{2.11}$$

The solution in (2.10) satisfying the constraint in (2.11) is the well-known WPA [2] for power allocation in MIMO channels, that is shown in Figure 2.5. It indicates that more power must be allocated to the eigenmodes with higher SNR denoted as used modes. If the value of SNR is below the threshold level in terms of P, the corresponding eigenmodes must not be used and no power is allocated to unused modes.

2.2.2 When CSI is not Known to the Transmitter Side

When the channel matrix $\mathbf{H}$ is not known at the transmitter side, the optimal strategy is to divide the total power equally across all the transmit antennas. The autocorrelation function of the transmit signal vector $\mathbf{x}$ can be represented as:

$$\mathbf{R}_{xx} = \mathbf{I}_{M_t} \tag{2.12}$$

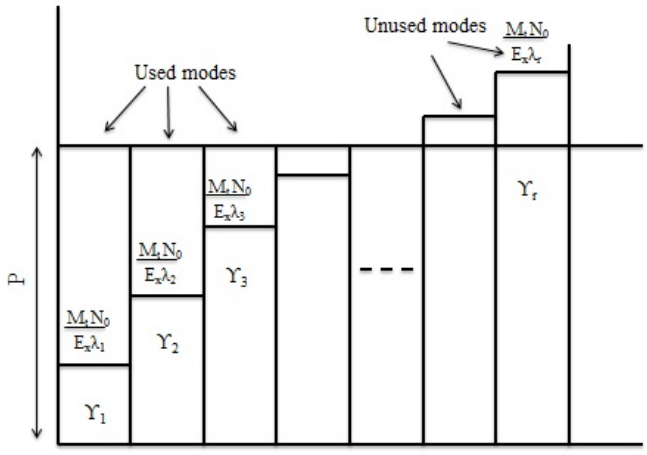

Figure 2.5: Water-pouring power allocation algorithm.

Without CSI at the transmitter, the channel capacity can be written as:

$$\overline{\mathbf{C}} = E\left\{ \sum_{i=1}^{r} log_2\left(1 + \frac{\mathsf{E_x}}{M_t N_0}\lambda_i\right)\right\} \tag{2.13}$$

where r represents the *rank* of $\mathbf{H}$ or the possible number of spatial links in the MIMO channel, or $rank(\mathbf{H}) = min(M_t, N_r)$. In (2.13), the channel gain for the ith SISO channel is λ_i. The total channel capacity in (2.13) is different from (2.8) without the knowledge of CSI at the transmitter and the total power is allocated uniformly to all transmit antennas.

2.3 MIMO Channel Quality Metrics

With the introduction of MIMO technology, a considerable amount of research has been published on eigenvalue statistics [10] [26] to explore the channel quality metrics. Knowledge of the eigenvalue statistics has shown the many advantages of MIMO in terms of SM gain, diversity order and beamforming gain [27] [28].

The eigenvalues of the correlation matrix reveal important characteristics in terms of the spatial domain of MIMO channels. The eigenvalue spread (EVS) indicates the spatial selectivity of the MIMO channels. It gives an indication about how many spatial links are possible within the MIMO system. If the eigenvalue spread is high, it shows the channel is more correlated with high difference between the eigenvalues. With knowledge of the EVS, it is possible to inject power effectively into the channels. In the high SNR regime, greater channel capacity can be achieved if the eigenvalues are less spread out. In the low SNR regime, all the power can be allocated to the strongest eigenmode to attain high beamforming gain.

Several studies have employed the eigenvalue-dependent channel quality metric as a switching criterion in adaptive MIMO systems [29] as depicted in Figure 2.6. The channel is estimated at the receiver end with the channel estimation techniques and the channel quality metric is computed based on these estimates. The transmitter is then informed with a low-rate feedback link.

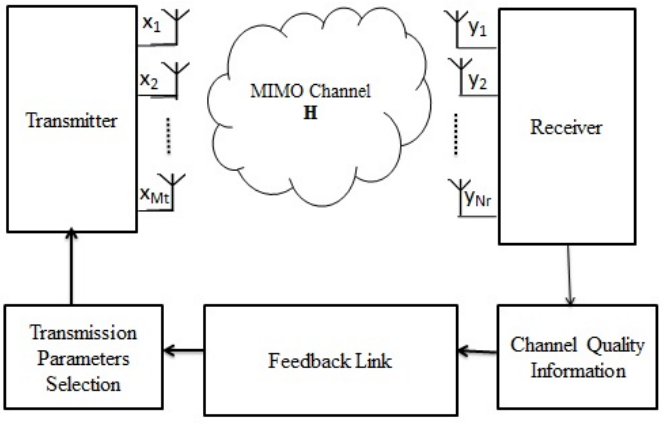

Figure 2.6: Adaptive MIMO system.

Based on feedback information, the transmitter selects the appropriate signalling parameters like modulation and coding techniques for the next transmission. This makes the system adaptive where the transmitter adapts to the changes of the propagation

channel. Thus, the channel quality metric acts as a switching criterion for certain adaptive MIMO systems [24] [30] to improve the link quality.

2.3.1 Rank

The MIMO channel capacity is highly dependent on the propagation channel characteristics even if the CSI is perfectly known at the transmitter (CSIT) and at the receiver side (CSIR). One of the important parameters of the MIMO channel matrix is the rank, which reveals important MIMO system characteristics in the spatial domain. It represents the effective spatial links that are possible within the MIMO channel. The rank of the MIMO channel matrix indicates the number of data streams that can be spatially multiplexed on a MIMO link.

A high rank of MIMO channel matrix indicates a radio channel with rich scattering, which leads to several independent spatial channels. A low channel rank indicates that spatial paths are highly correlated. With the channel rank one, only a principal propagation direction is possible as in the case of beamforming. For adaptive transmission, rank has been used as a channel metric to improve the detection performance of the Bell Laboratories Layered Space-Time (BLAST) in spatially correlated MIMO channels [31].

2.3.2 Condition Number

The condition number (CN) is another channel quality metric which reveals the multipath richness of the MIMO channel [32]. It measures the amount of correlation present in the MIMO channel. A channel rank only provides the possible number of spatial links but does not give any information about the quality of the links. A CN indicates the channel quality and is related to the EVS of the channel matrix. The

CN denoted as (κ) can be defined as the quotient of maximum eigenvalue and the minimum eigenvalue of the channel matrix as:

$$\kappa = \frac{\lambda_{max}}{\lambda_{min}} \tag{2.14}$$

where the λ_{max} and λ_{min} represent the maximum eigenvalue and the minimum eigenvalue, respectively. A detailed knowledge of the eigenvalue spread is highly desirable to characterize the MIMO propagation channel for future wireless communication systems.

Most research work has used the CN as a selection criterion for several purposes in MIMO systems. Heath and Love [30] used a CN of the MIMO channel to perform multimode antenna selection with limited feedback. In another study [33], Heath and Paulraj used CN of the MIMO channel to perform switching between diversity and multiplexing gain purposes. In a similar way, Piazza et al. [34] used CN to switch between different modes of circular patch reconfigurable antennas. For the adaptive modulation scheme, CN was used by Forenza et al. [35] to obtain the spatial selectivity of the channel. Previous work in [36], demonstrates the use of regular CN (or its reciprocal) to evaluate the quality of the channel matrix as it provides some intuition on channel quality.

Heath and Paulraj have proposed another switching criterion to choose between SM and diversity schemes in [33], known as the Demmel condition number. It has been shown that the Demmel condition number (κ_D) of the matrix channel provides a sufficient condition for multiplexing to outperform diversity. The Demmel condition number is the ratio of the Frobenius norm and the smallest singular value. A Demmel condition denoted by κ_D can be written as:

$$\kappa_D = \frac{\sum_{i=1}^{m} \sigma_i}{\sigma_{min}} \tag{2.15}$$

where λ_{min} is the minimum singular value of the channel matrix. In [37], MIMO Orthogonal Frequency Division Multiplexing (OFDM) channel measurements have been carried out to study the statistical properties of κ_D in various propagation environments.

A CN is a metric of the channel quality and also indicates the sensitivity of the MIMO channel matrix. A value of CN close to one indicates a well-conditioned matrix with almost equal eigenvalues. A high value of CN indicates a correlated channel with a large difference between all the eigenvalues of the channel matrix. Thus, high CN also signifies the *rank* drop and degenerates into a *rank-1* channel matrix. Statistically, if the channel condition number is low then the channel will be more suitable for large capacity gains for SM in MIMO wireless systems [32]. The importance of the condition number in the area of MIMO communications has been discussed by many authors in [38–42].

The condition number also indicates the behaviour of the channel matrix **H**: as an ill-conditioned channel matrix or a well-conditioned channel matrix. An ill-conditioned channel matrix means that small changes at the input side can make drastic changes in the solution channel matrix. During matrix computations, these small changes are caused by round-off errors and the solution of the channel matrix becomes unreliable. The ill-conditioning of the matrix also shows the singularity property of the matrix, which thus becomes non-invertible. Moreover, this computational complexity also makes the architecture design of the receiver more complicated [19].

If the CN of a matrix approaches 1, then that matrix is known as well-conditioned matrix. In the high SNR regime, a well-conditioned MIMO channel matrix, can facilitate communication with high SM gain. In the low SNR regime, allocating power to the strongest eigenmodes and leaving the weak eigenmodes with no power allocation is the best policy to attain beamforming gain. The achieved channel capacity in terms

of eigenmodes can be written as [43]:

$$\mathbf{C} \approx \frac{P}{N_0}\Big(\max_i \lambda_i\Big) log_2 e, \qquad bits/s/Hz \tag{2.16}$$

where $max_i \lambda_i$ is the maximum power gain provided by the MIMO channel. In the low SNR regime, the effect of the *rank* or CN of the MIMO channel matrix becomes negligible.

2.4 MIMO Channel Modelling

When communicating over MIMO fading channels, it is necessary to consider the system architecture and the particular propagation environment conditions. The distribution of the channel matrix **H** can be drawn from a certain probability function. It characterizes the MIMO system with the propagation scenario of interest and is known as the channel model. The modelling of MIMO channels captures the key properties of the propagation environment and evaluates the system performance. It is also important in system analysis, network planning and design in terms of signalling and detection schemes. It also enables the performance prediction and comparison of different system configurations in various propagation environments.

2.4.1 MIMO Channel Models

Several channel models for MIMO systems have been proposed previously in the literature [44–46], and can be classified in different ways. Two main categories of MIMO channel models are: Propagation-based models and Analytical models.

- Propagation-based models: are also known as physical channel models. The

physical channel model chooses physical parameters to describe the MIMO propagation channels. These parameters include angle-of-departure (AoD) at transmitter, angle-of-arrival (AoA) at receiver, antenna spacing at both ends and path attenuation [7]. This channel model reproduces the physical wave propagation in a deterministic or stochastic way.

The deterministic models aim to characterize the actual physical radio propagation environment channel. The channel matrix can be generated based on a geometrical description of the propagation environment by employing ray-tracing techniques combined with knowledge of the propagation environment. The mathematical derivation of these models is complex and time consuming. Thus, they are used only to cover specific small indoor environments.

The stochastic models aim to consider the channel behavior as a random variable with a certain statistical distribution depending on the propagation environment. These models are often based on large measurement data. Empirical models, which are based on channel measurements, also fall into this category.

- Analytical channel models focus on modelling the spatial structure of the channel without considering the characteristics of the propagation environment. Two popular models which characterize the MIMO channel matrix in terms of the correlation between the matrix coefficients are: independent identically distributed (i.i.d.) Rayleigh fading, and Kronecker channel models [44].

This thesis focuses on MIMO channels which follows the Rayleigh fading channel model. There are various models for the correlation structure on this fading. Depending on the structure, the correlation can be exploited on transmit/receive or on both sides.

2.4.2 Classical i.i.d. Rayleigh Fading Channel Model

The i.i.d. model is the simplest analytical model, in which all the channel coefficients of the channel matrix are assumed uncorrelated. In the literature [5], [13], [47] [48] used the i.i.d. Rayleigh fading channel as the channel model for traditional MIMO systems. The MIMO system performance in terms of bit error rate (BER) and channel capacity has been derived as well. In a rich scattering environment with suitable array element spacing,the entries of $\mathbf{H}$ can be assumed independent, zero-mean, unit-variance, circularly symmetric complex Gaussian random variables [4] [10] [14], and, the entries can be defined as:

$$h_{M,N} = \mathcal{N}\left(0, \frac{1}{2}\right) + j\mathcal{N}\left(0, \frac{1}{2}\right) \tag{2.17}$$

where $j = \sqrt{-1}$ and $\mathcal{N}(\mu, \sigma^2)$ denotes a Gaussian random variable with mean μ and variance σ^2 and $\mathbf{H} = \mathbf{H}_w$ or all the channel coefficients are uncorrelated as in the i.i.d. Rayleigh fading channel model.

2.4.3 Kronecker Model

When there is a low scattering environment or the antenna elements are placed close to each other, there will be correlation between the channel coefficients of channel matrix $\mathbf{H}$ [49] [50]. With the correlation structure, a correlation matrix needs to be constructed with the correlation model. This correlation effect is often modelled by using the Kronecker model. The total spatial correlation matrix can be created by the Kroncker product of the spatial correlation matrices at the transmitter and receiver sides [45].

The Kronecker model is a simple MIMO channel model with the assumption that no relation exists between the transmitter and receiver side correlation matrices. This

means the correlation present at the receiver side is independent from the correlation present at the transmitter side. Thus, each transmitter shows its own transmit correlation matrix, regardless of the receiver, and each receiver shows its own receive correlation matrix, regardless of the transmitter.

The Kronecker channel model approximates the correlation matrices by using transmitter and receiver correlation matrices and can be written as [45] [51–53]:

$$\mathbf{H} = \mathbf{R}_R^{1/2} \mathbf{H}_w \mathbf{R}_T^{1/2} \tag{2.18}$$

where $\mathbf{R}_T$ and $\mathbf{R}_R$ represents the correlation matrices at the transmitter and receiver sides, respectively. The channel matrix $\mathbf{H}_w$ is represented with i.i.d. zero-mean complex-Gaussian entries.

2.5 Role of Channel State Information

In MIMO systems, knowledge of the channel state at the transmitter/receiver or on both sides improves the system performance. The importance of channel knowledge has been previously discussed [54], and results showed the loss of degree-of-freedom (DoF) with the lack of availability of perfect CSIT. The performance in MIMO systems is degraded with no channel information available at the transmitter side, even if the receivers have CSIR. CSIT can be achieved either by exploiting the channel reciprocity principle in a TDD system or by means of a limited feedback channel in FDD system.

2.5.1 Channel Knowledge at the Transmitter

It is often assumed that the receiver can track the channel perfectly and thus complete CSI is possible at the receiver side (CSIR). But the transmitter can have different levels of CSIT, ranging from no CSIT at all to full CSIT. The assumption of accurate channel information is possible at the receiver side especially in the downlink. It is possible by using channel estimation techniques employing a common pilot-symbol channel shared between both terminals. The transmitter relies on the channel measurements at the receiver side and can be informed by the receiver in an implicit or explicit way.

Channel acquisition at the transmitter mainly relies on channel reciprocity or feedback. In FDD systems, where channel reciprocity cannot be exploited, the need for CSIT places a significant burden on the bandwidth constraints of the feedback channels. These feedback requirements further worsen in high-mobility systems (such as 3GPP-LTE,WiMAX etc.) where the channel conditions change rapidly and in wideband systems with frequency selective channels that require more feedback bits.

2.5.2 Statistical Channel Knowledge at the Transmitter

Because of the feedback bandwith constraint (availability) in wireless communication systems, it is not possible to send back all of the information from the receiver to the transmitter. Another option is to send partial channel state knowledge with less feedback overhead, also known as statistical CSIT. The reason for using statistical feedback is that the second-order information of the channel statistics vary much more slowly in comparison to the channel realization itself. This statistical CSIT can be conveyed periodically to the BS resulting in little uplink overhead in terms of feedback bits.

In the literature [44] [55], two common models for statistical CSIT that have been

studied extensively are:

- Channel Mean Information (CMI): refers to the case where the channel at the transmitter is assumed with a nonzero mean while the covariance matrix is unknown and often assumed as white.
- Channel Covariance Information (CCI): refers to the case where the channel at the transmitter is assumed with zero mean while the information regarding the relative geometry of the propagation path is available through a non-white spatial covariance matrix.

Channel knowledge acquisition at the transmitter side using covariance feedback can be applied to both TDD and FDD systems.

2.6 Antenna Selection in MIMO Systems

The use of multiple antennas at both ends of a wireless link offers significant improvements in terms of channel capacity and link reliability. The deployment of MIMO systems with multiple antennas is the major limiting factor in wireless systems. In fact, antenna elements are cheap but the RF chains connected to antennas increase the complexity in terms of space, and hardware requirements. In general, RF chains include amplifiers, mixers, up-and-down converters and analog-to-digital converters (ADC) on both sides, increasing the cost and power consumption as well. As discussed in the last section, there is another constraint of bandwidth requirement for the feedback link to send the CSI back to the transmitter. An effective solution to overcome all these disadvantages is antenna selection, which reduces the cost and size while providing as high a data rate as conventional MIMO systems [56] [57–59].

A typical MIMO system, as in Figure 2.7, shows an antenna selection scheme at the

transmitter and receiver side. The system consists of M_t transmit and N_r receive antennas, whereas a lower number of RF chains have been selected at the transmitter side ($L_{M_t} < M_t$) and at the receiver side ($L_{N_r} < N_r$). The best sub-set of L_{M_t} transmit and L_{N_r} receive antennas are selected with the antenna selection schemes. In this way, it reduces the number of RF chains from M_t to L_{M_t} at the transmitter side and from N_r to L_{N_r} at the receiver side, and therefore reduces the complexity of the system. Thus, MIMO systems using AST employ a reduced number of RF chains at the transmitter and receiver side.

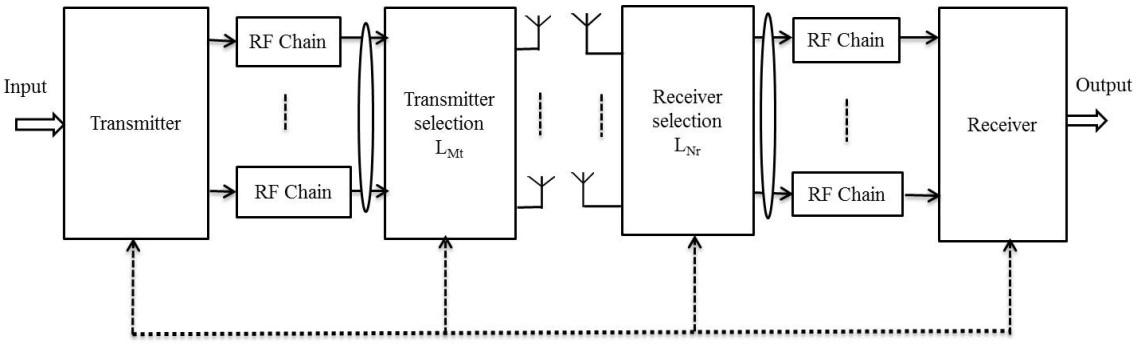

Figure 2.7: Block diagram of MIMO system with antenna selection.

As shown in Figure 2.7, it is possible to select the subset of the best antennas at the transmitter and receiver side. The feedback overhead can also be reduced by using transmit antenna selection. The receiver can send back the CSI with a low-rate feedback channel and select the antennas at the transmitter side. Thus, AS reduces cost, space and complexity in terms of RF chains and feedback bits.

The antenna selection process, selects the subset of antennas that maximizes some channel metrics in the system. The difference between antenna selection at the transmitter and the receiver side is the usage of the feedback. The selection of the transmit antennas can be selected at the receiver side and the information can be fed back to the transmitter. As only indices of the transmit antennas need to fed back, it reduces

the feedback overhead.

The optimal choice for antenna selection in MIMO systems requires knowledge and estimation of the full channel matrix **H**. To estimate all the channel coefficients with all the antennas, it seems necessary to make available all the RF chains on both sides. But this goes against the goal of reducing the number of RF chains. In the antenna selection process, when the environment changes slowly and with the help of a training sequence, antennas can be multiplexed to different RF chains so that the channel is estimated successively antenna by antenna.

Many algorithms for antenna selection have been investigated in the literature [60–62], which can be classified as transmit antenna selection, receive antenna selection, or joint transmit-receive antenna selection. The antenna selection criteria can be chosen to optimize different performance metrics, such as maximizing theoretic capacity [63] [64–66], maximizing SNR, or minimizing error rate [67] [68] [69] etc. These algorithms can be applied at the either side of the link [70].

Some algorithms in the literature are related to the topic of this thesis, and can be summarized as follows:

- Incremental antenna selection technique (IAST)
- Decremental antenna selection technique(DAST)

In IAST, each antenna is added successively at each step, the antenna that contributes most to the increase of the channel capacity is added to the set of selected transmit antennas. The antenna that provides the highest capacity is selected first, then the antenna which provides second highest, and so on. This process continues until all transmit antennas are selected [56].

Another antenna selection algorithm, DAST, can be implemented by deleting each

antenna in descending order of decreasing channel capacity. It starts with all the available transmit antennas and selects the antenna that contributes least to the channel capacity. One antenna in each step is discarded according to its capacity contribution. Thus, DAST identifies and discards the antenna that yields the minimum contribution to the capacity. The complexity of the DAST is higher than the IAST [25].

The straightforward approach for selecting the optimal subset of antennas is to exhaustively search over all the possibilities. The complexity of MIMO transceiver algorithms increases exponentially with the number of transmit and/or receive antennas. The selection of the subset antennas affects the channel capacity equation in an iterative algorithm, which evaluates all possible antenna combinations to get the highest channel capacity. In practice, fast and precise subset antenna selection methods are required. However, the success of these selection algorithms depends on the knowledge of CSI available at the transmitter and receiver side to select the best subset of antennas respectively [71] [72] [73].

2.7 Antenna Array Design

Wireless communication system performance depends on the characteristics of the propagation environment and the antenna array structure. Since the antenna interface is also included in the communication channel between transmitter and the receiver, the properties of the antennas also affects the signal quality of the system. Traditional antennas integrated on devices such as laptops or on portable devices have fixed radiation patterns. The properties of these radiation patterns do not change with the changing environmental conditions. Thus, the performance of the communication system degrades as the antennas do not operate optimally, according to the changing conditions of the channel. To solve this antenna problem, reconfigurable antennas

that can change their properties such as operating frequency, radiation pattern and polarization, have gained significant interest. These antennas are considered smart antennas and can maximize the capacity of wireless systems [74].

MIMO system performance is strongly influenced by the interaction between the propagation channel and the antenna array arrangement. The arrangement of the antenna arrays in MIMO is mostly affected by these three parameters: spatial correlation, mutual coupling and diversity. Thus, these three parameters should be taken into account when evaluating the performance of the MIMO array.

2.7.1 Correlation

MIMO channel capacity increases linearly with the minimum number of transmit and receive antennas when the channel coefficients are i.i.d complex Gaussian random variables. But putting too many antennas on a portable device leads to high spatial correlation. The correlation between the output signals reduces the spectral efficiency and degrades the system performance of the MIMO system. To gain the benefits of MIMO systems, it is important to find the methods to control the correlation effect in the antenna array design.

2.7.2 Mutual Coupling

Mutual coupling has a significant impact on the implementation of MIMO technology, especially on the portable devices where inter-element distance between antenna terminals is very low. When antennas are placed close to each other, the electromagnetic interaction between the closely spaced antennas is known as mutual coupling. Due to this interaction, the current on each antenna not only attains its own current from the feeding point but also induced current from the neighboring elements [75].

The mutual coupling between antenna elements depends on a number of factors, including inter-element spacing, operating frequency of the antennas, antenna array structure, antenna array geometry, the radiation patterns of the antenna elements and near-field scatterers. Most of these parameters can be estimated except the near-field scatterers. Moreover, these scatterers in the propagation environments are random in nature and increase the mutual coupling between the antenna elements.

Due to the close proximity of the antenna terminals, there are electromagnetic interactions between the antennas that alter the radiation properties of the array. These radiation patterns are not independent in the case of a MIMO system where the multiple antenna elements are placed with small separation. The negative effect of the mutual coupling is the impedance matching that reduces the received power and SNR.

Mutual coupling not only influences the antenna efficiency [76] but also affects the correlation. In the literature [77], it has been is shown that mutual coupling shown significantly reduces the correlation and thus increases the channel capacity. It has also been shown that mutual coupling can have a negative effect where it increases the correlation and decreases the channel capacity.

High mutual coupling creates pattern diversity, where the individual patterns may change, and reduces the correlation between the signals at the receiver. High mutual coupling between the radiation signals at the receiver increases the spatial correlation and impacts on the MIMO channel capacity [78] [79]. Different radiation patterns means each antenna element radiates through different propagation links with different portions of the scatterers. This is very helpful in MIMO systems especially in the case of poor scattering environments. Thus, mutual coupling shows different radiation patterns even when the antenna elements are separated with small spacings. These radiation patterns can be calculated and measured with the S_{ij} parameters of the scattering matrix.

Many studies have investigated the effect of mutual coupling on the MIMO systems. Research has shown [80–82] the benefits in terms of the MIMO diversity gain by reducing the signal correlation for a specific range of antenna separations. Other studies [49] [83] showed that mutual coupling degrades the MIMO performance in terms of channel capacity and impedance mismatch between antennas and their termination loads.

2.7.3 Diversity

MIMO antenna arrays can be designed with diversity techniques to reduce the signal correlation between the antenna elements and hence can improve the system performance. To obtain uncorrelated signals, different antenna diversity techniques are as follows:

- **Spatial diversity**: This is the simplest and most common form of diversity technique used in MIMO systems. The antennas are placed far apart from each other to produce the phase delay between the received signals at the antennas. Thus, the signal received at the first antenna is uncorrelated from the signal received at the second antenna. When the antenna terminals are placed far apart, propagation multipath impinges different array elements with different phases, producing uncorrelated signals across different antennas.

  Uncorrelated signals at the receiver depend on the appropriate spacing between the antennas and the width of the multiple angle of arrival depending on the scattering environment. However, benefits of the space diversity can be achieved by producing uncorrelated signals. So if one of the signal is in deep fade, the output signal can be recovered from the other antenna terminal. In typical MIMO systems, where size and cost are the primary constraints, for example

in mobile phones, placing antennas far apart is not possible for future wireless communication systems.

- **Pattern diversity**: produces uncorrerlated signals across different array elements with orthogonal radiation patterns. These different radiation patterns provide a high gain in a large portion of angle space, known as angle diversity. The antennas are located in the same physical space but the multipath signals come from the different angles. All the antenna array elements have a different radiation pattern that points in a different direction, and thus receives uncorrelated signals.

  Vaughan [84] discussed reconfigurable antennas with different radiation patterns to exhibit pattern diversity. The beamforming antenna provides an example of pattern diversity, as it can direct its radiation pattern in different directions. The radiation beams departing and arriving in different directions are added destructively or constructively resulting in different channels. The pattern diversity helps to achieve independent multipath signals at antenna elements.

- **Polarization diversity**: obtains uncorrelated signals across different antenna array elements by using cross-polarized antennas [85]. These antennas receive multipath signals with different polarizations of the electric and magnetic field. Unlike spatial diversity, these antennas can be located at the same position but receive orthogonal polarization signals. A polarization reconfigurable antenna can be designed to switch between linear polarizations, clockwise or counterclockwise in circular polarizations and different axial ratios and tilt angles of elliptical polarizations [74].

2.8 Induced EMF method

The induced electro motive force (EMF) method is a classical method to calculate the self and mutual impedances of the antenna array elements. This method is easy to calculate, gives a good approximation which leads to closed-form solutions to provide very good design data [86]. When antennas placed in the close proximity, the mutual coupling effect can not be ignored. The mutual impedance between the antenna array elements is used to measure these mutual coupling effects.To analyze mutual coupling effect between closely spaced antenna elements, it is necessary to know the fields produced by the antenna at near distances [87].

Consider two parallel linear dipoles as shown in Figure 2.8, to calculate self and mutual impedances of the antennas placing close to each other [87]. The distance between two-dipoles along the x-direction is d and their centers are offset by b along the z-axis direction.

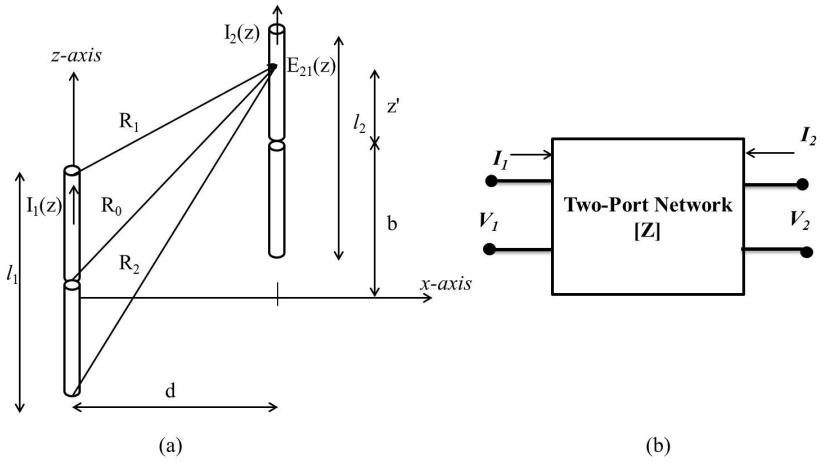

Figure 2.8: (a) Two parallel linear dipoles (b) Equivalent Two-port network.

When antenna element-1 acts as driven element and other antenna element-2 acts as open-circuited, there will be open-circuit voltage ($V_{21,OC}$) on antenna-2, due to the

mutual coupling effect. The mutual impedance at antenna element-2 due to antenna element-1 with input current I_1 on antenna element-1 can be written as :

$$Z_{21} = \frac{V_{21,OC}}{I_1} \tag{2.19}$$

With the reciprocity theorem, $Z_{12} = Z_{21}$. In the presence of incident field E_{in}, the short-circuit current can be defined as [87]:

$$I_{SC} = \frac{1}{V_0} \int_{-h}^{h} E_{in}(z) I(z) dz \tag{2.20}$$

where h defines the length of the antenna. and open-circuit voltage can written as:

$$V_{OC} = -\frac{1}{I_0} \int_{-h}^{h} E_{in}(z) I(z) dz \tag{2.21}$$

The z-component of the electric field generated by antenna element-1 and incident on antenna element-2 can be represented by $E_{21}(z)$. If antenna element-2 is open-circuited then according to (2.21), the induced open-circuit voltage can be written as:

$$V_{21,OC} = -\frac{1}{I_2} \int_{-h_2}^{h_2} E_{21}(z) I_2(z) dz \tag{2.22}$$

where $h_2 = l_2/2$ and $I_2(z) = I_2(0)$ is the current on antenna element-2.

Substitute (2.22) in (2.19), the mutual-impedance at antenna element-2 due to antenna element-1 will be:

$$Z_{21} = -\frac{1}{I_1 I_2} \int_{-h_2}^{h_2} E_{21}(z) I_2(z) dz \tag{2.23}$$

Current on antenna element-1 can be written as [87]:

$$\begin{aligned} I_1(z) &= I_1 \frac{sin(k(h_1 - |z|))}{sin\, kh_1} \\ &= I_{m1} sin(k(h_1 - |z|)) \end{aligned} \tag{2.24}$$

where $h_1 = l_1/2$, $k = 2\pi/\lambda$ is the free space wave-number and λ is the wavelength.

Current on antenna element-2 can be written as [87]:

$$\begin{aligned} I_2(z) &= I_2 \frac{sin(k(h_2 - |z|))}{sin\, kh_2} \\ &= I_{m2} sin(k(h_2 - |z|)) \end{aligned} \tag{2.25}$$

As shown in Figure R_0, R_1, R_2 are the distances from the center and the two ends of the antenna terminals. The electric field with the z-components can be written as [87]:

$$E_z(z) = -\frac{j\eta I_{m1}}{4\pi} \left[\frac{e^{-jkR_1}}{R_1} + \frac{e^{-jkR_2}}{R_2} - 2\, cos kh_1 \frac{e^{-jkR_0}}{R_0} \right] \tag{2.26}$$

where $-h_2 \leq z \leq h_2$, $\eta = 377\Omega$ is the wave impedance of the free space.

Based on Figure 2.8, R_0, R_1, R_2 can be represented as [87]:

$$\begin{aligned} R_0 &= \sqrt{d^2 + (z+b)^2} \\ R_1 &= \sqrt{d^2 + (z+b-h_1)^2} \\ R_2 &= \sqrt{d^2 + (z+b+h_1)^2} \end{aligned} \tag{2.27}$$

By substituting (2.26) into (2.23), the mutual impedance can be calculated as:

$$Z_{21} = \frac{j\eta}{4\pi\, sin\, kh_1\, sin\, kh_2} \int_{-h_2}^{h_2} F(z)\, dz \tag{2.28}$$

where F(z) is:

$$F(z) = \left[\frac{e^{-jkR_1}}{R_1} + \frac{e^{-jkR_2}}{R_2} - 2\cos kh_1 \frac{e^{-jkR_0}}{R_0}\right] sin\left(k(h_2 - |z|)\right) \tag{2.29}$$

Equation (2.23) referred as the mutual impedance across the input terminals of the antennas. By normalizes (2.23), by the factor $I_{m1}I_{m2}$, the mutual impedance in (2.23) can be represented as:

$$Z_{21m} = \frac{j\eta}{4\pi}\int_{-h_2}^{h_2} F(z)\, dz \tag{2.30}$$

The self-impedance can also be calculated with (2.28) by setting $h_2 = h_1$ and $d = a$, where a is the radius of the antenna element.

Thus, self-impedance can be written as :

$$\begin{aligned} Z_{11} &= -\frac{1}{I_1}\int_{-h_1}^{h_1} E_{11}(z)I_1(z)dz \\ &= \frac{j\eta}{4\pi} sin^2 kh_1 \int_{-h_1}^{h_1} F(z)\, dz \end{aligned} \tag{2.31}$$

where F(z) is:

$$F(z) = \left[\frac{e^{-jkR_1}}{R_1} + \frac{e^{-jkR_2}}{R_2} - 2\cos kh_1 \frac{e^{-jkR_0}}{R_0}\right] sin\left(k(h_2 - |z|)\right) \tag{2.32}$$

By substituting $d = a$ and $b = 0$ in (2.27):

$$\begin{aligned} R_0 &= \sqrt{a^2 + (z)^2} \\ R_1 &= \sqrt{a^2 + (z - h_1)^2} \\ R_2 &= \sqrt{a^2 + (z + h_1)^2} \end{aligned} \tag{2.33}$$

The values of mutual impedance between the antenna elements and self-impedance of

an antenna can be calculated by using (2.28) and (2.31) and respectively.

2.9 Reconfigurable MIMO Systems

Employing multiple antennas at both ends of the MIMO system provides diversity and spatial multiplexing gain. The advantage of using such techniques increases the reliability and spectral efficiency by taking the advantage of multipath propagation. MIMO systems can adapt to varying channel conditions by adjusting the modulation and coding rate and transmission signalling schemes according to the user's need. Placing multiple antennas at the transmitter and the receiver ends within a confined space, especially on mobile terminals, puts a burden on the communication system.

Reconfigurable antennas are a promising solution to this problem. Reconfigurable antennas act as smart antennas in which the system uses an antenna array and the radiation pattern is dynamically adjusted by the system as required. Smart antenna systems exploit their intelligence in order to generate or receive the desired radiation pattern based on the RF environment. They have the ability to modify the antenna characteristics by changing its frequency of operation, pattern and polarization characteristics. Thus, reconfigurable antennas add an additional DoF in the MIMO systems and can improve the overall system performance.

2.9.1 Techniques for Pattern Reconfigurable Antennas

Reconfigurable antennas have been studied over a decade for a variety of applications. These antennas need various switching mechanism to achieve antenna reconfiguration and optimal performance. There are different mechanisms in order to reconfigure the antenna characteristics [74] [88]:

2.9.1.1 Mechanical and Structural Changes

The antenna reconfiguration is achieved by modification of the mechanical changes by using motors, actuators or other tools to move some parts in the antenna structure. The change in the physical structure makes changes in the electrical properties of the antennas and alters the radiation patterns. A mechanically movable mesh reflector is used for a reflector antenna to achieve pattern reconfiguration as demonstrated in [85]. The physical shape of a sub-reflector made of flexible conductor material can be changed dynamically [89] to change the radiation patterns.

2.9.1.2 Electrical changes

Antenna reconfigurability can be achieved by using electronic switches to redistribute the antenna surface currents. The electronic switches can connect and disconnect to the antenna parts to redistribute the antenna currents. The integration of switches to the antenna structures makes it possible to get the required pattern reconfigurability. Electronics components such as positive intrinsic negative PIN diodes, micro-electromechanical systems (MEMS) switches, optoelectronic switches and varactor diodes can be used to redirect the surface current of antennas.

Different examples of electrically reconfigurable antennas are described below:

- **PIN diode**: The PIN diode is a semiconductor device, in which resistance varies in accordance with the voltage applied through the anode and cathode nodes. It operates in two states: in the *on* state, where the diode is forward biased and this electronic component acts as short circuit and in the *off* state, where the diode is reverse biased and this electronic component acts as open circuit. It is a low-cost component with switching speed in the range of 1-100 ns [74]. In communication devices, it can handle power up to 40 dB.

PIN diodes have been used in many antennas such as printed dipoles, slot antennas, microstrip patch antennas, planar inverted-F antennas (PIFA), and dielectric resonator antennas [90] owing to their high dynamic reconfigurable ability. They have some drawbacks in terms of nonlinearity and DC power consumption.

- **MEMS switch**: MEMS switches rely on mechanical movement to achieve reconfiguration. These switches have advantages over PIN diodes such as: lower insertion loss, higher isolation, minimum DC power consumption, and relatively high power handling. They have very low switching speed in the range of 1-200 μs [74].

- **Varactor diode**:

  The variation of the voltage levels in a varactor results in a change in its capacitance. Thus, they can tune the antenna operation in different regions. As compared to PIN diodes, varactor diodes allow a tunable response. The advantage of this type of component is its low DC consumption with efficient reconfigurable ability [74] and it can be used in some adaptive wireless applications.

- **Optoelectronic switch**: Optical reconfiguration techniques based on the photoconductive switches. The optoelectronic switch can reconfigure the patterns in an antenna structure by using optical bias. An optical switch is formed when a laser beam is incident on the semiconductor material. The shining light of optical beam changes the activation and deactivation level of the photoelectronic switch. It does not produce any harmonics and inter-modulation distortion due to their linear behavior. Optoelectronic switches have some advantages such as low losses, being lightweight, noise immunity, and RF-circuit isolation. Despite all the advantages, optical switches have some issues in terms of integration with antenna structures and require a complex activation mechanism [74].

2.9.1.3 Material changes

Reconfigurable properties can also be attained through material changes. Change in material characteristics alter the current distribution of the antenna element resulting in steering the radiation pattern in different directions. The changes in the material characteristics contribute to shift the antenna frequency and changing the permittivity of the material alters the antenna length.

Antenna substrate characteristics can be changed by using materials like liquid crystals and ferrites. The changes in these materials can be obtained by changing the relative magnetic permeability or electric permittivity. In a liquid crystal material, the orientation of the liquid crystal molecules can be altered. By doing this, the dielectric constant can be changed with different voltage levels. For ferrite materials, permittivity and permeability can be changed with applied electric and magnetic fields respectively [88].

In non-resonant antennas, the beam steering capabilities can be changed with the propagation speed of the traveling waves. Two-dimensional grid array of resonant slot antennas can be built on a conventional substrate using ferrostrate material. By changing the permittivity of the ferroelectric superstrate, beam steering capability can be attained [91]. Other antenna designs have been investigated [92] that used this technique to steer the beampatterns. Slab in [93] also studied leaky wave antennas that rely on material changes to steer the beam in different directions. This has some drawbacks such as slow tuning speed, small reconfiguration capabilities and high voltage requirements.

2.9.2 Types of Pattern Reconfigurable Antennas

In pattern reconfigurable antennas, a single or a small number of active elements is surrounded by a ring of parasitic elements loaded at their base with some load in the form of a reactance or switch. The antenna elements connected to the RF source are referred to as active or driven elements. The parasitic elements are not active because they are not connected to any RF source. They are placed in close-proximity to the active elements. The loads can be electrically controlled to form and steer the radiation pattern of the array. The signals are coherently combined before being detected by the elements, and therefore they do not suffer from quantization errors in individual elements. The radiation pattern control is achieved by adjusting the phases of currents in the passive radiators via electronically controlling the impedance loads connected to the parasitic elements. Antenna symmetry allows these beams to be repeated through the azimuth plane with appropriate stepping of loading configurations around the parasitic ring.

There are two general categories of pattern reconfigurable antenna systems, namely the adaptive array and switched array as discussed below [94] [95]:

2.9.2.1 Adaptive array system

An adaptive array system is a smart antenna system configuration with an infinite number of patterns based on the propagation scenario. In adaptive array design, radiation patterns alter dynamically in response to the changing RF environment. With the use of signal processing algorithms, adaptive systems are able to distinguish between the desired signal and the interference signal. In a fully adaptive array, the beam patterns can be pointed into arbitrary directions. This allows direction the main beam to the desired user and at the same time nullifies the interference. By

doing this, the signal-to noise and interference ratio (SINR) can be maximized.

Based on N-port scatterer theory, Harrington proposed, a seven-element dipole array, in which one active radiator is surrounded by six equivalent parasitic elements. These parasitic elements are loaded at their center with a variable reactance. These reactances are typically produced with varactor diodes. The depletion level of the diode can be controlled with reverse bias magnitude. The variable reactances afford fine analog control of radiation. The variable loads alter the values of the reactance and steer the beam in different directions.With appropriate algorithms, the antenna can be termed as adaptive due to the load's ability to form a main lobe in one direction and nulling others. The control circuitry for the varactor requires a digital to analog converter for analog reverse bias, and RF chokes to isolate the DC path from the element. This control circuitry is simple to manufacture and relatively inexpensive compared to the active phased array.

Harrington in [96] presented numerous load configurations to illustrate the antenna's beam steerability. This work is further investigated for path and monopole antennas by Thiel and Smith [94], Thiel et al. [97], Sibille et al. [98], Preston and Thiel [99] and Vaughan [100].

2.9.2.2 Switched array system

The switched array system is a smart antenna system configuration with an finite number of patterns. These multiple fixed patterns are formed with different sensitivity levels in the predefined directions. The switched array concept originates from the Yagi-Uda dipole array [101]. The Yagi-Uda linear array comprises a reflective dipole, single active dipole and numerous director dipoles to achieve highly focused radiation [94] [87]. The reflector dipoles constitutes the backbone of a switched parasitic array.

Gueguen in [102] describes a switchable antenna where several Yagi-Uda dipole arrays share an active element. A diode is at the center of each reflector and acts as *in* resonance when short circuited, allowing radiation scattering. On the other hand, an open diode leaves the dipole *out* of resonance and lets radiation pass. This work has been investigated for wire and patch structures by Thiel and Smith [94], Thiel et al. [97], Sibille et al. [98], Preston and Thiel [99] and Vaughan [100].

A switched parasitic array consists of one active (driven) element connected to the RF source of the transceiver. There are a number of parasitic elements terminated with resistive loads surrounding the active element. When the parasitic element is loaded with an inductive load, it acts as director. Then the parasitic element radiated away from the driven element. When the parasitic element is loaded with an capacitive load, it acts as a reflector. Then the parasitic element radiates toward the driven element.

Both adaptive array and switched array systems attempt to increase the gain according to the location of the user. The adaptive system provides optimal gain while simultaneously identifying, tracking, and minimizing interfering signals. But the implementation cost of adaptive array systems in terms of complexity and hardware effort is more than the switched beam array.

2.10 Related Work

Work in the literature related to the topic of this thesis can be summarized as follows:

2.10.1 Related Work on Switched Parasitic Antennas

- Migliore et al. [7] proposed an adaptive MIMO system employing parasitic elements to improve the channel capacity. The antenna array design consists of a set of active antennas coupled to a set of parasitic elements that are terminated with complex loads. They discussed adaptive MIMO numerically and experimentally to show the performance improvement with less complexity and cost. In the classical MIMO approach, antennas need a rich-scattering environment to achieve the best performance. On the other hand, in adaptive MIMO due to its adaptivity, it is able to achieve satisfactory performance even in a poor scattering environment. The results of adaptive MIMO have also been compared with the antenna selection technique. The behavior of parasitic elements in adaptive MIMO described is in three different ways:

  i. Firstly, the parasitic elements are able to exploit the electromagnetic field in a much wider space as compared to the conventional MIMO. With parasitic elements, the adaptive MIMO system has the capability to collect the information smartly not only on the active elements but also collects the information on the parasitic elements. It, provides the freedom of collecting more information by properly varying the parasitic loads.

  ii. Secondly, the parasitic elements act as local scatterers around the active elements. By changing the configurations of the terminated loads, the parasitic elements acts *in* and *out* of resonance. Thus, they modify the propagation scattering environment.

  iii. Finally with parasitic elements, the MIMO antenna array can form different working states compared to the conventional MIMO with a fixed channel state with all active elements only. By selecting one of the radiation pattern configuration states, the overall radiation pattern of the array

can be modified. Moreover, the adaptive MIMO antenna array can adapt to the propagation environment.

An evolutionary algorithm has been used for experimental results and achieved the maximum channel capacity in less than 10 iterations. Channel estimation has not been discussed, since each new configuration with changing parasitic elements results in a different channel realization. It has not been described how this information can be fed back to transmitter with limited feedback overhead.

- Wennstrom and Svantesson [103] introduced an antenna design with SPA to steer the radiation patterns electronically in MIMO systems. The design consists of one active element that is connected to the transceiver and several parasitic elements terminated with switchable loads. The parasitic elements switched between in and out of resonance in the same manner as the Yagi-Uda antennas, to form diverse radiation patterns. By changing the controllable loads terminated on parasitic elements, the current distribution on the parasitic elements also changed on the elements of the array, altering the radiation patterns. They introduced the oversampling approach that samples the electromagnetic field at various angular directions within a symbol period.

  In their work, parasitic elements are designed as monopoles on a ground plane to achieve omni-directional properties. The SPA configuration proposed in this paper was designed with 5-element and 7-element monopole wires to form 4-direction and 3-direction symmetric antennas, respectively. In the 7-element monopole SPA, an additional circle of parasitic elements were hardwired to ground to increase the directivity.

  The authors adopted the Space Time Block Code (STBC) concept [104] to exploit the correlation effects to evaluate the channel capacity in MIMO systems. It was shown that the channel capacity obtained with the SPA was approxi-

mately the same as the capacity obtained by conventional MIMO antenna arrays.

The authors exploit the characteristics of SPA that offer several fixed beams but in a small size for utilisation on mobile terminals.They showed that diversity is possible by quickly switching the parasitic loads at the receiver with an oversampling approach. But they have not discussed about the bandwidth expansion and the increased adjacent channel interference.

- Bains and Muller [105] proposed a low-complexity receiver architecture using parasitic elements for implementing a rotating antenna for MIMO receivers. The parasitic elements give the possibility of creating a directive antenna beam that is rotated 360° degree within the duration of a symbol period. By doing this, spatial multiplexing is converted into frequency multiplexing and different sub-channels are created in the frequency domain.

  Instead of sampling the electromagnetic field with antennas at discrete spatial points, they proposed oversampling of the electromagnetic field by using the rotating receive antenna to maximize the channel capacity. Using a rotating receive antenna maximizes the link capacity, but sampling at a rate higher than the symbol rate causes a bandwidth expansion issue. At the receiver end the bandwidth expansion makes it sensitive to adjacent channel interference. Channel-statistics have not been discussed that can impact the MIMO channel capacity. The authors have not mentioned the channel quality parameter which can be sent back to the transmitter.

- Vaughan [100] presented SPAs through antenna pattern diversity. These low-cost antennas provide diversity gain in hand-held terminals. The antenna design gives an efficient radiation pattern to reduce the bit errors of the received signals. The basic principle was explained for examples of wire antennas. The per-

formance of four wire antenna configurations was evaluated through computer simulation using the method-of-moments (MoM) process. The four different configurations are described as follows:

i. A wire antenna configuration with the two radiation patterns forming a compact antenna. The experiment set up includes one active element surrounded with three parasitic elements. One of the parasitic elements is short-circuited and the other two are terminated with switchable loads.

ii. A wire antenna configuration with two radiation patterns in the half space. The experimental set up is same as the first wire antenna configuration but the short-circuited parasitic element is replaced by a ground plane.

iii. A wire antenna configuration the same as the multiple elements of a Yagi-Uda antenna. In this, one active element is surrounded with multiple parasitic elements separated with 0.2λ distance. The parasitic elements are switchable and change their states from short-circuited to open-circuited.

iv. A wire antenna configuration with a lower directivity beam with fine rotational control using 16-parasitic elements with a separation distance of 0.25λ. By switching the parasitic elements, adjacent patterns can be obtained with the angle of $360°/15=22.5°$. Thus, a large number of decorrelated patterns can be obtained through 16-parasitic element configurations.

- Sohn and Gwak [106] proposed a single-RF MIMO-OFDM system with a Beam Switching Antenna (BSA) at the receiver side. The single-RF MIMO-OFDM used a single front-end and steered the beam patterns in predefined directions. The oversampling effect at the receiver side induces replicas in the frequency domain. These replicas interfere with the desired signals at the receiver side and degrade the system performance. The authors investigated this problem in a more realistic environment with the OFDM system with co-existing systems in

the neighboring frequency bands. Beam-steering is done with PIN diodes for fast switching speed. Different replica interference avoidance (RINA) strategies are proposed for co-existing and co-operating network situations. They presented two important findings to avoid adjacent channel interference:

i. replica interference without co-existing systems can be reduced with proper switching rate at the BSA receiver. The beam pattern switching rate at the receiver should be an integer multiple of the product of the orthogonal frequency division multiplexing (OFDM) sampling rate and the number of receiving beam patterns.

ii. replica interference with co-existing systems cannot be avoided completely. The replica interference depends on the status of the coexisting user and beam switching capability of the user.

For the simulation results and analysis, three different RINA approaches are suggested: maximum-capability RINA (MAX-RINA), Static RINA (S-RINA), and Dynamic RINA (D-RINA). In addition to that, the overall network operation principles of the replica interference avoidance strategies are also presented in the different scenarios.

- Piazza et al. [34] demonstrates a technique for antenna configuration selection for reconfigurable circular patch antennas. They investigated the benefits of MIMO reconfigurable antennas through a combination of adaptive antenna array structure and adaptive algorithm to select the optimal pattern configuration at the receiver. Three different novel classes of electrically multi element reconfigurable antennas have been proposed in their work:

  i. a reconfigurable printed dipole array that exploits the inter-element mutual coupling between closely spaces dipoles to exploit pattern reconfigurability,

ii. circular patch antennas capable of exciting higher order modes to exploit pattern and polarization reconfigurability, and

iii. a two-port meta-material leaky wave array that can be reconfigured in number of array configurations to achieve pattern reconfigurability.

The antenna configuration selection algorithm includes knowledge of the second-order statistics and average SNR. The performance of the proposed algorithm is also compared to the conventional MIMO system that estimates each antenna configuration and then selects the optimal configuration. With the selection algorithm, there is only need to estimate the channel for a single antenna configuration independently of the number of array configurations. The training sequence is allocated to only a single antenna to estimate the channel instead of estimating all the array pattern configurations. This improved channel estimation shows better SNR level at the receiver.

Authors showed the functionality of the selection algorithm depends on the differences existing between the antenna array configurations. Their work focused on the switching between the circular patch modes.

- Forenza et al. [35] proposed a reduced-complexity adaptive MIMO transmission technique for exploiting the capacity of spatially correlated channels. The adaptive switching algorithm designed to switch between different transmission schemes depending on the changing channel statistics. The switching criteria is based on the statistical knowledge of the channel rather than the instantaneous CSI. The algorithm used spatial correlation and average SNR information to select the link-quality region for a given transmission mode. The switching algorithm showed substantial capacity improvement in various propagation environment scenarios. The simulation results revealed significant improvement in system performance in terms of capacity and error-rate over non-adaptive

systems.

- Yoshida et al. [107] presented a compact transceiver structure to enable the mobile terminals to be miniaturized with a single front-end. The parasitic elements provides adaptive analog beam-forming, and switching between parasitic elements provides the spatial multiplexing. In the single RF front-end MIMO, the parasitic antenna elements are terminated with variable reactances. By controlling the parasitic elements interdependently, orthogonal directivity patterns are generated and receive spatially diverse signals.

  This paper considers both advantages of adaptive beam-forming and spatial multiplexing for compensating the switch penalty. The proposed architecture requires the antenna switching frequency to be higher than the signal bandwidth. Furthermore, statistical analysis of the antenna switching system with parasitic elements is discussed theoretically. The simulation results confirmed that the performance does not degrade with the increase of spatial correlation. The results are also compared with the conventional MIMO in a high spatial correlation environment. The computer simulation results are same as that of the conventional MIMO with a distance of $\lambda/8$ between the elements.

- Jo et al. [108] achieved full spatial multiplexing gain with single radio in their research. The SNR is measured at the receiver with a beam switching antenna to obtain spatial multiplexing gain in an indoor MIMO environment. The transient time of the switches is reduced by using a fast-response switching device. To achieve beam-steering at the transmitter and receiver, a single active element is surrounded with two parasitic elements. The values of the reactive loads terminated on the parasitic elements are pre-defined. Four different case scenarios have been discussed for the analysis and experiment results. These results revealed SM gain with a Long-Term Evolution (LTE) FDD downlink signal. The

performance of the beam switching antenna is improved by 10 dB by reducing the switching rate.

Jo et al. [109] recreated the experimental results by employing 4×4 MIMO signals by using a beam-switching technique at the receiver side. Demodulating the MIMO signal with a single-RF shows some degrading factors in terms of bandwidth expansion and SNR reduction.

2.10.2 Related Work on MIMO Channel Capacity with AS and CSI

Work in the literature that is related to the MIMO channel capacity in this thesis is summarized as follows:

- Cuan-Cortes et al. [18] showed MIMO channel capacity improvements by employing antenna selection and power allocation algorithms. IAST selects the antennas in increasing order of their contribution to the channel capacity. Then an optimal power allocation algorithm allocates the transmit power to those antennas accordingly. They discussed the influence of the correlation matrix on the channel capacity. The effect of the covariance matrix is shown in correlated and uncorrelated propagation environments. A comparison was presented between the traditional MIMO that allocates power uniformly to all the transmit antennas and WPA that allocates more power to the antennas that contribute more to the channel capacity.

  The antennas are selected first with IAST and then the covariance matrix is improved by allocating the transmit power to the antennas with WPA. The results showed the optimal covariance matrix improves the channel capacity significantly with proper selection of antennas and power distribution among all

the transmit antennas. A comparison of results reveals that the channel capacity has been improved with the modified covariance matrix. It has been presented that the channel capacity shows upper bounds with the improved covariance matrix.

Chapter 3

Switched Parasitic Antennas

This chapter gives a brief introduction of parasitic arrays and their fundamental mechanism of operation. The concept of N-port network theory is reviewed with the antenna modelling concept in MIMO systems. Electromagnetic mutual coupling is the basic concept that defines the directive nature of the parasitic array. The switching parasitic array structure is described with structural parameters and controllable loading configurations. Based on the switching state of the parasitic elements, the impedance matrix is calculated and different radiation patterns are attained. In the simulation scenario, different testing platforms are studied to generate a number of pattern configurations with switched parasitic antennas.

3.1 Basics of Parasitic Arrays

Smart antenna systems have the ability to adapt according to the system requirements. They can adjust transmit and receive radiation patterns of the antennas based on the propagation environment. The use of parasitic elements in the smart antenna reconfigures the radiation patterns in order to improve the system performance. Par-

asitic antennas have been widely used in military and commercial purposes.

The Yagi-Uda [101] antenna is the classical example of using parasitic element for analog TV reception signal. As discussed in [87], the antenna array consists of one driven element with several parasitic elements in a linear array. The driven (active) element is connected to the RF port and has a resonant length. Multiple parasitic elements control the radiation pattern by changing the mutual coupling between the antenna elements. When the length of the parasitic element is slightly longer than the driven element it acts as a reflector. Therefore it radiates the beam towards the driven element. When the length of the parasitic element is slightly shorter than the driven element it acts as a director. It then radiates the beam away from the driven element. The length of the parasitic elements is mechanically fixed in the Yagi-Uda antenna structure.

In this thesis, MIMO-SPA follows the same mechanism of Yagi-Uda with few active elements connected to the transceiver and several parasitic elements arranged in a circular array fashion. As opposed to the Yagi-Uda antenna, the length of the parasitic elements can be varied by using terminated loads on the parasitic elements. The resonant length of the parasitic elements can be switched between different levels. Depending on the switching position, parasitic elements act as reflector and director states. Thus, loading the parasitic elements by electronic means enables the radiation patterns to be steered in different directions. This process is also known as electronic beam-steering.

The beam steering capability can be achieved through the use of optimal impedance load values that can be controlled adaptively or manually. Parasitic arrays loaded with adaptively tunable loads are known as ESPAR. Alternatively, the parasitic array loaded with switchable impedance loads are known as switchable parasitic antennas. In both techniques, optimal combination of load values steer the beam patterns in dif-

ferent directions. The difference between these two techniques is the type of circuitry used. The tunable loads in ESPAR antennas are usually reactive (inductive/capacitive) in nature, whereas in SPA the switchable loads are usually resistive in nature. The switching between the load values tunes the parasitic elements *in* and *out* of resonance and toggles the parasitic elements between reflector and director states respectively. The symmetry property of antenna arrays also plays a significant role in the design and optimization process. Some of the radiation patterns show similar pattern configurations owing to the symmetry property of the antennas. The symmetry property occurs in antenna arrays with an even number of parasitic elements. The number of radiation patterns depends on the number of parasitic elements and the load combinations terminated on the parasitic elements.

Most of the literature [110] [111] [112] has presented ESPAR and SPA antenna geometries, where the active element is placed in the center and parasitic elements are placed in a circle equidistant from the origin. By doing this, beam-steering can be achieved only in the azimuth plane. With more than one ring of parasitic elements the beam-steering can be achieved in both planes i.e. elevation and azimuth planes. In 1978, Harrington [96] introduced parasitic elements terminated with tunable impedance loads to obtain the radiation patterns. Later, Milne [113] replaced these tunable loads with switchable loads to direct the beam patterns in different directions.

3.1.1 ESPAR

The electronically steerable parasitic array radiator (ESPAR) is a smart antenna that reconfigures the radiation patterns electronically by changing the load values. The structure of these antennas consists of one active element situated at the center and surrounded with a number of parasitic elements. The active element is connected

to the RF port and the parasitic elements are terminated with the reactance loads. These reactance loads can be realized with varactor diodes [112] and the beam steering can be achieved by tuning these varactor diodes. A DC voltage supply is required for these varactor diodes. The capacitance value of these diodes can be changed by varying the voltage levels. This changes the distribution of currents on the antenna elements and tunes the radiation patterns of the ESPAR antennas [74].

In 2000, the ATR labs in Japan introduced an ESPAR antenna [110] [111] with (K+1) elements as shown in Figure 3.1. The active element is placed in the middle and connected to the transceiver. There is only one active element connected to the RF port and it requires only one RF chain. Six parasitic elements (K=6) are placed around the periphery of the active element. The parasitic elements are terminated with varactor diodes.

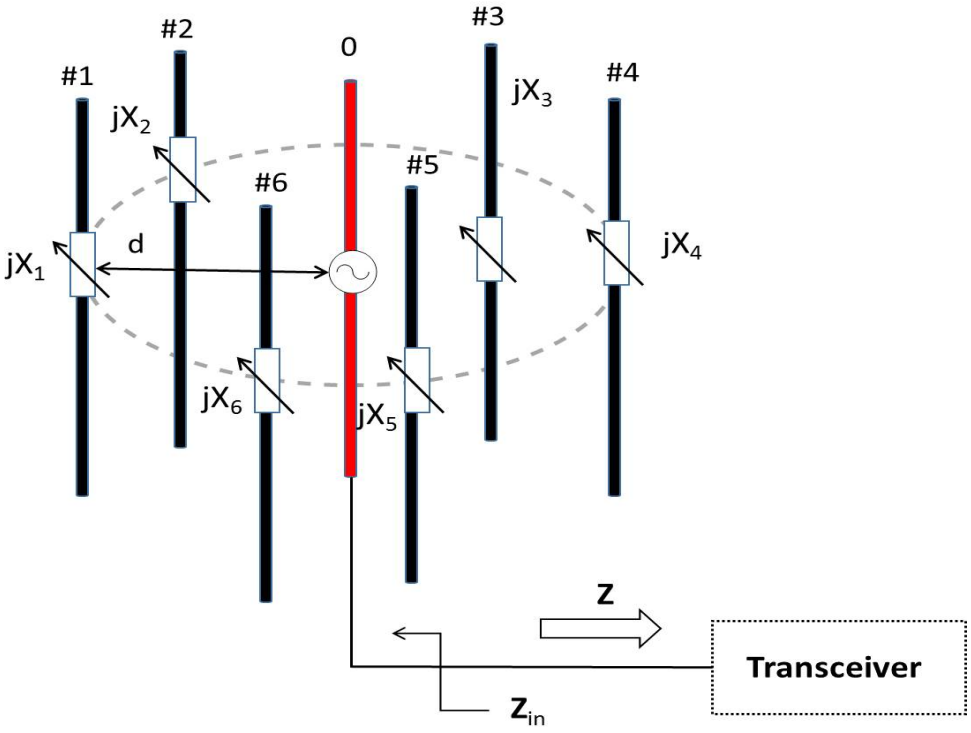

Figure 3.1: Structure example of (K+1)-element ESPAR.

By controlling the values of the varactor diodes, the mutual coupling varies between the active and parasitic elements. The configuration of the parasitic elements can be switched between director and reflector states. Thus, the radiation patterns can be exploited in different directions.

ESPAR antennas achieve high DoF for fully adaptive arrays with reactively controlled parasitic elements. They also provide high beam steering resolution but introduce delays during re-radiation in adaptive applications. These antenna designs require more hardware components to control the varactor diodes. Several DAC circuits are required to convert the digital microcontroller output to an analog voltage level.

3.1.2 Switched Parasitic Antennas

Switched parasitic antennas (SPA) are another option for reconfigurable antennas to provide a pre-defined fixed number of radiation patterns. As compared to ESPAR, SPA antennas are terminated with electronically switchable loads. The parasitic elements can be switched between reflector and director states through the use of RF switches. These switches can be toggled between two states which are open-circuited or short-circuited. Beam steering can be achieved in a fixed number of directions by switching the parasitic elements.

When the RF switch is in the *on* state it is short-circuited and corresponds to the parasitic element acting as a reflector. When the RF switch is in the *off* state it is open-circuited, with the corresponding parasitic element acting as a director. The possible number of directive patterns can be obtained from the available number of parasitic elements and the switchable states. The switching operation can be performed very rapidly by using RF switches like PIN diodes [74].

SPA offers several advantages including low-cost, space, low power requirements and

needing a smaller number of components compared to ESPAR antennas. It has some drawbacks such as poor elevation control, large beam-width, problems with DC switches and poor angle positioning precision.

3.2 N−Port Network Representation of Antenna Array

For modelling and analyzing purposes, the antenna array elements need to be represented by their electrical equivalent circuits. With the N-port network representation, appropriate parameters in terms of impedances (Z-parameters) and scattering (S-parameters) can be used to access the important characteristics of the antenna array elements. Figure 3.2 depicts the two-port network representation with Z-parameters.

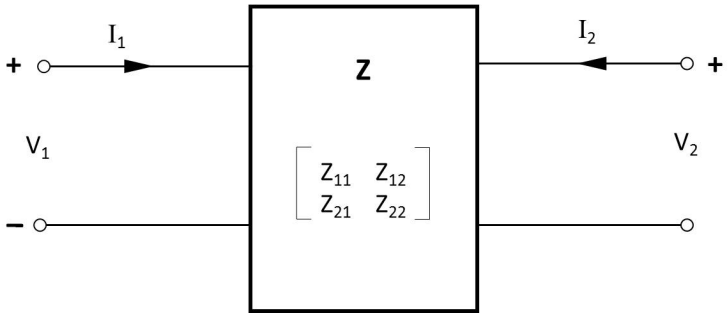

Figure 3.2: Two-Port Network.

In the design process of multiple antenna systems, diversity performance is also affected by others factors such as electromagnetic mutual coupling, the impedance matching network and the number of parasitic elements. The electromagnetic coupling effect can be measured in terms of the mutual impedance.

3.2.1 Port Theory

The electromagnetic mutual coupling effect can be analyzed with the port theory of the network. The network model of an antenna array can be represented by impedances connected to transmission lines. The antenna array elements can be represented with Z-parameters that show the relation between the voltage and current across the elements. As shown in Figure 3.2 the two-port network relationship between the voltage and current can be represented as:

$$\begin{bmatrix} V_1 \\ V_2 \end{bmatrix} = \begin{bmatrix} Z_{11} & Z_{12} \\ Z_{21} & Z_{22} \end{bmatrix} \begin{bmatrix} I_1 \\ I_2 \end{bmatrix} \tag{3.1}$$

where V_i and I_i are the voltage and current values of the ith port, and $Z_{11}, Z_{12}, Z_{21}, Z_{22}$ represents the impedance values. These values can be represented with impedance matrix $\mathbf{Z}$. The impedance parameters of the array antennas can be calculated as: self-impedance and mutual impedance. The self-impedance of array-element Z_{nn} can be calculated as the ratio of the voltage to the current at its terminals while the rest of the antenna terminals are open-circuited.

$$Z_{nn} = \left.\frac{V_n}{I_n}\right|_{I_m=0} \qquad n = 1, 2 \quad m = 1, 2 \quad n \neq m \tag{3.2}$$

The mutual-impedance of array-element Z_{mn} results from the electromagnetic coupling effect and can be calculated as the ratio of the voltage at one terminal to the current at the other terminal while the rest of the antenna terminals are open-circuited.

$$Z_{mn} = \left.\frac{V_m}{I_n}\right|_{I_m=0} \qquad n = 1, 2 \quad m = 1, 2 \quad n \neq m \tag{3.3}$$

This two-port network can be extended for arrays of multiple antennas by connecting impedance loads. The system performance can be realized by the Z-parameters across the array elements. Calculation of the impedance matrix ($\mathbf{Z}$) is important in the pres-

ence of parasitic elements. In the case of a multiple antenna system, the impedance matrix $\mathbf{Z}$ of a coupled array can be described as follows:

$$\mathbf{Z} = \begin{bmatrix} Z_{11} & Z_{12} & \dots & Z_{1M} \\ Z_{21} & Z_{22} & \dots & Z_{2M} \\ \vdots & \vdots & \ddots & \vdots \\ Z_{M1} & Z_{M2} & \dots & Z_{MM} \end{bmatrix} \tag{3.4}$$

where Z_{ii} is the self-impedance of the ith antenna for $(i = 1, 2, ..., M)$ and Z_{ij} represents the mutual impedance between the ith and jth antenna elements for $(i \neq j, and\ i, j = 1, 2, ..., M)$.

The self-impedance and the mutual-impedances of the antenna elements can be calculated in a number of ways such as using the classical induced electromotive force (EMF) method [87] or with the Method of Moments [86]. Calculation of the impedance matrix ($\mathbf{Z}$) in this thesis uses the EMF method [87]for the several array structures.

3.2.2 Antenna Modelling

The antenna equivalent circuit with two antenna elements is shown in Figure 3.3. The voltage sources across the antenna elements are represented as $\mathbf{V_{S1}}$ and $\mathbf{V_{S2}}$. The self-impedances of antenna 1 and antenna 2 are $\mathbf{Z_{11}}$ and $\mathbf{Z_{22}}$ respectively. The source impedance is denoted as Z_0. With the electromagnetic mutual coupling effect, the mutual impedances are represented with Z_{12} and Z_{21}.

According to N-port network theory, two-port antenna elements can be represented in voltage and current forms as:

$$\mathbf{V_{S}}_i = (\mathbf{Z_A} + \mathbf{Z_S})\mathbf{I} \tag{3.5}$$

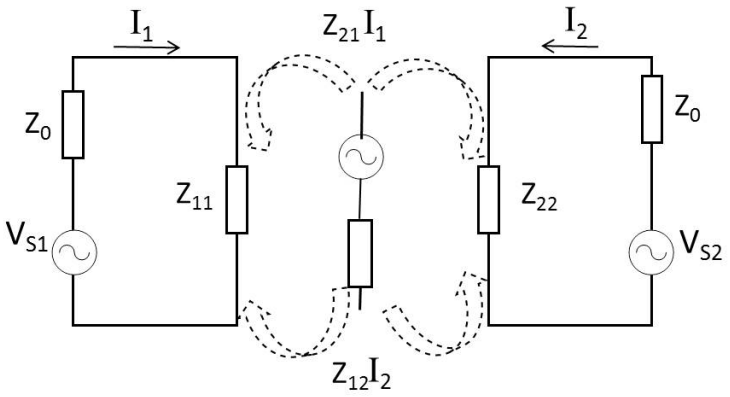

Figure 3.3: Antenna equivalent circuit for two-antenna elements.

where $\mathbf{V_{S}}_i$ represents the source voltage of ith antenna element. $\mathbf{Z_A}$ is the antenna impedance matrix and $\mathbf{Z_S}$ is the source impedance matrix. $\mathbf{I}$ is a vector containing the respective currents across the antenna elements.

The elements of the antenna impedance matrix $\mathbf{Z_A}$ are self-impedances such as, Z_{11} and Z_{22} and mutual-impedances Z_{12} and Z_{21}. The source impedance matrix $\mathbf{Z_S}$ represents the source impedances of two antenna elements in matrix form as well.

$$\mathbf{Z_A} = \begin{bmatrix} Z_{11} + Z_{12} & Z_{12} \\ Z_{21} & Z_{22} + Z_{21} \end{bmatrix} \tag{3.6}$$

$$\mathbf{Z_S} = \begin{bmatrix} Z_0 & 0 \\ 0 & Z_0 \end{bmatrix} \tag{3.7}$$

3.3 Mutual Coupling

The antenna elements placed close to each other interact electromagnetically with each other. This interaction is known as the electromagnetic mutual coupling effect. The mutual coupling between the antenna elements affects the antenna characteristics

in terms of antenna radiation patterns, terminal impedances and array gain [114]. The interaction between the antenna elements alters the current distribution on the individual antenna elements and thus, modifies the radiation patterns of the antenna array.

The mutual coupling effect in MIMO-SPA can be discussed in two ways: mutual coupling between active elements only and mutual coupling between active and parasitic elements.

3.3.1 Mutual Coupling between Active Elements

The mutual coupling effect between two active elements can be examined with two parallel dipole elements placed close to each other. This structure can be represented with the two-port network shown in Figure 3.4, where voltages V_1 and V_2 can be seen from the two end terminals with the currents I_1 and I_2 respectively.

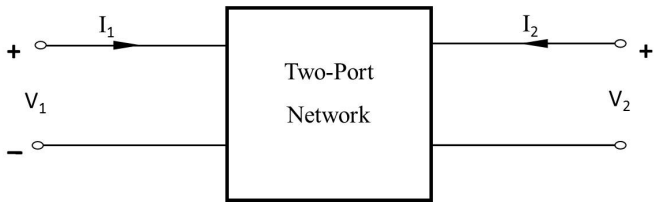

Figure 3.4: Two-Port network model for two active elements.

From two-port network theory, the relationship between the voltages and currents can be represented in the equation form [86] [115]:

$$\begin{aligned} V_1 &= Z_{11}I_1 + Z_{12}I_2 \\ V_2 &= Z_{21}I_1 + Z_{22}I_2 \end{aligned} \tag{3.8}$$

where Z_{nn} and Z_{mn} represents the self-impedance and the mutual impedance of the

antenna elements. The self-impedance Z_{nn} is defined as the ratio of voltage at terminal n due to the current on its own terminal. The mutual-impedance Z_{mn} is the ratio of voltage at terminal m with the current induced by the neighboring terminal n owing to the mutual coupling effect. Antennas follow the reciprocity principle thus, $Z_{mn} = Z_{nm}$.

These two-port network theory equations (3.8) can be extended to an N-port array [86] [115]:

$$\begin{aligned} V_1 &= Z_{11}I_1 + Z_{12}I_2 + \cdots + Z_{1N}I_N \\ V_2 &= Z_{21}I_1 + Z_{22}I_2 + \cdots + Z_{2N}I_N \\ \vdots &= \\ V_N &= Z_{N1}I_1 + Z_{N2}I_2 + \cdots + Z_{NN}I_N \end{aligned} \tag{3.9}$$

These equations can be rewritten in matrix form:

$$\begin{bmatrix} V_1 \\ V_2 \\ \vdots \\ V_N \end{bmatrix} = \begin{bmatrix} Z_{11} & Z_{12} & \dots & Z_{1N} \\ Z_{21} & Z_{22} & \dots & Z_{2N} \\ \vdots & \vdots & \ddots & \vdots \\ Z_{N1} & Z_{N2} & \dots & Z_{NN} \end{bmatrix} \begin{bmatrix} I_1 \\ I_2 \\ \vdots \\ I_N \end{bmatrix} \tag{3.10}$$

or

$$\mathbf{V} = \mathbf{ZI} \tag{3.11}$$

Impedance matrix $\mathbf{Z}$ shows the mutual coupling effect between the antenna terminals. The current distribution on the antenna elements can be calculated with knowledge of the impedance matrix. The current vector $\mathbf{I}$ contains all the current distribution information in the antenna array. If the mutual coupling effect is ignored in the network, the impedance matrix $\mathbf{Z}$ acts as the identity matrix. Then the input currents will be proportional to the driving voltages $\mathbf{V}$. With the mutual coupling effect, the current distribution can be calculated from the solution [87]:

$$\mathbf{I} = \mathbf{Z}^{-1}\mathbf{V} \tag{3.12}$$

The current information leads to the re-distribution of the current on the antenna elements and alters the radiation properties of the antenna array. In this thesis, the impedance matrix $\mathbf{Z}$ is calculated with the induced EMF method as discussed in section 2.8.

3.3.2 Mutual Coupling between Active and Loaded Parasitic Elements

Since the introduction of Yagi-Uda antennas, the use of parasitic elements is common in directive antennas that provide high gain. Based on the fundamental principle of electromagnetic mutual coupling, the directivity property of the antennas can be exploited. The use of parasitic elements offers advantages in terms of bandwidth and gain. These elements also combat the negative effect of mutual coupling by decorrelating the antenna signals. Thus, parasitic elements convert the curse of the mutual coupling effect to a benefit for antenna arrays. The characteristics of the antenna array in terms of the radiation pattern can be modified by altering the properties of the parasitic elements.

The mutual coupling between antenna elements can be altered by changing these three factor: length, width and the relative positioning between the antenna elements. In classical Yagi-Uda antennas, the length of the antenna elements is mechanically fixed. The length of the parasitic elements can be changed electronically by using RF switches. The terminated loads on the parasitic elements alter the impedance load values with these switches. The electromagnetic interaction between the active and parasitic elements can be affected by the length variation and the relative distance between the antenna elements. It has been mentioned in [116] [117] that the mutual

coupling between two printed antennas is reduced around 40 dB by using printed parasitic elements.

The effect of mutual coupling between antenna elements is explained with the simple structure of one active dipole *(ad)* element and one parasitic dipole *(pd)* element as shown in Figure.3.5. The active dipole has a length of (l_{ad}), the parasitic dipole length is (l_{pd}), and the distance between the two dipoles is represented as (d_{ap}).

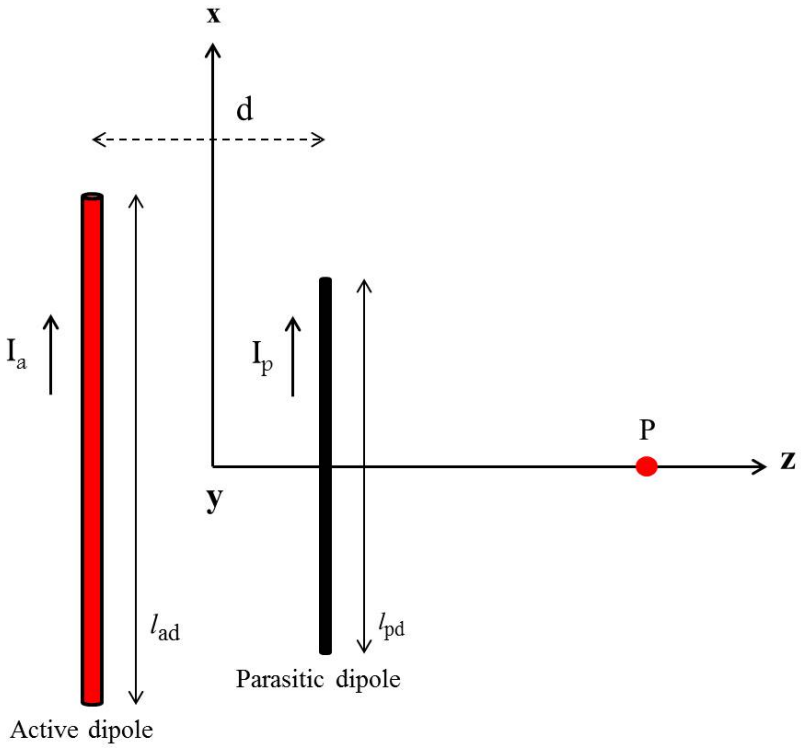

Figure 3.5: Active dipole and parasitic dipole.

- when the length of the parasitic dipole (l_{pd}) is slightly longer than the length of active dipole (l_{ad}), it is known as a reflector. The reflector with a length longer than the resonant length makes the dipole inductive in nature. Hence, the current lags the voltage and this causes the RF antenna to radiate more power away from the parasitic element.

- when the parasitic dipole (l_{pd}) has the same length as the active dipole (l_{ad}), the radiation pattern shape is almost symmetrical.

- when the parasitic dipole (l_{pd}) is slightly shorter than the active dipole (l_{ad}), it is known as a director. The director with a length shorter than resonant length makes the dipole capacitive in nature. Hence, the current leads the voltage and this causes the RF antenna to radiate more power in the direction of the parasitic element.

The total field produced by the active dipole and the parasitic dipole at point P, as shown in Figure 3.5 can be represented with Thevenin's-equivalent circuit equations as:

$$\begin{aligned} V_{1\mathrm{a}}^{\mathrm{ad}} &= Z_{11}^{\mathrm{ad}} I_a + Z_{12}^{\mathrm{pd}} I_p \\ 0 &= Z_{21}^{\mathrm{pd}} I_a + Z_{22}^{\mathrm{pd}} I_p \end{aligned} \tag{3.13}$$

where

I_a represents the current through the active dipole,

I_p represents the induced current of the parasitic element by the active dipole,

$V_{1\mathrm{a}}^{\mathrm{ad}}$ is the voltage at the active dipole that is connected with the voltage source and $V_{1\mathrm{p}}^{\mathrm{pd}}$ is the voltage across the parasitic element, with $V_{1\mathrm{p}}^{\mathrm{pd}} = 0$ because it is not connected to any voltage source. The induced current at the parasitic dipole can be obtained as [118]:

$$\begin{aligned} I_p &= \frac{-Z_{21}^{\mathrm{pd}}}{Z_{22}^{\mathrm{pd}}} I_a \\ Z_{\mathrm{in}}^{\mathrm{ad}} &= Z_{11}^{\mathrm{ad}} + Z_{22}^{\mathrm{pd}} \frac{I_p}{I_a} \end{aligned} \tag{3.14}$$

The voltage across the parasitic dipole element due to the induced current of active element can be defined as:

$$V_{1\mathrm{p}}^{\mathrm{pd}} = -Z_{L2} I_p \tag{3.15}$$

To examine the network equations, consider the Thevenin's equivalent circuit where

one active dipole is connected to the ideal generator then $Z_{11}^{\mathrm{ad}} = 0$ and $V_1 = V_{1\mathrm{a}}^{\mathrm{ad}}$. The parasitic element is terminated with some load $Z_{22}^{\mathrm{pd}} = Z_{L2}$. The network equations of (3.13) become:

$$\begin{aligned} V_{1\mathrm{a}}^{\mathrm{ad}} &= Z_{11}^{\mathrm{ad}} I_a + Z_{12}^{\mathrm{pd}} I_p \\ -Z_{L2} I_p &= Z_{21}^{\mathrm{pd}} I_a + Z_{22} I_p \\ \textit{or} & \\ V_{1\mathrm{a}}^{\mathrm{ad}} &= Z_{11}^{\mathrm{ad}} I_a + Z_{12}^{\mathrm{pd}} I_p \\ 0 &= Z_{21}^{\mathrm{pd}} I_a + (Z_{22}^{\mathrm{pd}} + Z_{L2}) I_p \end{aligned} \tag{3.16}$$

However, the current convention in (3.16) can be extended to an N-port system with all parasitic port voltages replaced by the negative product of their current and load impedance as in (3.15). The antenna array with only a single active element and N parasitic elements in (3.10) becomes:

$$\begin{bmatrix} V_{1\mathrm{a}}^{\mathrm{ad}} \\ V_{1\mathrm{p}}^{\mathrm{pd}} \\ V_{2\mathrm{p}}^{\mathrm{pd}} \\ \vdots \\ V_{\mathrm{Np}}^{\mathrm{pd}} \end{bmatrix} = \begin{bmatrix} Z_{11}^{\mathrm{ad}} & Z_{12}^{\mathrm{pd}} & \dots & Z_{1\mathrm{N}}^{\mathrm{pd}} \\ Z_{21}^{\mathrm{pd}} & (Z_{22}^{\mathrm{pd}} + Z_{L2}) & \dots & Z_{1\mathrm{N}}^{\mathrm{pd}} \\ Z_{31}^{\mathrm{pd}} & (Z_{33}^{\mathrm{pd}} + Z_{L3}) & \dots & Z_{2\mathrm{N}}^{\mathrm{pd}} \\ \vdots & \vdots & \ddots & \vdots \\ Z_{\mathrm{N1}}^{\mathrm{pd}} & Z_{\mathrm{N2}}^{\mathrm{pd}} & \dots & (Z_{\mathrm{NN}}^{\mathrm{pd}} + Z_{LN}) \end{bmatrix} \begin{bmatrix} I_{1a} \\ I_{1p} \\ I_{2p} \\ \vdots \\ I_{Np} \end{bmatrix} \tag{3.17}$$

or simply:

$$\mathbf{V} = [\mathbf{Z} + \mathbf{Z}_L]\mathbf{I} \tag{3.18}$$

where the diagonal matrix:

$$\mathbf{Z}_L = \begin{bmatrix} 0 & 0 & \dots & 0 \\ 0 & Z_{L2} & \dots & 0 \\ \vdots & \vdots & \ddots & \vdots \\ 0 & 0 & \dots & Z_{LN} \end{bmatrix} \tag{3.19}$$

contains the load impedances terminated at each parasitic element.

Equation (3.18) has been well analyzed in parasitic arrays by Harrington [96], Mautz and Harrington [119], and later by Dinger [120]. Any change in the loading configuration of the parasitic elements only affect the load impedance matrix. Hence, $\mathbf{Z}_L$ can be calculated independently without making any amendments in the antenna array design. According to (3.17), the values of self-impedances Z_{11}^{ad} and mutual-impedances $Z_{\mathrm{NN}}^{\mathrm{pd}}$ need to be calculated by considering the mutual coupling effect.

As already discussed in chapter 2 (section 2.8) of this thesis, the values of mutual impedance between the active and parasitic elements and self-impedance of an antenna can be calculated by using (2.28) and (2.31) and respectively. The MATLAB simulation code function 'impedmat' is used for solving these impedances of the parasitic arrays is presented in the Appendix-B.

3.4 SPA System Description

In this thesis, a low-cost beam steering SPA is used to consider the radiation patterns in the azimuth plane with an operating frequency of 2.4 GHz in the industrial, scientific, and medical radio (ISM) band. The parasitic elements are terminated with load impedance with the use of ideal RF switches. The switching between *on/off* states, results in fixed radiation patterns in different directions.

When the RF switch is in the *on* state, the parasitic element is short-circuited and acts as a reflector with an assumed theoretical value of the load impedance $\approx 10000\,\Omega$. When the RF switch is in the *off* state, parasitic element is open-circuited and act as director and assumed with theoretical value of the impedance load $\approx 0\Omega$. As the RF switches are assumed ideal, no insertion losses are considered in the calculation of the impedance matrices.

The number of radiation patterns can be determined by the number of parasitic elements and the switching load configurations of the parasitic elements. The performance and functionality of using SPA depends on the basic principle of electromagnetic mutual coupling. The design procedure of MIMO-SPA requires the structural parameters of the antenna elements and the load configuration parameters terminated on the parasitic elements [121]. The structural parameters of the antenna elements include :

- Total number of elements (T=A+P), where T is the total number of the elements in the antenna array, A is the number of active elements and P is the number of parasitic elements.
- The length of the active elements (l_{ad});
- The length of the parasitic elements (l_{pd});
- The width of the elements, (W); and
- The distance of the parasitic elements from the active elements, (d).

The load configuration parameters can be set as reactive loads or resistive loads. The reactive loads with varactor diodes provide the tuning between the loads over an infinite number of levels. The resistive loads can provide switching in fixed or pre-defined levels.

In this thesis, the parasitic elements are terminated with impedance loads. The length of the parasitic elements is the same in order to achieve omni-directional patterns [122]. An even number of parasitic elements is used to attain the antenna symmetry property [121] [123]. However, the structural and load configurations can be optimized for the better system performance. In the literature, most researchers have used optimization algorithms and numerical analysis for the optimization purpose [124]. In this work,

the structural parameters are assumed based on the array theory and the geometry used for the array design is presented as by Varlamos et al. [125].

3.4.1 Beam Steering of SPA

In the MIMO-SPA antenna geometry, there are two active elements encircled with P parasitic elements. The beam steering property of SPA depends on the number of parasitic elements. The beam steering property can be exploited by switching the parasitic elements with RF switches. Different pattern configurations can be obtained by open-circuiting one parasitic element at a time and leaving the other (P-1) elements short-circuited. The permutation of the load configurations of the parasitic elements gives the total number of radiation patterns. The number of possible angular directions into which the main beam can be directed can be calculated from the number of parasitic elements. The beam steering resolution in the azimuth plane can be defined as [121]:

$$Resolution = \frac{360^o}{P}. \tag{3.20}$$

Thus, the beam resolution of SPA can be defined as the number of different directions into which the main beam can be directed with maximum gain. The resolution defines the directivity and the angles of the radiation patterns that direct the main beam. More resolution can be achieved with reactive loads, which have the capability to steer the narrow-beam patterns in several directions.

By increasing the number of parasitic elements, the beam steering capability can be increased. But increasing the number of parasitic elements gives beam resolution with smaller angles and radiation patterns which are more correlated to each other. It will not increase the cost and hardware complexity of the system but will clutter the space.

3.4.2 Loading Configurations

The number of radiation patterns not only depends on the number of parasitic elements but also on the switching capability of the load configurations. In this thesis, with the use of RF switches, only two switching states *on/off* are possible with the terminated load impedances.

$$Total\ number\ of\ pattern\ configurations = (L_s)^P \tag{3.21}$$

where P is the total number of the parasitic elements used in the single ring circular SPA antenna array and L_s denotes possible values of the load impedances terminating the parasitic elements.

All the loading configurations will provide different pattern configurations depending on the loading values of the parasitic elements. These radiation patterns can be selected with some objective function in terms of maximum gain or minimum insertion loss.

3.5 SPA Performance Evaluation

SPA antennas with a smaller number of parasitic elements provides a limited number of directions into which the main beam can be direct with maximum gain. The number of directions can be increased with the switching configuration capability of the loading configurations.

In the SPA evaluation performance, the radiation elements operate at a frequency of 2.4 GHz. The specification of the antenna elements are based on the antenna array theory of half-wave dipoles, The length of the parasitic elements is changed with RF switches to act as reflectors and directors as in the Yagi-Uda antenna.

3.5.1 Simulation Procedure

The beam-steering capability of SPA has been simulated with the MATLAB. Two ideal RF switches are used with the *on/off* states i.e.($L_s = 2$). In order to see the mutual coupling effect on all the elements, the impedance matrix needs to be calculated first. A change in the number of parasitic elements and the loading configurations results in a change only in the loading matrix. The switching between the controllable impedance loads changes the distribution of currents and radiation patterns of the antenna array.

3.5.2 Testing Platforms

The case studies are as follows:

- Case-I. Loading configurations for the 4-Elements SPA geometry;
- Case-II. Loading configurations for the 6-Elements SPA geometry; and
- Case-III. Loading configurations for the 8-Elements SPA geometry.

3.5.2.1 Case-I. Loading configurations for the 4-Elements SPA antenna geometry

The MIMO-SPA antenna geometry with total four elements consists of two active elements and two parasitic elements as shown in Figure 3.6. The total loading configurations with two switching levels *(on/off)* gives four ($2^2 = 4$) beam pattern configurations.

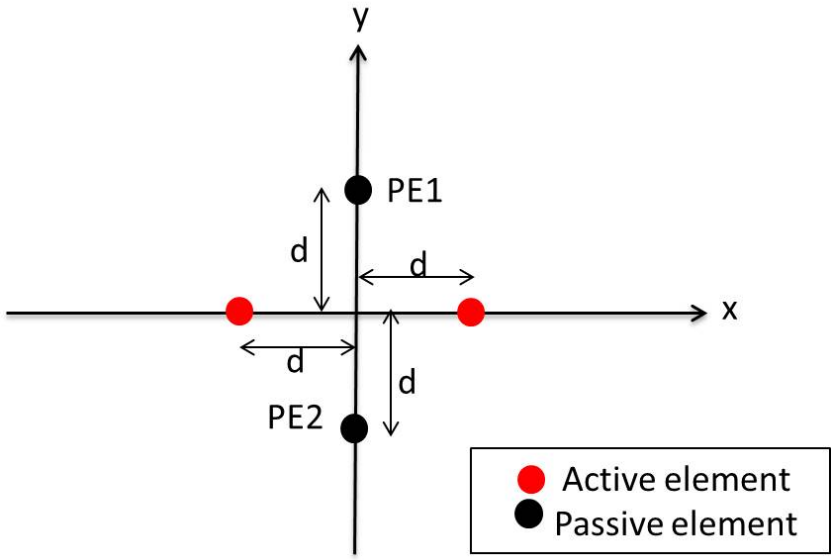

Figure 3.6: Structure example of two active elements and two parasitic elements.

As shown in Table 3.1, there are total four pattern configurations denoted as (P1, P2, P3, P4). The switching state of two parasitic elements (PE1, PE2) is represented as open-circuited and short-circuited. When the RF switch is in the *on*-state, the corresponding parasitic element is short-circuited and the load state is denoted by SC. Whereas, when the RF switch is in the *off*-state, the corresponding parasitic element is open-circuited or isolated from the ground plane and the load state is denoted by OC. The theoretical impedance load values corresponding to the *off*-switch state is $\approx 10000\,\Omega$ and is represented in binary form as *State=0*. The load value corresponding to *on*-switch state is $\approx 0\,\Omega$ and is represented in binary form as *State=1*.

Table 3.1: Pattern configurations using two parasitic elements

No.	**PE1**	**PE2**	**Pattern Configurations**
P1	OC	OC	States=00
P2	OC	SC	States=01
P3	SC	OC	States=10
P4	SC	SC	States=11

Figure 3.7 shows four different radiation pattern configurations with two active elements and two parasitic elements. The first beam pattern configuration P1, when both switches of the Parasitic Elements (PE) are in the *off* state shows *(States=00)*, in second beam pattern configuration P2 with PE1 in *off* state and PE2 in the *on* state shows*(States=01)*, in the third beam pattern configuration P3, with PE1 in *on* state and PE2 in the *off* state shows *(States=10)*, and in the last beam configuration P4, with both PE1 and PE2 are in *off* states shows *(States=11)*.

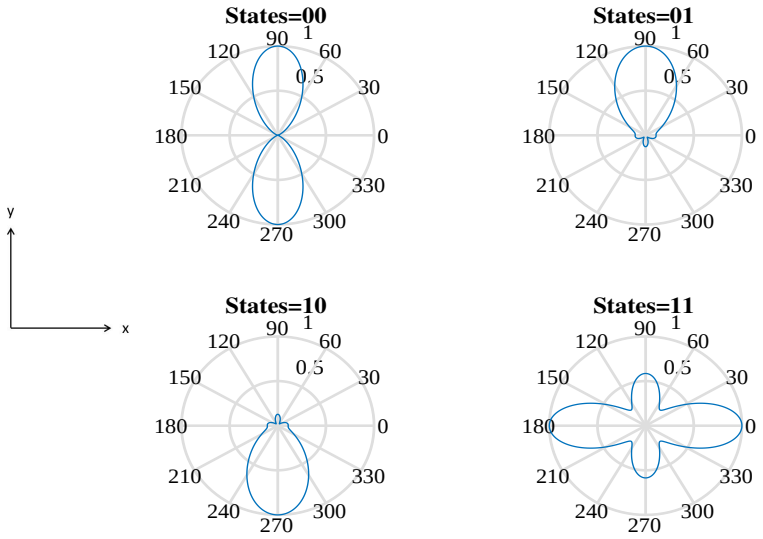

Figure 3.7: Radiation patterns with two active elements and two parasitic elements.

Table 3.2 shows the antenna parameters by using SPA configurations. Due to the antenna symmetry property some of the parameters show same results.

Table 3.2: Antenna parameters with corresponding pattern configurations

Pattern No.	**Gain** (dBi)	**Z_{in}** (Ω)	**Return Loss** (dB)	**Reflection Coefficient** (Γ)
P1	2.6150	87.0223 +73.2088i	12.7705	0.4323 + 0.3033i
P2	2.2754	96.5057 +48.7038i	16.5941	0.3854 + 0.2043i
P3	2.2754	96.5057 +48.7038i	16.5941	0.3854 + 0.2043i
P4	2.0525	85.9698 +24.0628i	23.2049	0.2869 + 0.1262i

3.5.2.2 Case-II. Loading configurations for the 6-Elements SPA antenna geometry

The SPA antenna geometry with total six elements consists of two active elements and four parasitic elements as shown in Figure 3.8. With four parasitic elements (PE1, PE2, PE3, PE4) having two switching states *(on/off)* gives sixteen ($2^4 = 16$) beam pattern configurations (P1, P2, ..., P16).

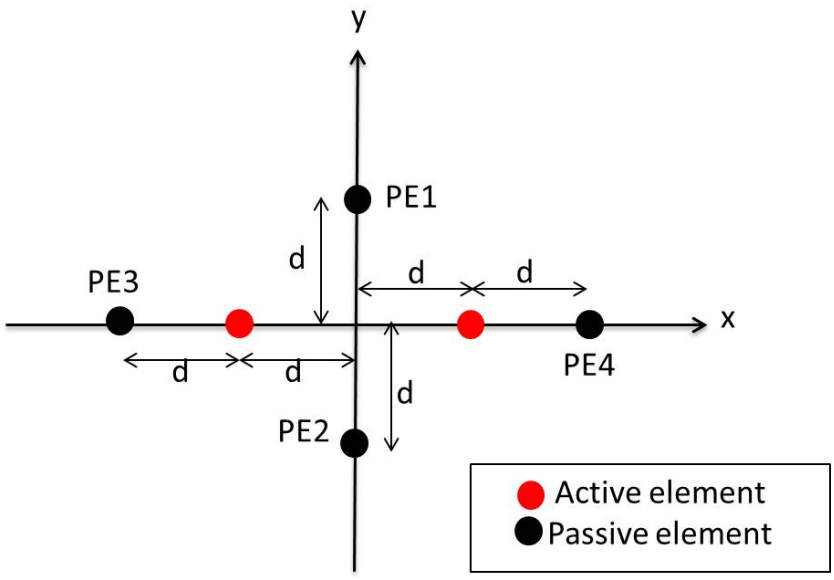

Figure 3.8: Structure example of two active elements and four parasitic elements.

As shown in Table 3.3, first beam pattern *(States=0000)*, when all the switches on PEs are in the *off* state and so on. With the SPA antennas symmetry property, some of the switching combinations result in similar antenna radiation patterns [121].

Table 3.3: Pattern configurations using four parasitic elements

No.	**PE1**	**PE2**	**PE3**	**PE4**	**Pattern Configurations**
P1	OC	OC	OC	OC	States=0000
P2	OC	OC	OC	SC	States=0001
P3	OC	OC	SC	OC	States=0010
P4	OC	OC	SC	SC	States=0011
P5	OC	SC	OC	OC	States=0100
P6	OC	SC	OC	SC	States=0101
P7	OC	SC	SC	OC	States=0110
P8	OC	SC	SC	SC	States=0111
P9	SC	OC	OC	OC	States=1000
P10	SC	OC	OC	SC	States=1001
P11	SC	OC	SC	OC	States=1010
P12	SC	OC	SC	SC	States=1011
P13	SC	SC	OC	OC	States=1100
P14	SC	SC	OC	SC	States=1101
P15	SC	SC	SC	OC	States=1110
P16	SC	SC	SC	SC	States=1111

Figure 3.9 shows sixteen different radiation pattern configurations with two active elements and four parasitic elements.

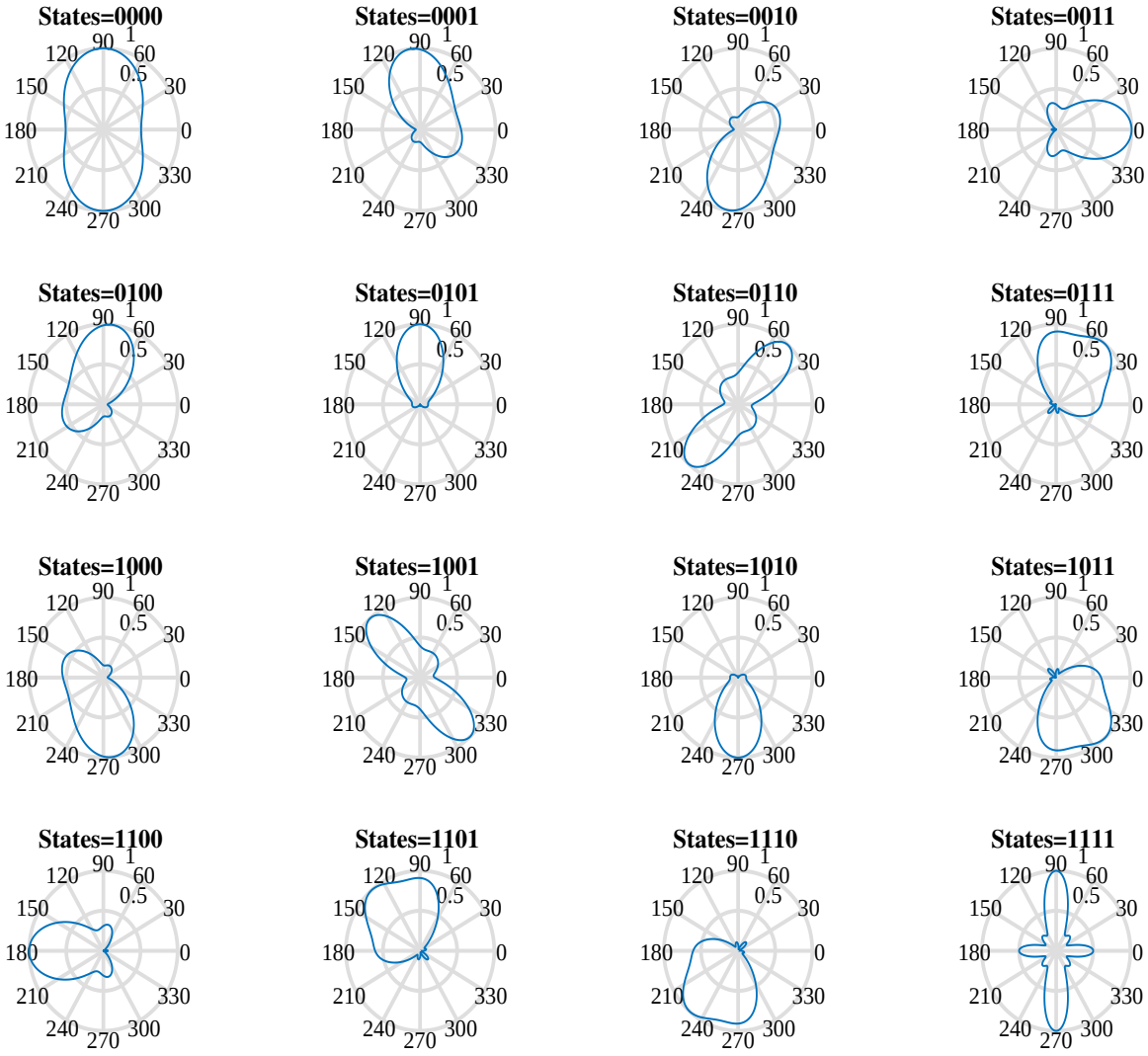

Figure 3.9: Radiation patterns with two active elements and four parasitic elements.

Table 3.4 shows the antenna parameters by using SPA configurations. Due to the antenna symmetry property some of the parameters show same results.

Table 3.4: Antenna parameters with corresponding pattern configurations

Pattern No.	**Gain** (dBi)	**Z_{in}** (Ω)	**Return Loss** (dB)	**Reflection Coefficient** (Γ)
P1	2.6241	0.9151 + 0.5786i	15.2801	0.3946 + 0.2476i
P2	2.1671	0.8952 + 0.5653i	15.6103	0.3843 + 0.2494i
P3	2.1671	0.8952 + 0.5653i	15.6103	0.3843 + 0.2494i
P4	2.2882	0.8691 + 0.5491i	16.0361	0.3708 + 0.2523i
P5	2.1671	0.9500 + 0.6273i	14.3214	0.4191 + 0.2513i
P6	2.6842	0.9278 + 0.6096i	14.6923	0.4076 + 0.2529i
P7	2.7476	0.9306 + 0.6086i	14.6988	0.4081 + 0.2518i
P8	2.6280	0.9017 + 0.5865i	15.1917	0.3929 + 0.2540i
P9	2.1671	0.9500 + 0.6273i	14.3214	0.4191 + 0.2513i
P10	2.7476	0.9306 + 0.6086i	14.6988	0.4081 + 0.2518i
P11	2.6842	0.9278 + 0.6096i	14.6923	0.4076 + 0.2529i
P12	2.6280	0.9017 + 0.5865i	15.1917	0.3929 + 0.2540i
P13	2.2882	1.0027 + 0.7022i	13.0538	0.4538 + 0.2552i
P14	2.6280	0.9801 + 0.6771i	13.4685	0.4413 + 0.2556i
P15	2.6280	0.9801 + 0.6771i	13.4685	0.4413 + 0.2556i
P16	2.5164	0.9503 + 0.6453i	14.0349	0.4244 + 0.2561i

3.5.2.3 Case-III. Loading configurations for the 8-Elements SPA antenna geometry

In SPA antenna geometry with a total of eight elements, there are four active elements and four parasitic elements as shown in Figure 3.10. The total load configurations with two switching levels *(on/off)* gives four ($2^4 = 16$) beam pattern configurations.

Figure 3.11 shows the sixteen different beam configurations with four active elements surrounded by four parasitic elements. There are four parasitic elements, the same as shown in Table 3.3, with two switching levels *(on/off)*, giving sixteen ($2^4 = 16$) beam pattern configurations. Due to the SPA antenna's symmetry property, some of the combinations result in similar antenna radiation patterns [121].

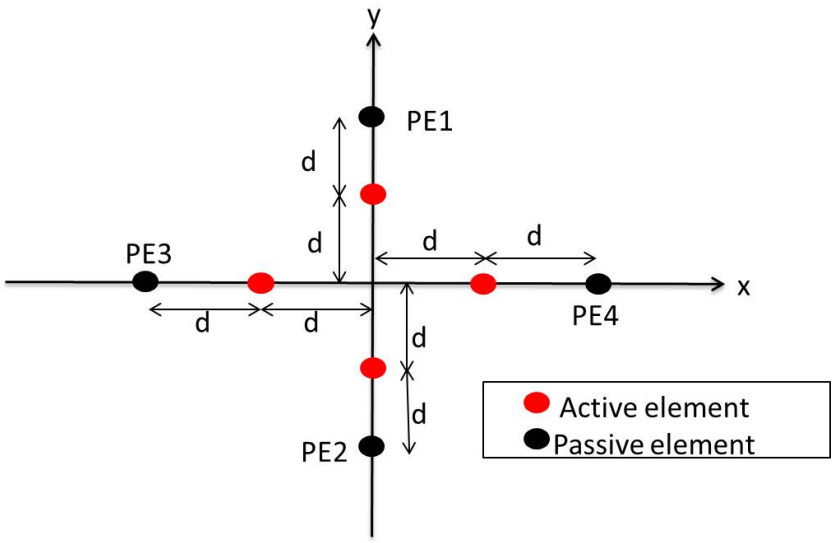

Figure 3.10: Structure example of four active elements and four parasitic elements.

Table 3.5 shows the antenna parameters by using SPA configurations. Due to the antenna symmetry property some of the parameters show same results.

Table 3.5: Antenna parameters with corresponding pattern configurations

Pattern No.	**Gain** (dBi)	**Z_{in}** (Ω)	**Return Loss** (dB)	**Reflection Coefficient** (Γ)
P1	2.9565	2.1303 + 0.7381i	8.4599	0.6476 + 0.0989i
P2	3.1229	0.9971 + 0.8081i	11.6796	0.4827 + 0.2792i
P3	3.1229	0.9971 + 0.8081i	11.6796	0.4827 + 0.2792i
P4	2.9137	0.6956 + 0.9448i	9.1410	0.4851 + 0.4069i
P5	1.7264	1.0529 + 0.4764i	16.0015	0.4114 + 0.1806i
P6	1.5181	0.8622 + 0.5944i	15.1705	0.3833 + 0.2691i
P7	1.5181	0.8622 + 0.5944i	15.1705	0.3833 + 0.2691i
P8	1.4798	0.8062 + 0.7541i	12.3378	0.4258 + 0.3315i
P9	1.7264	0.7216 + 1.1079i	7.5636	0.5508 + 0.4074i
P10	1.5181	0.6566 + 0.9106i	9.3152	0.4662 + 0.4202i
P11	1.5181	0.6566 + 0.9106i	9.3152	0.4662 + 0.4202i
P12	1.4798	0.5341 + 0.8758i	8.7153	0.4369 + 0.4769i
P13	2.5668	0.6868 + 0.9541i	8.9744	0.4882 + 0.4114i
P14	2.7955	0.6734 + 0.8418i	10.3790	0.4374 + 0.4036i
P15	2.7955	0.6734 + 0.8418i	10.3790	0.4374 + 0.4036i
P16	2.8682	0.5917 + 0.8234i	10.0206	0.4162 + 0.4404i

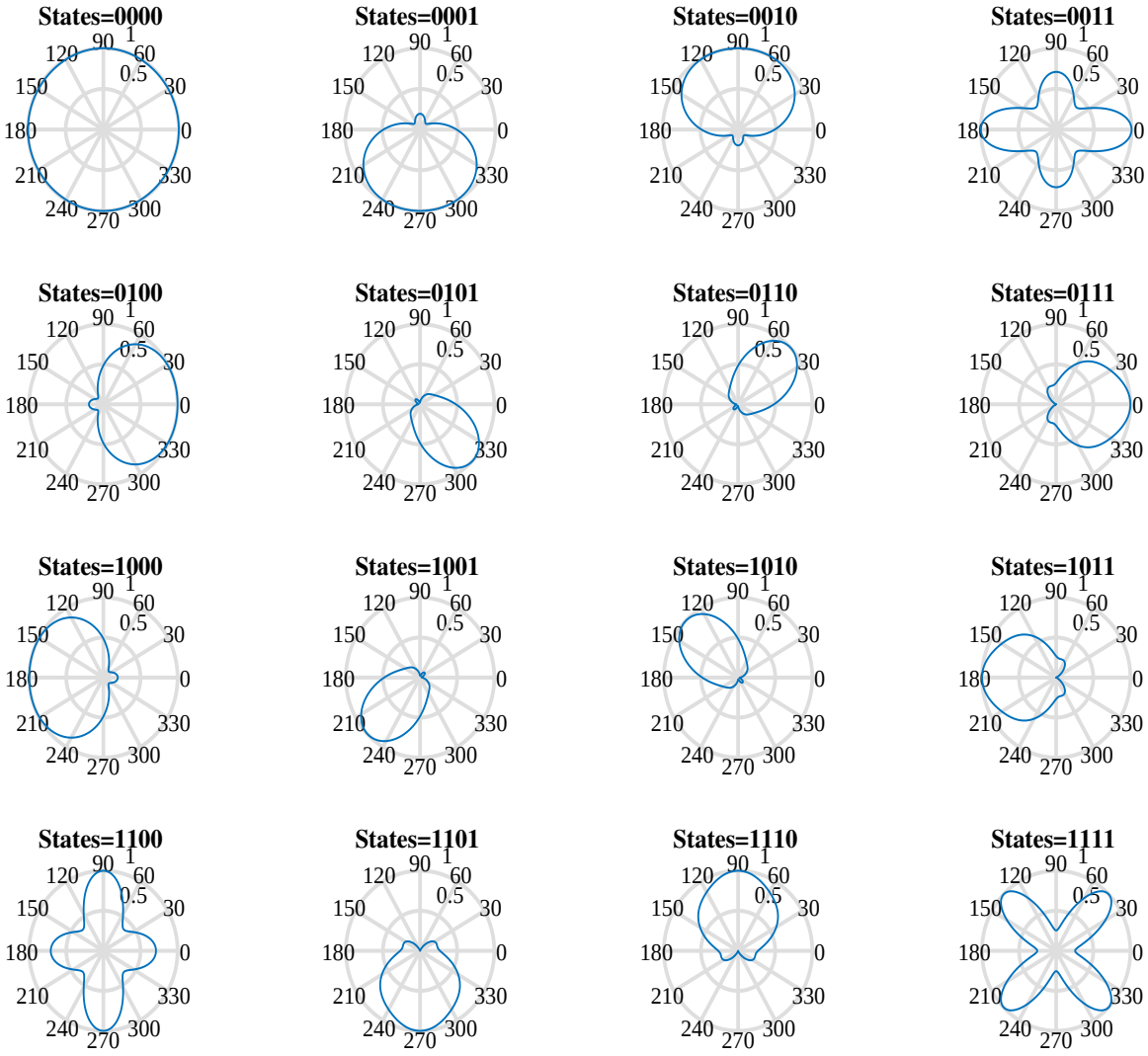

Figure 3.11: Radiation patterns with four active elements and four parasitic elements.

3.6 Conclusion

This chapter has presented a low-cost beam-steering antenna based on parasitic elements that can steer the beam pattern into a fixed number of directions. The pattern diversity property is exploited with the use of parasitic elements. The antenna elements have been analyzed with N-port network theory. The mutual coupling effect forms the foundation of the operation between the antenna elements and is repre-

sented with the calculation of impedance matrices. The impedance matrices provide the current distribution on each antenna element. The current redistribution alters the radiation pattern of the antenna array. Different radiation pattern configuration are obtained by changing the structural geometry of SPA and the loading configurations of the parasitic elements.

Chapter 4

MIMO Channel Capacity Analysis using Switched Parasitic Antennas

In this chapter, the main consideration is to achieve spatial multiplexing gain in the MIMO system using parasitic elements at the receiver side, where size, cost, power and complexity are the primary constraints. The design is basically intended to exploit pattern diversity by using the parasitic elements. It consists of few active elements coupled to set of parasitic elements terminated with impedance loads. By switching the impedance loads, the radiation patterns can be configured into different angular positions. It gives the flexibility to the receiver to sense information from various portions of the space. The influence of the covariance matrix is also shown in the calculation of channel capacity for various pattern configurations. This covariance matrix shows upper bounds on the channel capacity with the antenna selection and proper power allocation techniques.

4.1 MIMO System Model

The block diagram of a narrow-band point-to-point MIMO ($M_t \times N_r$) system consists of transmitting antennas and receiving antennas with the voltage and impedances sources at the both ends as shown in Figure 4.1. In this conventional MIMO system, the number of RF chains are same as the number of antenna terminals on both sides of the MIMO system. By using SPA approach, a smaller number of antennas can be used at the front-end connected to the transceivers and other antenna elements can be replaced with parasitic elements. This MIMO-SPA system reduces the size, cost and power constraint, especially in portable devices.

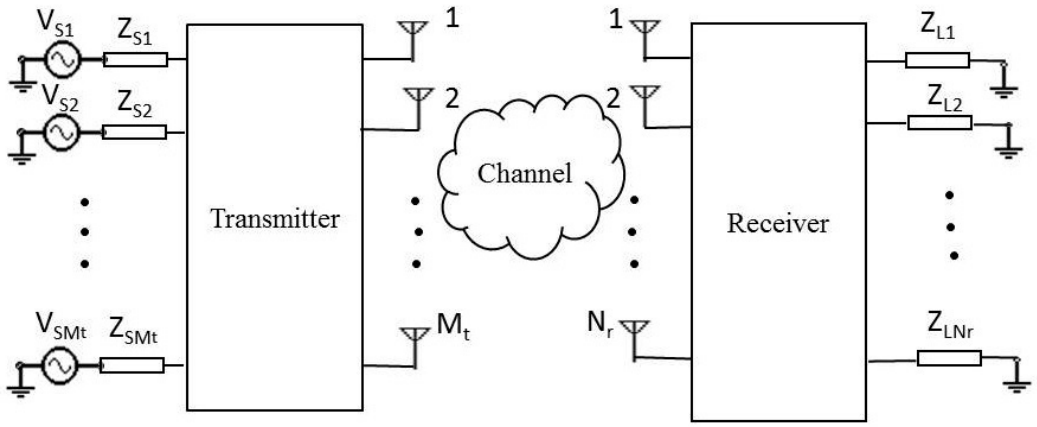

Figure 4.1: Block diagram of a $M_t \times N_r$ MIMO system.

The performance of the MIMO-SPA system can be represented in the terms of channel capacity. The channel capacity of a MIMO-SPA system not only depends on the characteristics of the channel in which the signal propagates but also on the properties of the radiating elements. It takes into consideration the effect of the propagation channel as well as the antenna elements in the system.

Use of parasitic elements in the antenna design is based on the fundamental concept of electromagnetic mutual coupling. This concept can be acquired on the antenna

terminals with the use of impedance matrices. Figure 4.2 depicts the MIMO-SPA model using antenna impedances $\mathbf{Z}_{TT}$ and $\mathbf{Z}_{RR}$ at the transmitting and the receiving sides respectively. To find out the effect of the antenna terminals on the MIMO channel capacity, it is necessary to consider the mutual coupling effect and calculate the impedance matrices using the antenna parameters.

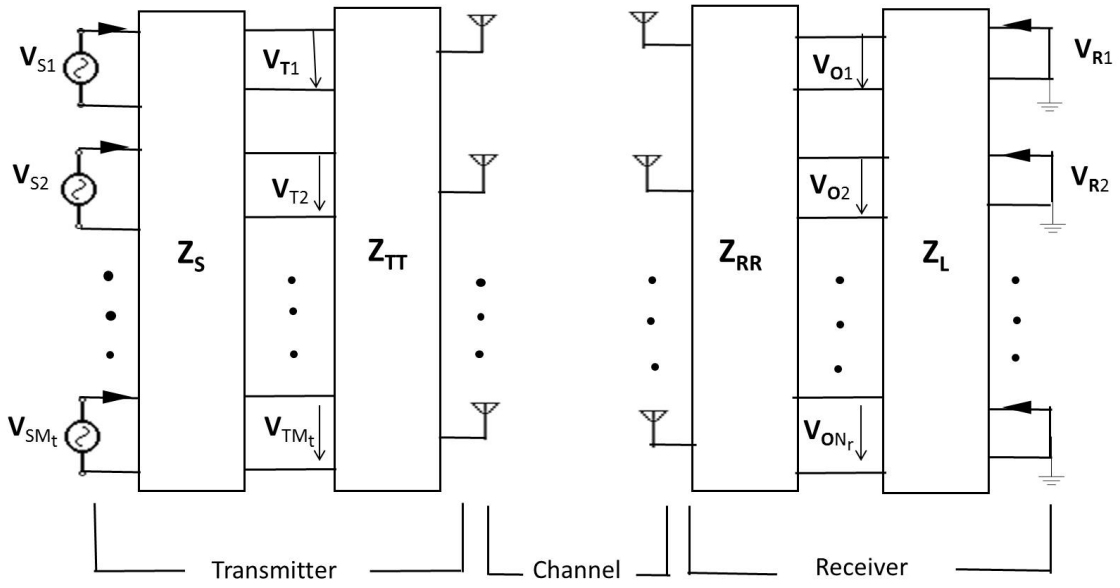

Figure 4.2: MIMO-SPA system with impedance matrices at both link ends.

Based on N-port theory, the voltage and current relationship between the transmit and the receive arrays can be represented as [115] :

$$\begin{bmatrix} \mathbf{V_T} \\ \mathbf{V_R} \end{bmatrix} = \begin{bmatrix} \mathbf{Z_{TT}} & \mathbf{Z_{TR}} \\ \mathbf{Z_{RT}} & \mathbf{Z_{RR}} \end{bmatrix} \begin{bmatrix} \mathbf{I_T} \\ \mathbf{I_R} \end{bmatrix} \tag{4.1}$$

where

$\mathbf{V}_T = [V_{T1}, V_{T2}, ..., V_{T_{M_t}}]^T$ is voltage source vector at the transmitting end,

$\mathbf{i}_T = [I_{T1}, I_{T2}, ..., I_{T_{M_t}}]^T$ is the current vector at the transmitting end,

$\mathbf{V}_R = [V_{R1}, V_{R2}, ..., V_{R_{N_r}}]^T$ is voltage source vector at the receiver end,

$\mathbf{i}_R = [I_{R1}, I_{R2}, ..., I_{R_{N_r}}]^T$ is the currents vector at the receiver end.
The diagonal matrices $\mathbf{Z}_{TT}$ and $\mathbf{Z}_{RR}$ are the self-impedance matrices at the transmitting and receiving antennas receptively. $\mathbf{Z}_{TR}$ and $\mathbf{Z}_{RT}$ are mutual-impedance matrices between transmitting and receiving antennas.

These voltage and current sources can be represented by means of Thevenin's theorem where an ideal voltage source V_{Si} is connected in series with source impedance Z_{Si} as [86]:

$$\tilde{\mathbf{V}}_\mathbf{S} = \tilde{\mathbf{I}}_\mathbf{S}(\mathbf{Z_{TT}} + \mathbf{Z_S}) \tag{4.2}$$

The currents at the transmitter side can be obtained as:

$$\tilde{\mathbf{I}}_\mathbf{S} = (\mathbf{Z_{TT}} + \mathbf{Z_S})^{-1}\tilde{\mathbf{V}}_\mathbf{S} \tag{4.3}$$

where $\tilde{\mathbf{I}}_\mathbf{S} = [I_{S1}I_{S2}...I_{SM_t}]^T$, $\tilde{\mathbf{V}}_\mathbf{S} = [V_{S1}V_{S2}...V_{SM_t}]^T$ and $\mathbf{Z_S} = diag(Z_{S1}Z_{S2}...Z_{SM_t})$.
Consider the parameter $\mathbf{G}$ relating the current at the transmitter side to the voltage at the receiver side. The parameter $\mathbf{G}$ also includes the electromagnetic effect of the propagation environment. The voltage-current relationship at the receiver side with the propagation effects can be denoted as:

$$\tilde{\mathbf{V}}_\mathbf{O} = \mathbf{G}\tilde{\mathbf{I}}_\mathbf{S} \tag{4.4}$$

At the receiver side, the output voltage with impedance matrices including antenna impedance matrix and loading matrix can be obtained as:

$$\tilde{\mathbf{V}}_\mathbf{O} = (\mathbf{Z_{RR}} + \mathbf{Z_L})\tilde{\mathbf{I}}_\mathbf{R} \tag{4.5}$$

or (4.5) can be written in the current form as:

$$\tilde{\mathbf{I}}_{\mathbf{R}} = (\mathbf{Z}_{\mathbf{RR}} + \mathbf{Z}_{\mathbf{L}})^{-1}\tilde{\mathbf{V}}_{\mathbf{O}} \tag{4.6}$$

where $\mathbf{Z}_{\mathbf{L}} = diag(Z_{L1}Z_{L2}...Z_{LN_r})$ is the diagonal loading impedance and $\mathbf{Z}_{\mathbf{RR}}$ is the antenna impedance matrix of the receiving array. On the receiver side, the voltage-current relationship in terms of the receiving impedance of the antennas can be written as:

$$\tilde{\mathbf{V}}_{\mathbf{R}} = \mathbf{Z}_{\mathbf{RR}}(\tilde{\mathbf{I}}_{\mathbf{R}}) \tag{4.7}$$

From (4.6), (4.7) can be re-written as:

$$\tilde{\mathbf{V}}_{\mathbf{R}} = \mathbf{Z}_{\mathbf{RR}}(\mathbf{Z}_{\mathbf{RR}} + \mathbf{Z}_{\mathbf{L}})^{-1}\tilde{\mathbf{V}}_{\mathbf{O}} \tag{4.8}$$

The relationship between the voltage at the source side $\tilde{\mathbf{V}}_{\mathbf{S}}$ and at the receiver side $\tilde{\mathbf{V}}_{\mathbf{R}}$ can be described as:

$$\tilde{\mathbf{V}}_{\mathbf{R}} = \mathbf{Z}_{\mathbf{RR}}(\mathbf{Z}_{\mathbf{RR}} + \mathbf{Z}_{\mathbf{L}})^{-1}\mathbf{G}(\mathbf{Z}_{\mathbf{TT}} + \mathbf{Z}_{\mathbf{S}})^{-1}\tilde{\mathbf{V}}_{\mathbf{S}} = \tilde{\mathbf{H}}\tilde{\mathbf{V}}_{\mathbf{S}} \tag{4.9}$$

With (4.9), it is easy to evaluate the voltage at the receiver side by calculating impedance matrices $\mathbf{Z}_{\mathbf{TT}}$ and $\mathbf{Z}_{\mathbf{RR}}$ at the transmitter and receiver sides respectively. These impedance matrices consider the effect of electromagnetic mutual coupling exists between the antenna terminals. The effect of the parasitic elements can also be realized with source impedance matrix $\mathbf{Z}_{\mathbf{S}}$ at the transmitter side and with the loading impedance matrix $\mathbf{Z}_{\mathbf{L}}$ at the receiver side. The number of parasitic elements can be changed independently at the transmitter and receiver sides. The loading effect at the transmitter and at the receiver side changes the source impedance $\mathbf{Z}_{\mathbf{S}}$ and the loading impedance $\mathbf{Z}_{\mathbf{L}}$ respectively.

These parasitic elements are the passive elements and are not connected to any RF source. Thus, it is not possible to access the voltages directly on the parasitic elements. The voltage can be obtained at the active elements by using permutation matrices as follows:

$$\mathbf{V_R} = \mathbf{S_R}\tilde{\mathbf{H}}\tilde{\mathbf{V}}_\mathbf{S} \tag{4.10}$$

where $\mathbf{S_R}$ is a permutation matrix of dimensions $(N_{ra} \times N_r)$, N_{ra} represents the number of active elements at the receiver side. It extracts the voltage at the active elements induced by the parasitic elements. Thus, the permutation matrix at the receiver side extracts the values of $\tilde{\mathbf{H}}$ that are relative to the active elements.

If the parasitic elements are connected at the transmitter side, the information across the parasitic elements can be accessed with the permutation matrix $\mathbf{S_T}$. The permutation matrix $\mathbf{S_T}$ has dimensions $(M_t \times M_{ta})$, where M_{ta} is the number of active elements at the transmitter side. With the use of permutation matrices $\mathbf{S_T}$ and $\mathbf{S_R}$ at the transmitter and receiver sides respectively, (4.10) can be written as:

$$\mathbf{V_R} = \mathbf{S_R}\tilde{\mathbf{H}}\mathbf{S_T}\mathbf{V_S} = \mathbf{H}\mathbf{V_S} \tag{4.11}$$

or

$$\mathbf{H} = \mathbf{S_R}\tilde{\mathbf{H}}\mathbf{S_T} \tag{4.12}$$

The effect of the parasitic elements can be realized with these permutation matrices $\mathbf{S_T}$ and $\mathbf{S_R}$, which select the rows and columns of $\tilde{\mathbf{H}}$ relative to the active elements connected to the transceivers.

4.2 Modelling the Effect of the Parasitic Elements

4.2.1 MIMO Channel Matrix (H) using SPA

The effect of the transmitting and receiving antenna terminals can be evaluated in terms of the impedance matrices. The impedance loads of the parasitic elements can also be represented in the form of matrices. The MIMO channel can be represented in the form of a channel matrix ($\tilde{\mathbf{H}}$) including antenna impedances matrices and loading parasitic elements matrices on both sides in the equation form as [7]:

$$\tilde{\mathbf{H}} = \mathbf{Z_{RR}}(\mathbf{Z_{RR}} + \mathbf{Z_L})^{-1}\mathbf{G}(\mathbf{Z_{TT}} + \mathbf{Z_S})^{-1} \tag{4.13}$$

where $\mathbf{G}$ is the propagation channel matrix including the effect of channel patterns and the scatterers. This modelling effect of the parasitic elements can be represented with a channel matrix at the transmitter and at the receiver side separately.

Consider a transmitting array with transmitting elements (M_t), with active elements (M_{ta}) and parasitic elements (M_{tp}), so that the total elements at the transmitter side are ($M_t = M_{ta} + M_{tp}$). With any change in the number of active and parasitic elements, (4.13) will be unchanged, only the values of the diagonal matrix $\mathbf{Z_S}$ will change in order to model the parasitic impedance loads at the transmitter side.

Equation (4.13) can be rewritten when parasitic elements are used at the transmitter side only:

$$\tilde{\mathbf{H}}_{tp} = (\mathbf{Z_{RR}} + \mathbf{Z_L})^{-1}\mathbf{G}(\mathbf{Z_{TT}} + \mathbf{Z_{S},}_{M_{tp}})^{-1}\mathbf{S_T} \tag{4.14}$$

where the subscript *tp* stands for parasitic elements at the transmitting side.

Equation (4.14) is similar to (4.13), the only change being the loading impedances terminating the parasitic elements in $\mathbf{Z_S}$.

Similarly to the transmitter side, parasitic elements can be used at the receiver side

as well. Consider a receiving array with active elements (N_{ra}) and parasitic elements (N_{rp}), so that the total elements are ($N_r = N_{ra} + N_{rp}$). Again, (4.13) will be unchanged, only the values of the diagonal matrix $\mathbf{Z_L}$ will change in order to model the parasitic impedance loads at the receiver side. Equation (4.13) can be rewritten when parasitic elements are used at the receiver side only:

$$\tilde{\mathbf{H}}_{rp} = \mathbf{S_R}(\mathbf{Z_{RR}} + \mathbf{Z}_{L,N_{rp}})^{-1}\mathbf{G}(\mathbf{Z_{TT}} + \mathbf{Z_S})^{-1} \tag{4.15}$$

where the subscript *rp* stands for parasitic elements at the receiving side.

The complete channel matrix with parasitic elements at both sides can be evaluated as [7]:

$$\tilde{\mathbf{H}}_{tp,rp} = \mathbf{S_R}(\mathbf{Z_{RR}} + \mathbf{Z}_{\mathbf{L},rp})^{-1}\mathbf{G}(\mathbf{Z_{TT}} + \mathbf{Z}_{\mathbf{S},tp})^{-1}\mathbf{S_T} \tag{4.16}$$

where the subscripts *tp*, *rp* represent the parasitic elements on the transmitting and receiving sides respectively. The permutation matrices $\mathbf{S_T}$ and $\mathbf{S_R}$ select the coefficients of $\tilde{\mathbf{H}}$ relative to the active elements connected to the transceivers.

Equation (4.16) shows the modification in the channel matrix by using parasitic elements at the transmitter and the receiver sides. Any modification in the loading impedance values of the parasitic elements can be realized in the form of the channel matrix. Hence, the effect of parasitic elements in the matrices $\mathbf{Z}_{\mathbf{S},tp}$ and $\mathbf{Z}_{\mathbf{L},rp}$, can change the coefficients of the channel matrix and can also vary the channel capacity. It should be noted that the relationship between $\tilde{\mathbf{H}}_{tp,rp}$ and the loading impedances $\mathbf{Z}_{\mathbf{S},tp}$ and $\mathbf{Z}_{\mathbf{L},rp}$, is non-linear because of the matrix inversion.

In this thesis, parasitic elements are used only at the receiver side for simplicity, thus changing the loads of impedance matrix $\mathbf{Z}_{\mathbf{L},rp}$ only. It is also possible to change the parasitic controlling impedances at the transmitter side $\mathbf{Z}_{\mathbf{S},tp}$ such as at a base station but it will make significant impact on all the users at the receiver side.

4.2.2 MIMO Channel Capacity using SPA

The channel realizations in a MIMO-SPA system change with the use of parasitic elements. To evaluate the channel capacity in MIMO-SPA, it is necessary to consider the parameters of the channel matrix **H**.

In flat-fading MIMO systems, the channel matrix depends on the system architecture and the particular channel propagation conditions. The coefficients of **H** can be considered with some probability distribution. With a large number of scatterers, the channel matrix coefficients can be assumed with zero-mean Gaussian distribution random variables. In the ideal case, when all the channel coefficients are uncorrelated, the highest channel capacity can be achieved. This is only possible in the case of rich scattering propagation environments, where the signals at the receiver are uncorrelated.

In MIMO systems, the transmitted symbol vector **s** transmits input symbol ($\mathbf{s} = s_1, s_2 ... s_{M_t}$) individually from transmit antennas (M_t) and the output can be defined as:

$$\mathbf{y} = \sqrt{\frac{E_s}{M_t}}\mathbf{Hs} + \mathbf{n} \tag{4.17}$$

where $\mathbf{n} = (n_1, n_2, ... n_{N_r})$ is a noise vector and is assumed to consists of zero-mean, circular symmetric, complex Gaussian random variables. The autocorrelation of the transmitted signal vector can be defined as: $\mathbf{R}_{ss} = E\{ss^H\}$. Assume transmit power across each antenna is 1, such as $Tr(\mathbf{R}_{ss}) = M_t$.

When CSI is available at the transmitter, the decomposition model gives information about the possible number of spatial links possible in the given MIMO system. By using SVD, it converts the multiple equations of the MIMO system into equivalent spatial links. The transmitter is pre-processed with **V** and the receiver signal is post-

processed with $\mathbf{U}^H$.

The output of the MIMO system (4.17) can be written by using SVD as:

$$\tilde{\mathbf{y}} = \sqrt{\frac{E_s}{M_t}}\mathbf{U}^H\mathbf{H}\mathbf{V}\tilde{\mathbf{s}} + \tilde{\mathbf{n}} \tag{4.18}$$

Using the SVD model, the number of MIMO channels is divided into a number of independent SISO channels. The channel matrix $\mathbf{H} \in \mathbb{C}^{M_t \times N_r}$ with SVD can be represented as:

$$\mathbf{H} = \mathbf{U}\Sigma\mathbf{V}^H \tag{4.19}$$

where $\mathbf{U} \in \mathbb{C}^{N_r \times N_r}$ and $\mathbf{V} \in \mathbb{C}^{M_t \times M_t}$ are unitary matrices and $\Sigma \in \mathbb{C}^{M_t \times N_r}$ is a rectangular matrix. The off-diagonal elements of Σ are zero and the diagonal elements of Σ are non-zero. These are known as singular values and can be denoted as $(\lambda_1, \lambda_2, ...\lambda_{min})$, where $N_{min} \triangleq min(M_t, N_r)$. The rank parameter of $\mathbf{H}$ represents the non-zero singular values, such that $rank(\mathbf{H}) \leq N_{min}$.

Thus, Shannon's channel capacity [126] of MIMO system can be evaluated as :

$$\mathbf{C} = \sum_{i=1}^{r} \log_2\left(1 + \frac{\alpha_i P_t {\sigma_i}^2}{N_0}\right) \qquad (bit/s/Hz) \tag{4.20}$$

where P_t is the total transmitted power, σ_i^2 is the ith singular value of the matrix $\mathbf{H}$, r is the rank of the matrix $\mathbf{H}$, N_0 is the noise variance at the receiver, and α_i shows the percentage of the transmitted power on the sub-channels. Equation(4.20) shows that the MIMO channel capacity depends on the singular values of the channel matrix $\mathbf{H}$.

4.3 MIMO Channel Capacity Analysis with Different Pattern Configurations

Conventional MIMO, gives only one channel matrix realization with the dimensions of the transmitting and receiver antenna elements. By using parasitic elements, there will be different channel realizations of the channel matrices depending on the loading configurations. The number of loading configurations can be calculated from the number of parasitic elements and the level of impedance loads terminated on them.

To see the effect of the parasitic elements on the MIMO channel capacity, it is necessary to obtain the channel matrix using (4.16) to evaluate $\tilde{\mathbf{H}}_{tp,rp}$. In this thesis, parasitic elements are only used at the receiver side, thus there is need to calculate $\tilde{\mathbf{H}}_{rp}$ only, as in (4.15).

The MIMO channel capacity can be evaluated by using Shannon's theory as follows [126]:

$$\mathbf{C} = E\left\{ \max_{Tr(R_{ss})=M_t} \log_2 \det\left(I_{N_r} + \frac{\mathsf{E_s}}{M_t N_0} \mathbf{H}_{rp} \mathbf{R}_{ss} {\mathbf{H}_{rp}}^H \right) \right\} \tag{4.21}$$

where $\mathsf{E_s}$ is the total transmitted power, N_0 is the variance of the additive white Gaussian noise at the receiver, $\mathbf{H}_{rp}$ represents the channel matrix using parasitic elements at the receiver side only, $\mathbf{R}_{ss}$ represents the covariance matrix and must be determined to satisfy the transmitter power constraints.

Compared to the traditional MIMO system, instead of finding the channel capacity for only one channel matrix, MIMO-SPA exploits the pattern diversity and provides a number of channel matrices. With the different load impedances across the parasitic elements, there will be different realizations of the channel matrices. The number of channel matrices depends on the number of parasitic elements and the available switching levels across the parasitic elements.

4.3.1 MIMO-SPA (2×2) using two Parasitic Elements

As discussed in chapter 3, section (3.4) showed SPA performance evaluation to create radiation patterns in three different cases. MIMO-SPA (2×2) using two parasitic elements represent the Case-I, where parasitic elements are used only at the receiver side. For the simulation purpose, the arrangement of array elements is same as shown in Figure 3.6.

Simulation scenario for MIMO-SPA system $(M_t \times N_r)$ using two parasitic elements at the receiver side only:

- Number of active elements at transmitter side M_{ta}=2
- Number of active elements at receiver side N_{ra}=2
- Number of parasitic elements at transmitter side M_{tp}=0
- Number of parasitic elements at receiver side N_{rp}=2
- Total number of elements at the transmitter side $M = M_{ta} + M_{tp}$=2+0=2
- Total number of elements at the receiver side $N = N_{ra} + N_{rp}$=2+2=4

In MIMO-SPA with (2×2) dimensions, using two parasitic elements gives four different channel matrices $(\mathbf{CH}_{00}, \mathbf{CH}_{01}, \mathbf{CH}_{10}, \mathbf{CH}_{11})$ according to the state of the switches *(on/off)*. The channel matrix $(\mathbf{CH}_{00})$ represents with both the parasitic elements are in the *off* state, which is similar to the conventional MIMO without using any parasitic elements.

Figure 4.3, shows the channel capacity with four different pattern configurations. The beam pattern configuration $(\mathbf{CH}_{00})$ shows the same channel capacity same as conventional MIMO (2×2) when there are only active elements present. In this

uncorrelated propagation environment simulation scenario, the channel coefficients of the four pattern configurations are uncorrelated in each case. Figure 4.3 shows that channel matrix ($\mathbf{CH}_{10}$) provides the highest channel capacity among the other pattern configurations.

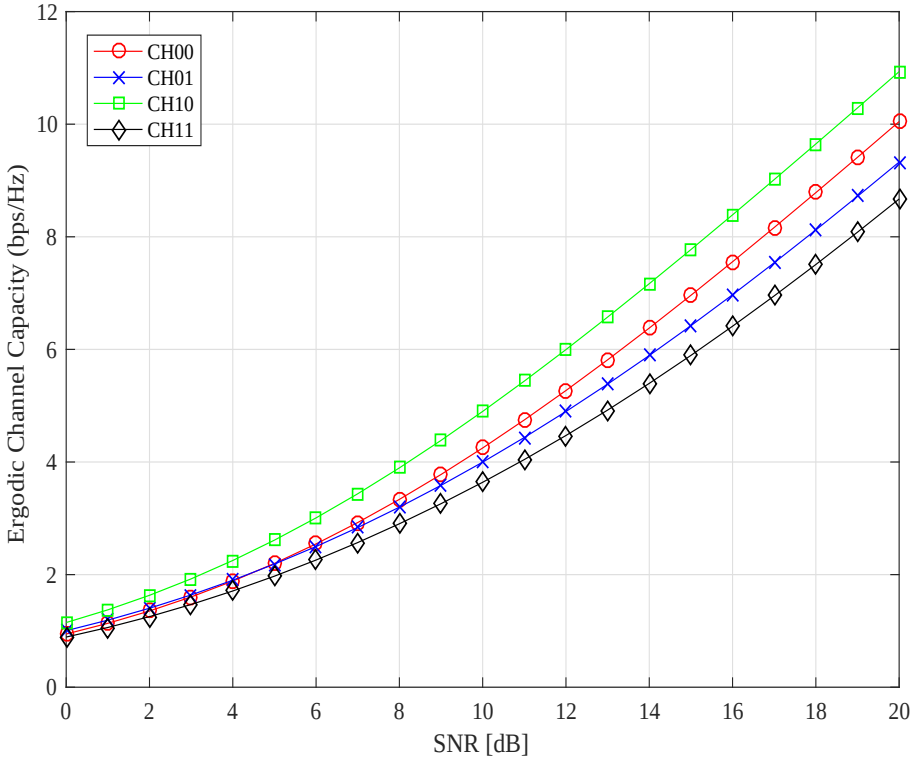

Figure 4.3: MIMO-SPA (2×2) with two parasitic elements.

The conventional MIMO (2×2) using only active elements gives average channel capacity 4.1 bit/s/Hz. MIMO-SPA (2×2) using two parasitic elements increases the average channel capacity to 5.3 bit/s/Hz. The simulation results show that by using parasitic elements, it is possible to increase the channel capacity.

4.3.2 MIMO-SPA (2×2) using four Parasitic Elements

Case-II in section (3.4), represents MIMO-SPA (2×2) using four parasitic elements. The arrangement of array elements at the receiver side is same as shown in Figure 3.8.

Simulation scenario for MIMO system $(M_t \times N_r)$ using four parasitic elements at the receiver side only :

- Number of active elements at transmitter side M_{ta}=2
- Number of active elements at receiver side N_{ra}=2
- Number of parasitic elements at transmitter side M_{tp}=0
- Number of parasitic elements at receiver side N_{rp}=4
- Total number of elements at the transmitter side $M = M_{ta} + M_{tp}$=2+0=2
- Total number of elements at the receiver side $N = N_{ra} + N_{rp}$=2+4=6

MIMO-SPA with (2×2) using four parasitic elements gives a total of sixteen ($2^4 = 16$) channel matrices ($\mathbf{CH}_{0000}, \mathbf{CH}_{0001}, ..., \mathbf{CH}_{1111}$) for sixteen different beam pattern configurations. As shown in Figure 4.4, pattern configuration *(States=0000)*, when all the switches on PEs are in the *off* state is equivalent to the conventional MIMO with only active elements are present. Due to the SPA antennas symmetry property, some of the pattern configurations shows similar results for ergodic channel capacity.

Figure 4.4 depicts the ergodic channel capacity in the uncorrelated propagation scenario for the sixteen pattern configurations. The simulation results show that the channel matrix ($\mathbf{CH}_{1101}$) provides the highest channel capacity among all the other pattern configurations.

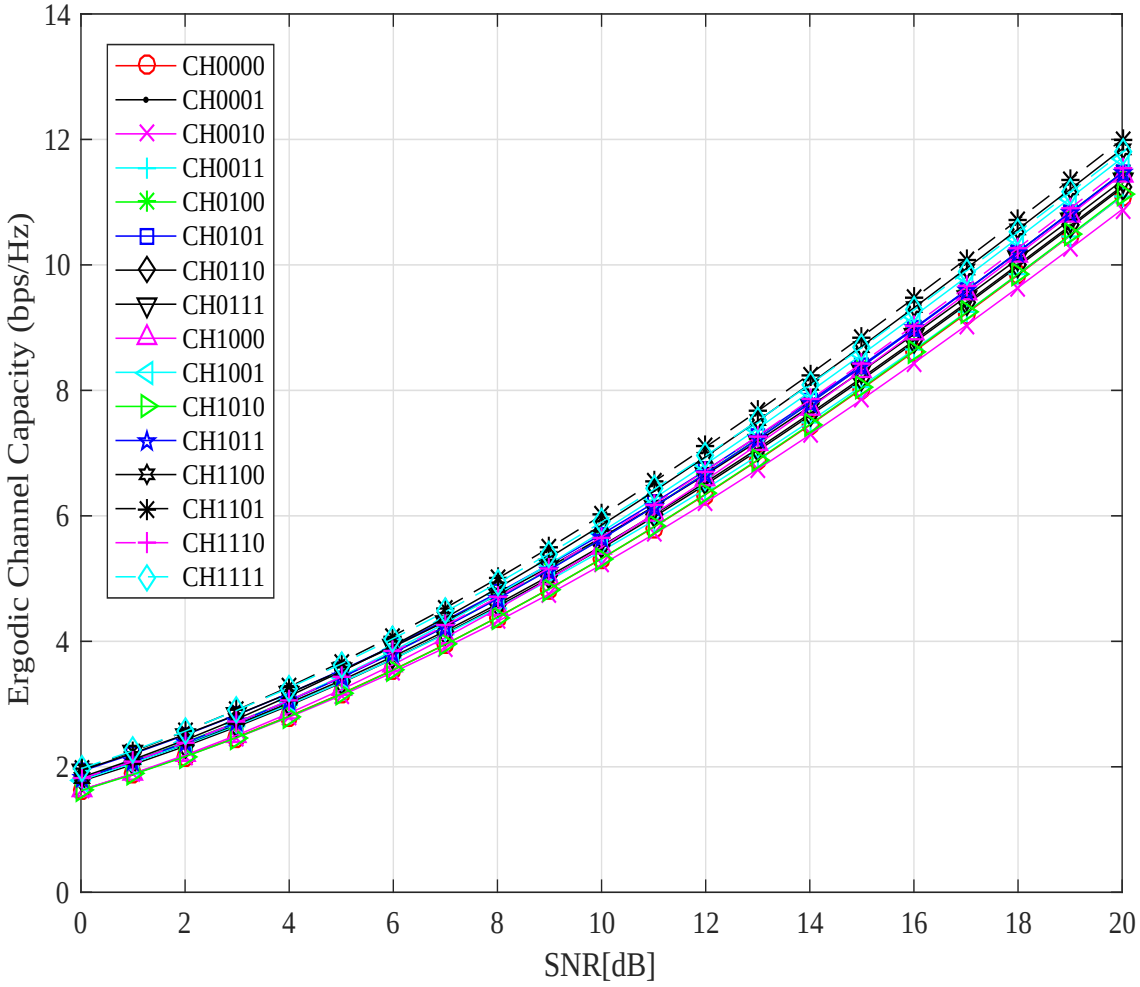

Figure 4.4: MIMO-SPA (2×2) with four parasitic elements.

In comparison conventional MIMO (2×2) using only active elements shows an average channel capacity of 5.3 bit/s/Hz and MIMO-SPA (2×2) using four parasitic elements increases the average channel capacity to 5.7 bit/s/Hz. The simulation results show improvement in the MIMO channel capacity by using parasitic elements with low-hardware complexity in the communication systems.

4.3.3 MIMO-SPA (4×4) using four Parasitic Elements

Case-III in section (3.4), represents MIMO-SPA (4×4) using four parasitic elements. The arrangement of array elements where four active elements are surrounded with four parasitic elements is same as shown in Figure 3.10.

Simulation scenario for MIMO-SPA system $(M_t \times N_r)$ using four parasitic elements at the receiver side only :

- Number of active elements at transmitter side M_{ta}=4
- Number of active elements at receiver side N_{ra}=4
- Number of parasitic elements at transmitter side M_{tp}=0
- Number of parasitic elements at receiver side N_{rp}=4
- Total number of elements at the transmitter side $M = M_{ta} + M_{tp}$=4+0=4
- Total number of elements at the receiver side $N = N_{ra} + N_{rp}$=4+4=8

Figure 4.5 shows MIMO-SPA (4×4) with four parasitic elements. Using four parasitic elements at the receiver side gives sixteen different beam pattern configurations. Four parasitic elements with two switching levels *(on/off)* gives sixteen $(2^4 = 16)$ pattern configurations corresponding to sixteen channel matrices $(\mathbf{CH}_{0000}, \mathbf{CH}_{0001}, ..., \mathbf{CH}_{1111})$. The first beam pattern *(States=0000)*, when all the switches of PEs are in the *off* state is equivalent to conventional MIMO with active elements only. In the uncorrelated propagation scenario, the channel matrix $(\mathbf{CH}_{1101})$ provides the highest channel capacity among all the other pattern configurations.

In a comparison of MIMO-SPA with standard MIMO, MIMO (4×4) using only active elements gives an average channel capacity of 8.5 bit/s/Hz, while MIMO-SPA

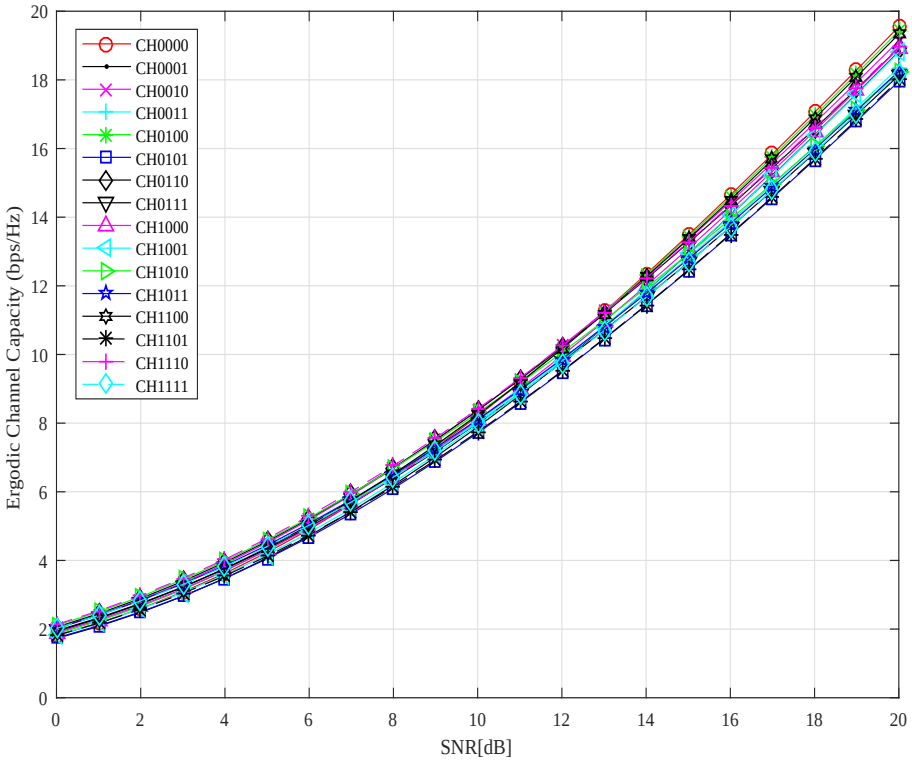

Figure 4.5: MIMO-SPA (4×4) with four parasitic elements.

(4×4) using four parasitic elements gives an average channel capacity of 9.2 bit/s/Hz. Thus, the simulation results show that the addition of parasitic elements provides low-complexity and higher channel capacity in MIMO systems.

4.4 MIMO System with Covariance Matrix

MIMO performance relies on the characteristics of the channel matrix and the availability of CSI on both sides of the communication link. At the receiver, it is possible to estimate this information by using channel estimation techniques with pilot training symbols. Often, the receiver feeds back this information to the transmitter. Instead of sending all this information, the receiver can send only the statistics of the channel in

the form of the covariance matrix. The advantage of using this information is that the statistics of the channel changes slowly as compared to the realization of the channel itself. MIMO-SPA channel capacity can be evaluated by using Shannon's theory as follows [126]:

$$\mathbf{C} = E\left\{ \max_{Tr(R_{ss})=M_t} \log_2 \det\left(I_{N_r} + \frac{\mathsf{E_s}}{M_t N_0} \mathbf{H}_{rp} \mathbf{R}_{ss} {\mathbf{H}_{rp}}^H \right) \right\} \tag{4.22}$$

where $\mathbf{R}_{ss}$ is the covariance matrix, which defines the presence of correlation in the propagation environment. If knowledge of the covariance matrix is available at the transmitter, it can distribute the power accordingly to the sub-channels.

The covariance matrix can be modified by using two techniques, IAST and WPA:

- IAST technique selects the subset of transmit antennas according to their contribution to the MIMO channel capacity. The antenna that contributes most to the channel capacity is selected first and then another antenna with the second highest contribution and so on. Thus, the selection process of antennas is in increasing order at the transmitter side.

- WPA technique allocates power to the selected antennas at the transmitter side. When CSI is available, WPA allocates the transmit power across all the transmit antennas in an optimal way. If the channel information is not available at the transmitter side then the optimal way is to distribute the power uniformly across all the transmit antennas.

The covariance matrix can be evaluated for these two techniques and can be defined as [18]:

$$\mathbf{R}_{ss}^{Imp} = \mathbf{V}\mathbf{R}_{ss}^{opt}\mathbf{V}^H \tag{4.23}$$

where $\mathbf{R}_{ss}^{opt} = \{\gamma_1^{opt}, \gamma_2^{opt} ... \gamma_{M_t}^{opt}\}$ is the optimal covariance matrix and $\mathbf{V}$ is the unitary

matrix that satisfies $V^H V = \mathbf{I}_Q$.

Hence, the improved channel capacity in MIMO-SPA according to the optimal covariance matrix is given by:

$$\mathbf{C}_{Imp} = E\left\{ \max_{\mathbf{R}_{ss}} \log_2 \det\left(I_{N_r} + \frac{\mathsf{E_s}}{M_t N_0} \mathbf{H}_{rp} \mathbf{R}_{ss}^{Imp} {\mathbf{H}_{rp}}^H \right) \right\} \tag{4.24}$$

4.4.1 Influence of Covariance Matrix

The covariance matrix shows the correlation present in the channel matrix **H**. The characteristics of the covariance matrix change according to the distribution of the channel-coefficients. Variation in the power allocation on the MIMO transmit antennas also makes changes in the correlation matrix. Hence, this effect can be analyzed in terms of channel capacity. The influence of the covariance matrix ($\mathbf{R}_{ss}$), with power constraints developed by [127] and has been used in [18] [128]:

$$\mathbf{R}_{ss}(\alpha) = \alpha I + (1-\alpha)\mathbf{u}\mathbf{u}^H \tag{4.25}$$

where $\mathbf{u} = [11...1]^T$, I is the identity matrix and α is a real number with power constraint which satisfies $0 \leq \alpha \leq \frac{P}{P-1}$.

- when α=0, then $\mathbf{R}_{ss}(0) = \mathbf{u}\mathbf{u}^H$ which shows that the covariance matrix $\mathbf{R}_{ss}$ has all elements of its matrix with value of 1. This means that all the channel coefficients correlated.
- when $\alpha = 1$, then $\mathbf{R}_{ss}(1) = \mathbf{I}$ which shows that the covariance matrix $\mathbf{R}_{ss}$ has all its elements are uncorrelated.
- when α parameter distributes power in the optimal way, it gives the improved correlation matrix. Thus, $\mathbf{R}_{ss}(opt) = \mathbf{R}_{ss}(Imp)$.

4.4.2 MIMO-SPA Channel Capacity with Different Covariance Matrices

MIMO-SPA channel capacity also shows impact on different pattern configurations with the improved covariance matrix. With the knowledge of these matrices, it is possible to evaluate Shannon's channel capacity as follows [126]:

$$\mathbf{C}_{Imp} = E\left\{ \max_{\mathbf{R}_{ss}} \log_2 \det\left(I_{N_r} + \frac{\mathsf{E_s}}{M_t N_0} \mathbf{H}_{rp} \mathbf{R}_{ss}^{Imp} {\mathbf{H}_{rp}}^H \right) \right\} \tag{4.26}$$

The covariance matrix $\mathbf{R}_{ss}$ needs to be determined to satisfy the transmitter power constraints. The covariance matrix can change the channel capacity across all the pattern configurations according to the power allocation at the transmitter side by using SVD. With the different realizations of the channel matrices, the MIMO channel capacity will be different across each pattern configuration. The more the channels are correlated, the lower will be the channel capacity and vice-versa.

4.5 MIMO-SPA Channel Capacity with IAST and WPA

When the channel conditions are known at the transmitter, the antenna can select the subset of antennas with incremental/decremental antenna selection techniques. The power allocation can be carried with WPA at the transmitter side.

In this thesis, incremental antenna selection technique (IAST) is used to select the best set of antennas at the transmitter side and power is allocated in an optimal way by using WPA. The variation in the channel capacity can be evaluated with different covariance matrices that change the power allocation at the transmitter side. The

comparison is discussed with three different covariance matrices as follows:

- IAST with correlated covariance matrix-$[\mathbf{R}_{ss}]_{corr}$
- IAST with uncorrelated covariance matrix- $[\mathbf{R}_{ss}]_{uncorr}$
- IAST with improved covariance matrix using WPA- $[\mathbf{R}_{ss}]_{WPA}$

4.5.1 MIMO-SPA (2×2) using two Parasitic Elements

4.5.1.1 IAST with correlated covariance matrix- $[\mathbf{R}_{ss}]_{corr}$

In the correlated case, when there is correlation present in the covariance matrix $[\mathbf{R}_{ss}]_{corr}$, all the elements of the matrix are set to one as in (4.25) with $\alpha = 0$. This means that all the channel coefficients are correlated. The covariance matrix according to (4.25) can be represented as $\mathbf{R}_{ss}(0)$ or $[\mathbf{R}_{ss}]_{corr}$.

Figure 4.6 shows the ergodic channel capacity across four pattern configurations with IAST and the correlated covariance matrix $[\mathbf{R}_{ss}]_{corr}$. The ergodic channel capacity does not show significant increase with respect to SNR. Due to the high correlation present between the channel coefficients, covariance matrix $[\mathbf{R}_{ss}]_{corr}$ represents a negative influence on the channel capacity.

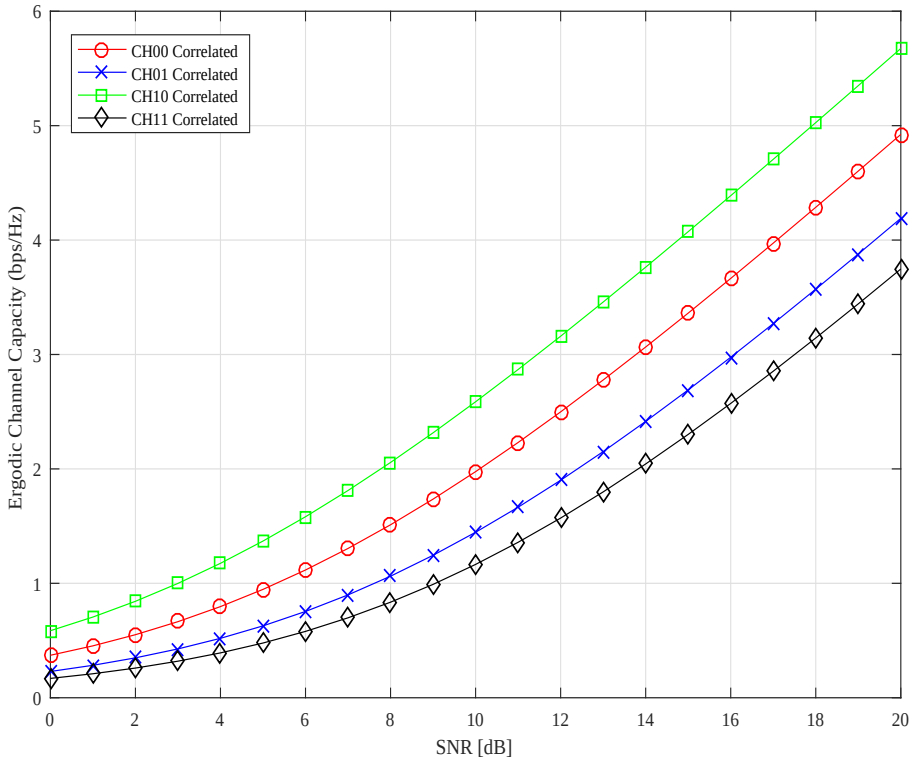

Figure 4.6: MIMO-SPA (2×2) channel capacity using two parasitic elements with matrix of all ones as correlation matrix.

4.5.1.2 IAST with uncorrelated covariance matrix- $[\mathbf{R}_{ss}]_{uncorr}$

In the uncorrelated case, the covariance matrix $[\mathbf{R}_{ss}]_{uncorr}$ is an identity matrix. The diagonal elements of the matrix are ones and all other elements are zeros as in (4.25) with $\alpha = 1$. This means that all the channel coefficients are uncorrelated. The covariance matrix according to (4.25) can be represented as $\mathbf{R}_{ss}(1)$. For the proper allocation of the power, IAST is used to select the antennas in particular order.

Figure 4.7 shows the ergodic channel capacity increases with respect to SNR in the uncorrelated case. The channel matrix ($\mathbf{CH}_{10}$) provides the highest channel capacity among all the other pattern configurations.

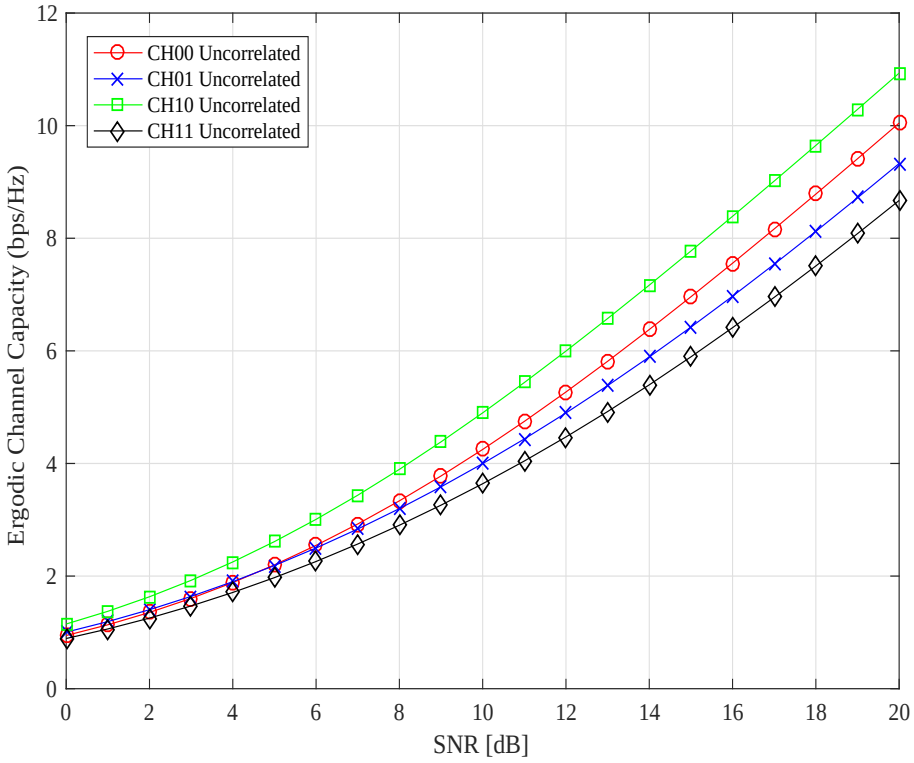

Figure 4.7: MIMO-SPA (2×2) channel capacity using two parasitic elements with identity matrix as correlation matrix.

4.5.1.3 IAST with improved covariance matrix using WPA- $[\mathbf{R}_{ss}]_{WPA}$

The improved covariance matrix is obtained by selecting the best set of antennas using IAST and then allocating optimal power using WPA. The improved covariance matrix is represented as $\mathbf{R}_{ss}(Imp)$.

The comparison of four different pattern configurations for correlated $[\mathbf{R}_{ss}]_{corr}$, uncorrelated $[\mathbf{R}_{ss}]_{uncorr}$ and improved covariance using WPA $[\mathbf{R}_{ss}]_{WPA}$ is shown in Figure 4.8. For all the parasitic configurations, the MIMO channel capacity is improved with the power allocation using WPA as compared to the equal power distribution across all the transmit antennas.

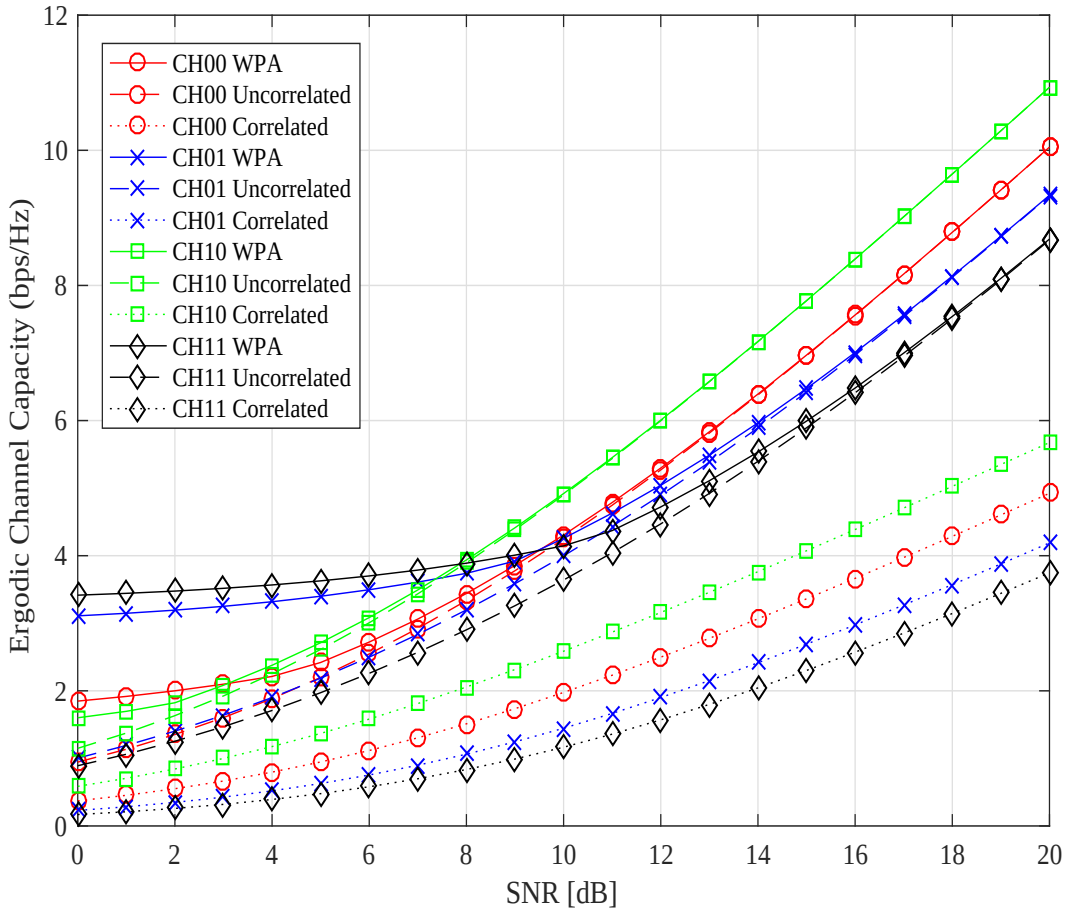

Figure 4.8: Comparison of the channel capacity using the three different methods for MIMO-SPA (2×2) using two parasitic elements.

The comparison of channel capacity for each beam pattern configuration can be plotted separately. Figure 4.9 shows the comparison for all the four channel matrices ($\mathbf{CH}_{00}, \mathbf{CH}_{01}, \mathbf{CH}_{10}, \mathbf{CH}_{11}$) with different covariance matrices. In each plot of channel matrix, the ergodic channel capacity performance improves with the covariance matrix using WPA $[\mathbf{R}_{ss}]_{WPA}$.

From Figure 4.9, the proposed system shows improvement from 4.9 bit/s/Hz of the conventional MIMO (2×2) to 5.3 bit/s/Hz in MIMO-SPA (2×2) using only two parasitic elements. Thus, the selection of best antennas with the optimal strategy of power allocation provides a higher channel capacity.

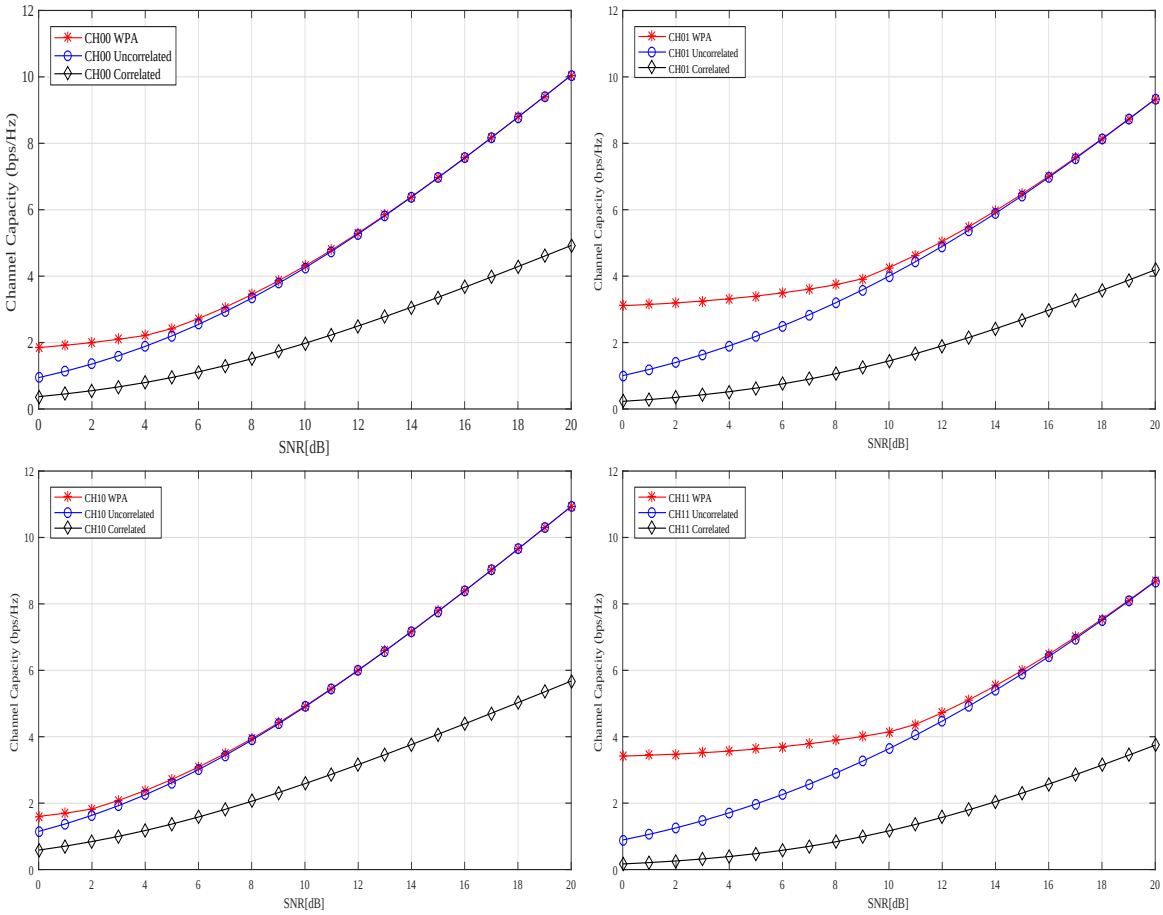

Figure 4.9: Comparison of the channel capacity using the three different methods for MIMO-SPA (2×2) using two parasitic elements.

4.5.2 MIMO-SPA (2×2) using four Parasitic Elements

4.5.2.1 IAST with correlated covariance matrix- $[\mathbf{R}_{ss}]_{corr}$

Figure 4.10 shows the comparison for all the sixteen channel matrices $(\mathbf{CH}_{0000}, \mathbf{CH}_{0001}, ..., \mathbf{CH}_{1111})$ with the correlated covariance matrix $[\mathbf{R}_{ss}]_{corr}$. In this case, all the channel coefficients of the MIMO-SPA channel matrices for all the sixteen configurations are correlated. The ergodic channel capacity for IAST is decreased for all the pattern configurations when the covariance matrix is correlated.

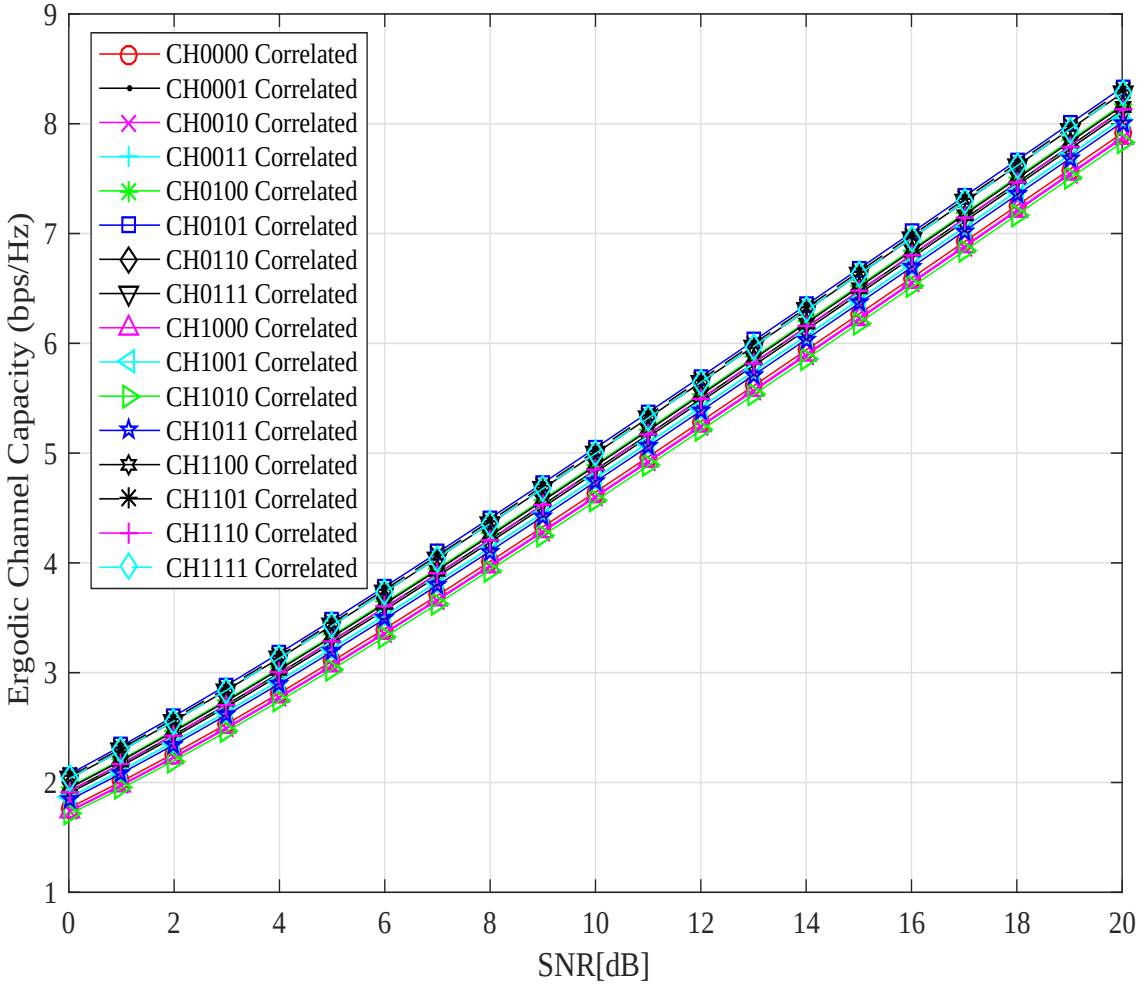

Figure 4.10: MIMO-SPA (2×2) channel capacity using four parasitic elements with matrix of all ones as correlation matrix.

4.5.2.2 IAST with uncorrelated covariance matrix- $[\mathbf{R}_{ss}]_{uncorr}$

Figure 4.11 shows the comparison for all the sixteen channel matrices ($\mathbf{CH}_{0000}, \mathbf{CH}_{0001}, ..., \mathbf{CH}_{1111}$) with the identity matrix $\mathbf{I}$ as the covariance matrix. In this case, all the channel coefficients of the MIMO-SPA channel matrices for all the sixteen configurations are uncorrelated. Figure 4.11 shows the pattern configuration ($\mathbf{CH}_{1101}$) provides the highest ergodic channel capacity as compared to all the other pattern configurations.

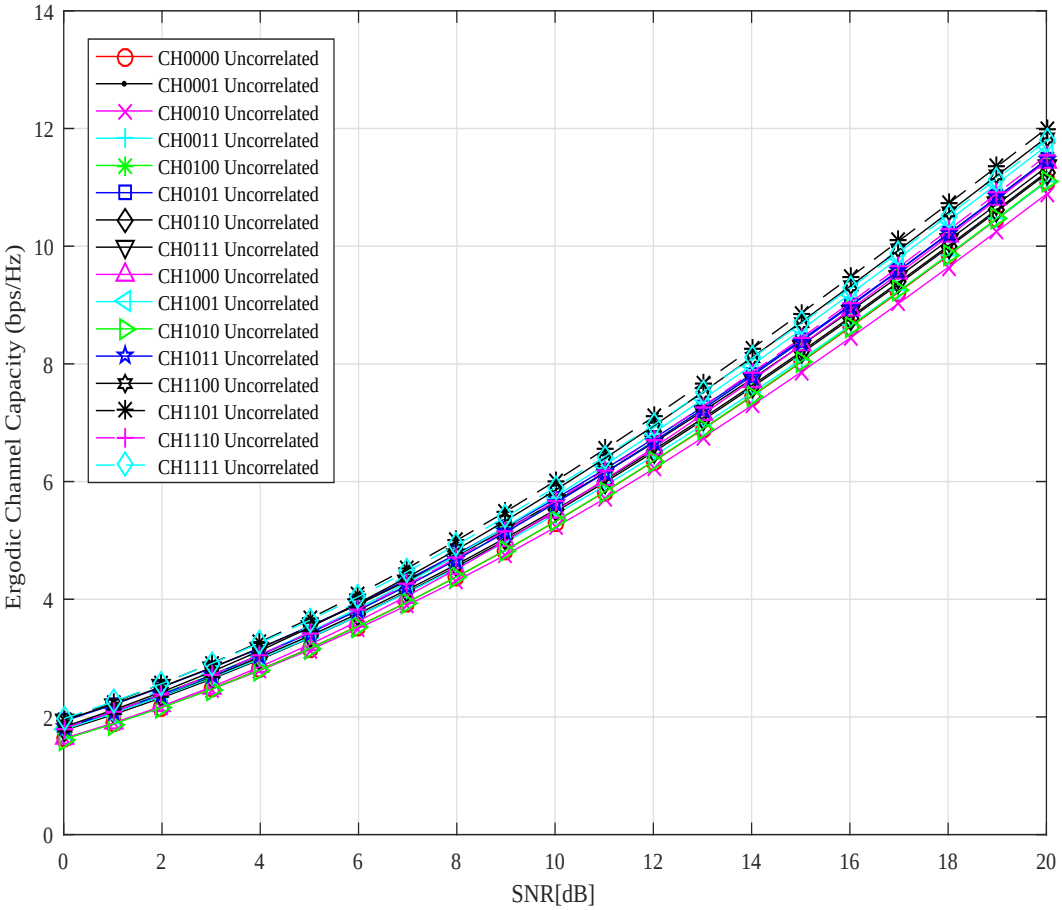

Figure 4.11: MIMO-SPA (2×2) channel capacity using four parasitic elements with identity matrix as correlation matrix.

4.5.2.3 IAST with improved covariance matrix using WPA- $[\mathbf{R}_{ss}]_{WPA}$

The comparison of channel capacity for each beam pattern configuration for MIMO-SPA (2×2) channel capacity using four parasitic elements can be plotted separately. Figure 4.12 shows the comparison for all the sixteen channel matrices $(\mathbf{CH}_{0000}, \mathbf{CH}_{0001}, \mathbf{CH}_{0010}, ..., \mathbf{CH}_{1111})$ with different covariance matrices. In each plot of channel matrix, the ergodic channel capacity performance improves with the covariance matrix using WPA $[\mathbf{R}_{ss}]_{WPA}$.

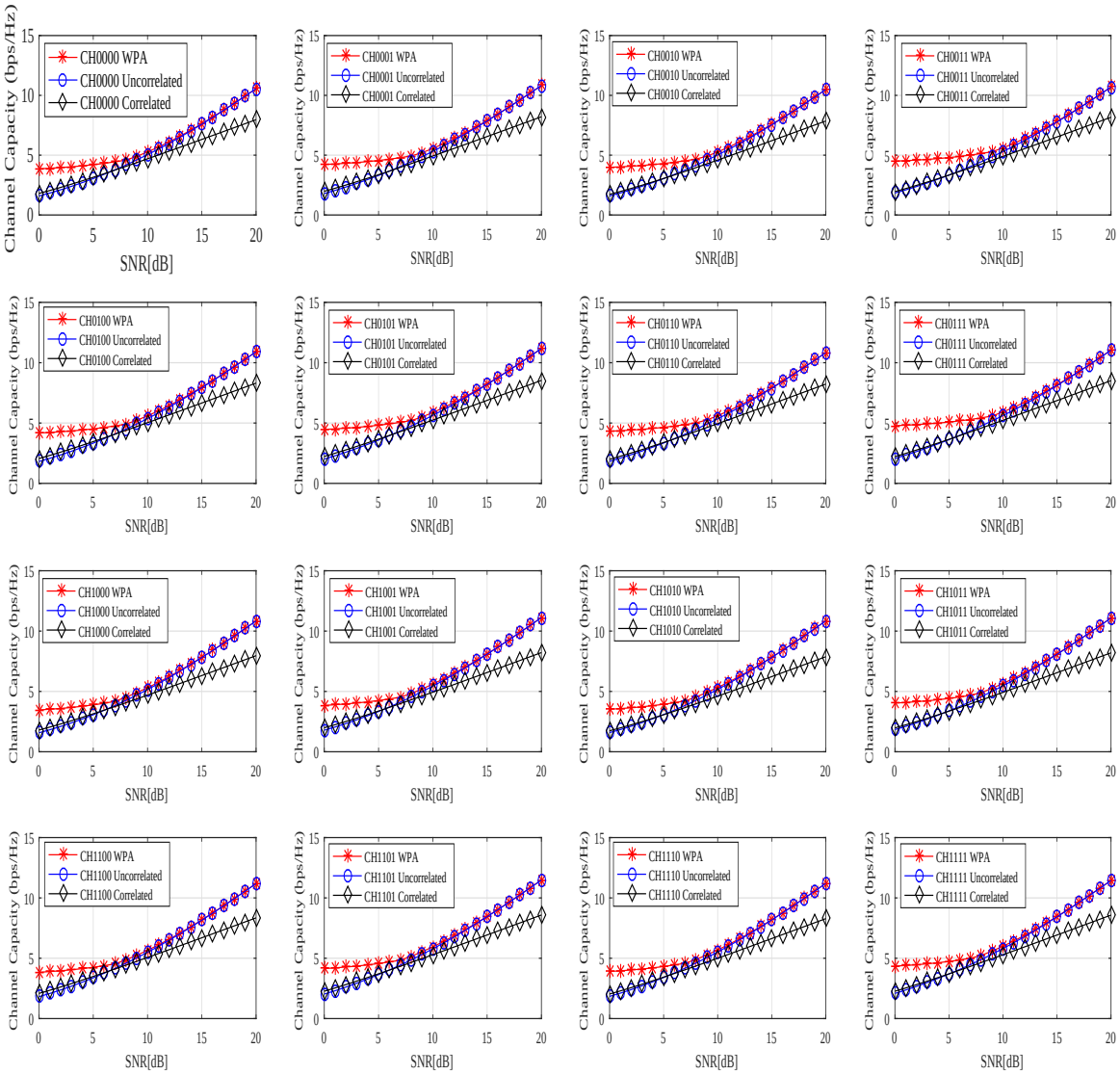

Figure 4.12: Comparison of the channel capacity using the three different methods for MIMO-SPA (2×2) using four parasitic elements.

Simulation results show that the conventional MIMO gives the channel capacity of 5.8 bit/s/Hz. It increases with improved covariance matrix to 6.2 bit/s/Hz in MIMO-SPA with four parasitic elements. Hence, the optimal covariance matrix with the proper selection of antenna with the optimal power allocation improves the channel capacity significantly.

4.5.3 MIMO-SPA (4×4) using four Parasitic Elements

4.5.3.1 IAST with correlated covariance matrix- $[\mathbf{R}_{ss}]_{corr}$

Figure 4.13 shows the comparison for all the sixteen channel matrices $(\mathbf{CH}_{0000}, \mathbf{CH}_{0001}, ..., \mathbf{CH}_{1111})$ with the correlated covariance matrix $[\mathbf{R}_{ss}]_{corr}$. In this case, all the channel coefficients of the MIMO channel matrices for all the sixteen configurations are correlated. The ergodic channel capacity for IAST is decreased for all the pattern configurations when the covariance matrix is correlated.

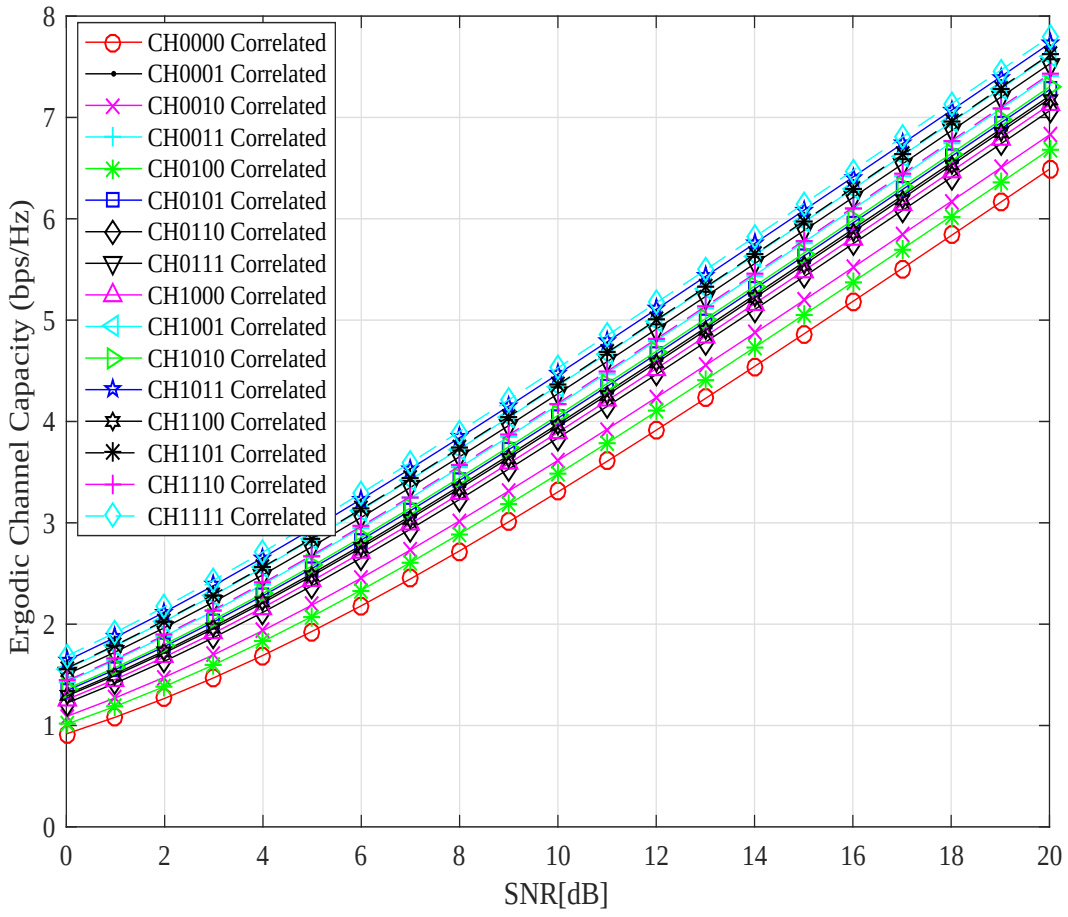

Figure 4.13: MIMO-SPA (4×4) channel capacity using four parasitic elements with matrix of all ones as correlation matrix.

4.5.3.2 IAST with uncorrelated covariance matrix- $[\mathbf{R}_{ss}]_{uncorr}$

Figure 4.14 shows the comparison for all the sixteen channel matrices ($\mathbf{CH}_{0000}, \mathbf{CH}_{0001}, ..., \mathbf{CH}_{1111}$) with the identity matrix as the covariance matrix. In this case, all the channel coefficients of the MIMO channel matrices for all the sixteen configurations are uncorrelated. Figure 4.14 shows the pattern configuration ($\mathbf{CH}_{1110}$) provides the highest ergodic channel capacity as compared to all the other pattern configurations. It also shows the improvement by using SPA with MIMO as compared to the conventional MIMO without parasitic elements.

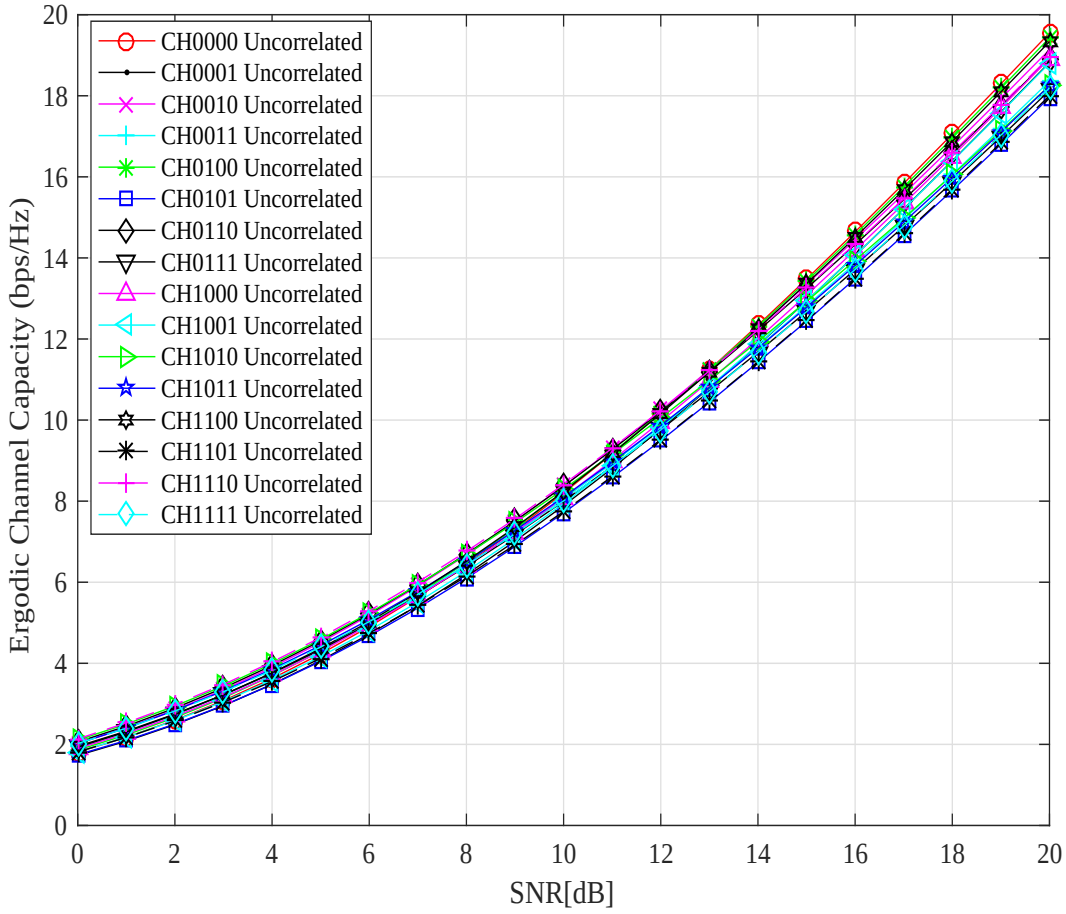

Figure 4.14: MIMO-SPA (4×4) channel capacity using four parasitic elements with identity matrix as correlation matrix.

4.5.3.3 IAST with improved covariance matrix using WPA- $[\mathbf{R}_{ss}]_{WPA}$

The comparison of channel capacity for each beam pattern configuration for MIMO (4×4) using four parasitic elements can be plotted separately. Figure 4.15 shows the comparison for all the sixteen channel matrices $(\mathbf{CH}_{0000}, \mathbf{CH}_{0001}, \mathbf{CH}_{0010}, ..., \mathbf{CH}_{1111})$ with different covariance matrices. In each plot of channel matrix, the ergodic channel capacity performance improves with the covariance matrix using WPA $[\mathbf{R}_{ss}]_{WPA}$.

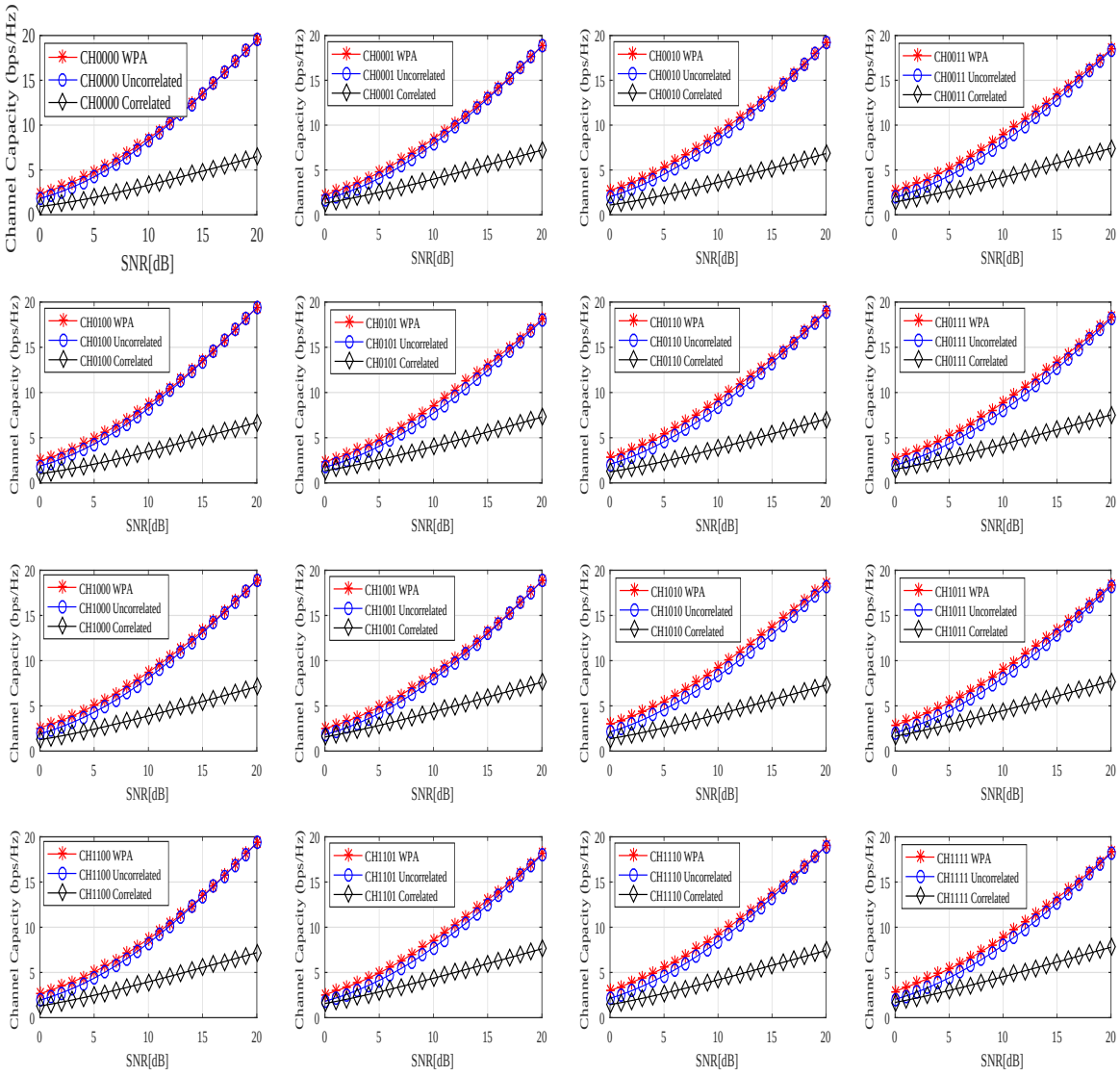

Figure 4.15: Comparison of the channel capacity using the three different methods for MIMO-SPA (4×4) using four parasitic elements.

Simulation results show that conventional MIMO gives a channel capacity of 9.1 bit/s/Hz, increasing with improved covariance matrix to 9.8 bit/s/Hz with MIMO-SPA with four parasitic elements. The optimal covariance matrix with the proper selection of antennas and optimal power allocation improves the channel capacity.

4.6 MIMO-SPA Channel Capacity with correlation matrix

In MIMO-SPA, the variation in the correlation matrix shows changes in the channel capacities for all the pattern configurations as shown in Figure 4.9, Figure 4.12 and Figure 4.15. Upper and lower bounds on channel capacity with the influence of covariance matrix in three different cases with (4.25) can be represented as:

- when α=0 then $[\mathbf{R}_{ss}]_{corr} = \mathbf{C}_{min}$, which gives lower-bounds on the channel capacity with all the coefficients of the channel matrix for each pattern configuration are correlated.
- when $\alpha = 1$ then $[\mathbf{R}_{ss}]_{uncorr} = \mathbf{C}_{max}$, which gives channel capacity with all the coefficients of the channel matrix for each pattern configuration are uncorrelated. The channel capacity shows better results than correlated environment.
- when α parameter allocates power in optimal way with IAST and WPA, it gives the improved correlation matrix. Thus, $[\mathbf{R}_{ss}]_{Imp} = \mathbf{C}_{Imp}$, shows upper-bounds on the channel capacity.

The comparison of channel capacity (4.26) with respect to the covariance matrix $\mathbf{R}_{ss}$ can be represented as:

$$\mathbf{C}_{min} = \mathbf{C}\Big|_{\mathbf{R}_{ss}(0)} \tag{4.27}$$

$$\mathbf{C}_{max} = \mathbf{C}\Big|_{\mathbf{R}_{ss}(1)} \tag{4.28}$$

$$\mathbf{C}_{Imp} = \mathbf{C}\Big|_{\mathbf{R}_{ss}(Imp)} \tag{4.29}$$

Therefore, lower and upper bounds for the channel capacity can be established with the corresponding correlation matrices as follows:

$$C_{min} \leq C_{max} \leq C_{Imp} \tag{4.30}$$

Equation (4.30) shows a lower-bound on the channel capacity C_{min} with the correlated covariance matrix $[\mathbf{R}_{ss}]_{corr}$ or $\mathbf{R}_{ss}(0)$. An intermediate channel capacity C_{max} achieved with the uncorrelated covariance matrix $[\mathbf{R}_{ss}]_{uncorr}$ or $\mathbf{R}_{ss}(1)$. An upper-bound on channel capacity C_{Imp} obtained with the optimal covariance matrix $[\mathbf{R}_{ss}]_{Imp}$. These channel capacity bounds show the influence of the covariance matrix with variations of the power parameter in MIMO-SPA systems.

4.7 Conclusion

MIMO-SPA presented in this chapter is capable of steering beam patterns in different directions by switching the parasitic elements. The use of pattern diversity is exploited with parasitic elements that use the electromagnetic mutual coupling principle. This effect on antenna elements is calculated by considering the impedance matrices. The effect of radiating elements and propagation medium is evaluated to find out the MIMO-SPA performance in terms of channel capacity. The ergodic channel capacity

have been calculated on all the pattern configurations. The influence of the correlation matrix on the channel capacity is also shown with IAST and WPA. The simulation results shows that the improved covariance matrix gives the upper bounds on the channel capacity in the MIMO-SPA systems. Hence, the most cost-efficient MIMO system is obtained by using IAST for the antenna subset selection and WPA for the optimal power allocation across all the transmit antennas.

Chapter 5

Pattern Configuration Selection

This chapter investigates the MIMO-SPA system behavior based on the statistical properties of the propagation environment. An overview of some important MIMO channel quality metrics such as condition number and channel capacity are presented in this chapter. A condition number is a channel quality indicator that represents the correlation present in the MIMO channel. This chapter proposes a novel optimal pattern configuration method based on channel statistics that can be sent back to the transmitter with a low-rate feedback link. The optimal pattern configuration based on the condition number at different SNR is also presented for different MIMO-SPA scenarios.

5.1 Exploiting CSI at the Transmitter Side

MIMO technology provides promising solutions for the increasing demands of high channel capacity and reliability in wireless communication systems. These advantages are possible with knowledge of channel fading at both ends of the communication link. In TDD systems, both links can exploit this information with the reciprocity

principle. In FDD systems, both links use different radio frequencies and do not follow the channel reciprocity principle.

Generally, the receiver can access the CSI by using channel estimation techniques but it is not possible for the transmitter to access its own channels by direct means. It relies on the receiver to get this information through the feedback channel. Thus, the receiver first estimates the channel parameters by using pilot symbols then feeds back this information to the transmitter.

In wireless communication systems, the main drawback is the requirement of an additional resource to provide this information back to the transmitter. The amount of feedback information also increases with the number of antennas used in the system. Due to the feedback requirements in terms of system bandwidth, it is not practically feasible to send full information on the channel to the transmitter. In time-varying channel conditions, it is not possible for the transmitter to track the channel completely. The information also become outdated when the transmitter uses it for the next transmission. At the transmitter, instead of sending the full CSI, statistical knowledge of the channel can be exploited. It reduces the feedback overhead and is updated only when there is significant change in the propagation channel.

The statistics of the changing environment can be sent back in the form of correlation matrices. Another approach to sending partial information of the channel status is to use the condition number of the channel matrix. A condition number reflects the eigenvalue spread of the MIMO channel. It gives indication of the multipath richness present in the given channel realization.

In long-term evolution (LTE), three indicators are used for the feedback purpose: rank indicator (RI), precoding matrix indicator (PMI) and channel quality indicator (CQI). The first two indicators are used for MIMO operation. CQI is the most important indicator for scheduling and link adaptation purposes. The adaptation of

the transmit signal to the channel variations improves the transmission rate of the system. This adaptation in the MIMO systems is possible with the availability of CSI at the transmitter by indirect means such as with channel estimation techniques and with a reliable feedback link.

5.2 Importance of Channel Quality Metrics

In adaptive MIMO systems, the transmitter tracks the changes in the channel with the information provided by the receiver. As shown in Figure 5.1, the receiver estimates the channel with channel estimation techniques and sends back the low-rate feedback link to the transmitter. The transmitter uses this information to adapt the channel such as in terms of modulation and coding schemes for the next signal transmission.

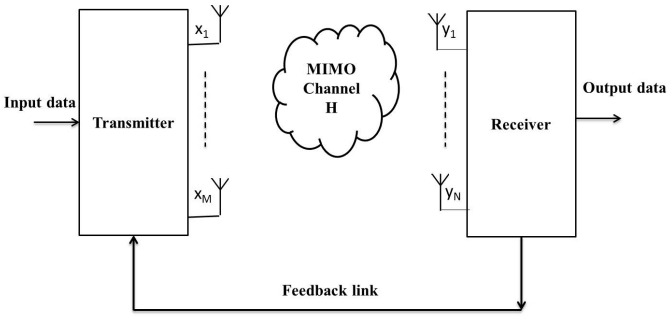

Figure 5.1: Feedback link with CSI

When CSI is not available at the transmitter, the best policy is to allocate the transmit power uniformly across all the transmit antennas. When the CSI is available at the transmitter, the optimal power is allocated based on the quality of the channel. The power allocation at the transmitter side is based on the eigenvalue spread of the channel. The eigenvalue spread indicates the correlation present in the multipath propagation channel. It signifies the orthogonality present between the spatial

channels. A low eigenvalue spread indicates that there is low correlation present in the channel, which increases the spatial multiplexing gain. A high eigenvalue spread indicates similarity between the spatial channels and provides limited or sometimes only one channel, as in the beamforming technique [47].

In the high SNR regime, a greater channel capacity can be achieved with low eigenvalue spread. In the low SNR regime, most or all of the power is allocated to the strongest eigenmode only. For high channel capacity or high spatial multiplexing gain, it is desirable to have low eigenvalue spread.

5.2.1 MIMO Channel Condition Number

In MIMO systems, EVS indicates the degree of correlation present in multipath channel. The rank indicator indicates the number of spatial links possible to provide the spatial multiplexing gain in the MIMO system. It only gives the information about the possible number of spatial channels but does not give any information about the quality of the spatial channels. Another channel metric is known as the condition number, which gives an indication about the quality of the channel. It characterizes the channel matrix in terms of the sensitivity of the channel matrix.

If the eigenvalues of the channel matrix are almost equal or the difference between the eigenvalues is very low, it will provide a low condition number. This is also known as a "well-conditioned channel" matrix. In the ideal case, with a rich-scattering environment, where all the channels are uncorrelated, the MIMO channel matrix provides the highest rank and the condition number is equal or close to 0 dB. This indicates the orthogonality of the sub-channels and provides comparable channel gains in different spatial directions. Due to the poor channel conditions with correlated channels, the rank of the channel matrix drops to zero and is known as a rank-deficient

channel matrix. The condition number of this channel matrix will be very high and it will be difficult to properly recover the MIMO signal. Thus, the condition number indicates whether the MIMO channel is capable of supporting spatial multiplexing in MIMO systems. It is also used as a short-term indication of the SNR required to properly recover a MIMO transmission.

As previously discussed in the literature [129] [130], a condition number can be defined in a number of ways:

- The condition number can be defined as the ratio of the largest eigenvalue(λ_{max}) to the smallest eigenvalue (λ_{min}). It can be obtained through eigenvalue decomposition (EVD) and can be represented as:

$$\kappa = \frac{\lambda_{max}(\mathbf{H})}{\lambda_{min}(\mathbf{H})}. \tag{5.1}$$

  The condition number can also be defined as the ratio of the largest singular value (σ_{max}) to the smallest singular value (σ_{min}), where (σ) is obtained via the SVD of the matrix. The eigenvalue and SVD produce the same result only when the matrix is both symmetric and positive definite.

- Another method of finding the condition number is by the product of the norms of the matrix and its inverse, such as: $\kappa = \|\mathbf{H}\|.\|\mathbf{H}^{-1}\|$, where $\|$ denotes the 2-norm and is referred as the Euclidean distance.

In matrix theory [19], the condition number indicates how sensitive the solution of the system is relative to its input. It tells about the stability of the system. If the channel matrix is an "ill-conditioned" matrix, it will show drastic changes in the output data with the small changes in the input. Thus, the system will be more prone to errors and sensitive to channel noise and other interference issues.

In an industrial publication [131], the relation between the condition number and its effect on the throughput is discussed as shown in Table 5.1. The channel condition number should be less than ($\leq 19dB$) to obtain the high throughput. With the high correlation ($\geq 19dB$) between the channels, MIMO would not be able to increase the throughput of the system. For the maximum throughput, the channels should be totally independent with minimum correlation. Thus, the quality of the MIMO system channel plays a vital role to optimizing the throughput of the LTE-A Downlink Physical Layer.

Table 5.1: Channel condition number and its indications

Condition Number	**Indication**
0dB	Totally independent channels, Ideal condition to achieve maximum throughput
$\leq$ 13dB	Favorable condition which enables higher throughput as compare to SIMO/MISO
13dB-19dB	Medium Correlation which provides marginal throughput improvement
$\geq$ 19dB	High correlation where MIMO would not be able to increase throughput

In the literature, the condition number has been used as a selection criterion for several purposes in MIMO systems. Many studies [30] [33] have used the condition number for switching between the diversity and spatial multiplexing schemes. Reconfigurable patch antennas use the condition number to select the antenna configuration [34]. The adaptive MIMO transmission techniques [35] have used the condition number to exploit the spatial selectivity of the wireless channels. Other research [36], demonstrates the use of the regular condition number to evaluate the quality of the channel matrix, as it provides some intuition on channel quality.

5.2.2 MIMO Channel Capacity

According to the Shannon's theorem [126], the MIMO channel capacity not only changes with SNR and bandwidth, it also depends on the status of the channel matrix. The quality of the channel matrix is also an important factor to evaluate the MIMO channel capacity [132].

Figure 5.2 depicts the relation between SNR and the condition number. It shows how the quality of the channel in terms of condition number decides the requirement for the SNR in the system. For example, for the requirement of a channel capacity of 6 bits/s/Hz, a condition number of 0 dB requires a SNR of 9 dB. As the condition number increases to 16 dB, it requires a SNR of 12 dB. For a condition number of 30 dB, it needs SNR of 15 dB for the same system data rate.

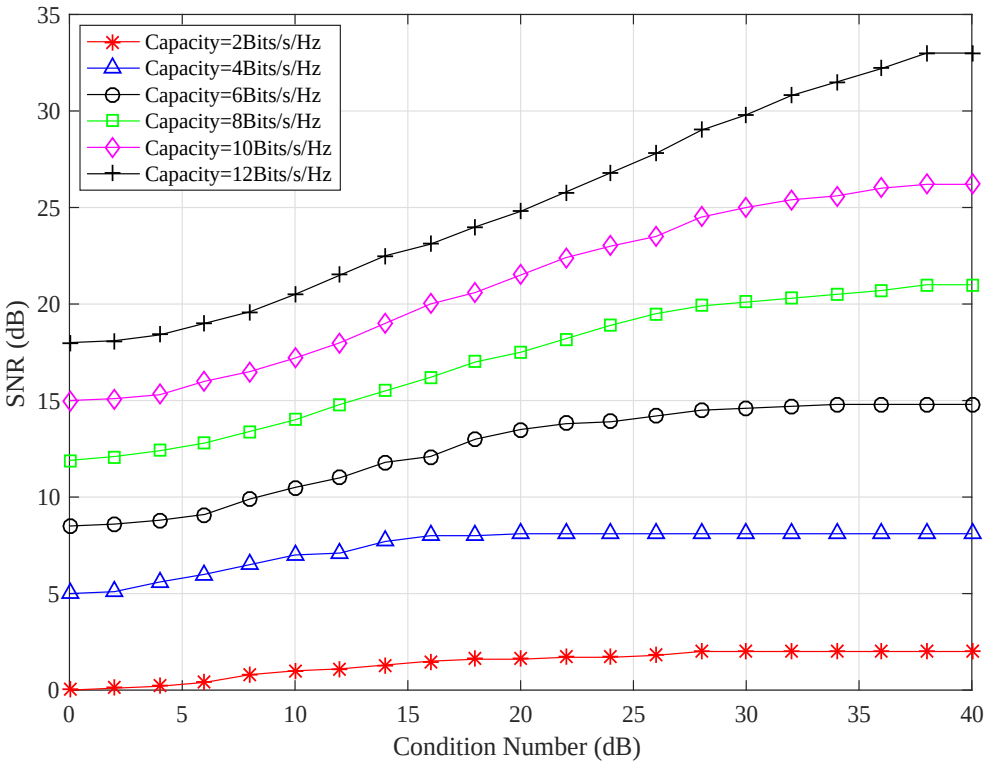

Figure 5.2: Signal-to-noise ratio and condition number

This shows that as the condition number increases, the system requires more SNR to achieve the same performance. Figure 5.2 shows that the same performance can be achieved even with low SNR values when the channel has a low condition number. However, the condition number represents the correlation present in the channel coefficients in the channel matrix. The greater the correlation between the coefficients, the higher will be the condition number. This correlation depends on a number of factors including: small antenna spacing, common antenna polarization and a narrow angular spread with a poor scattering environment.

The relationship between correlation and channel capacity in terms of cumulative distribution function (cdf) is shown in Figure 5.3.

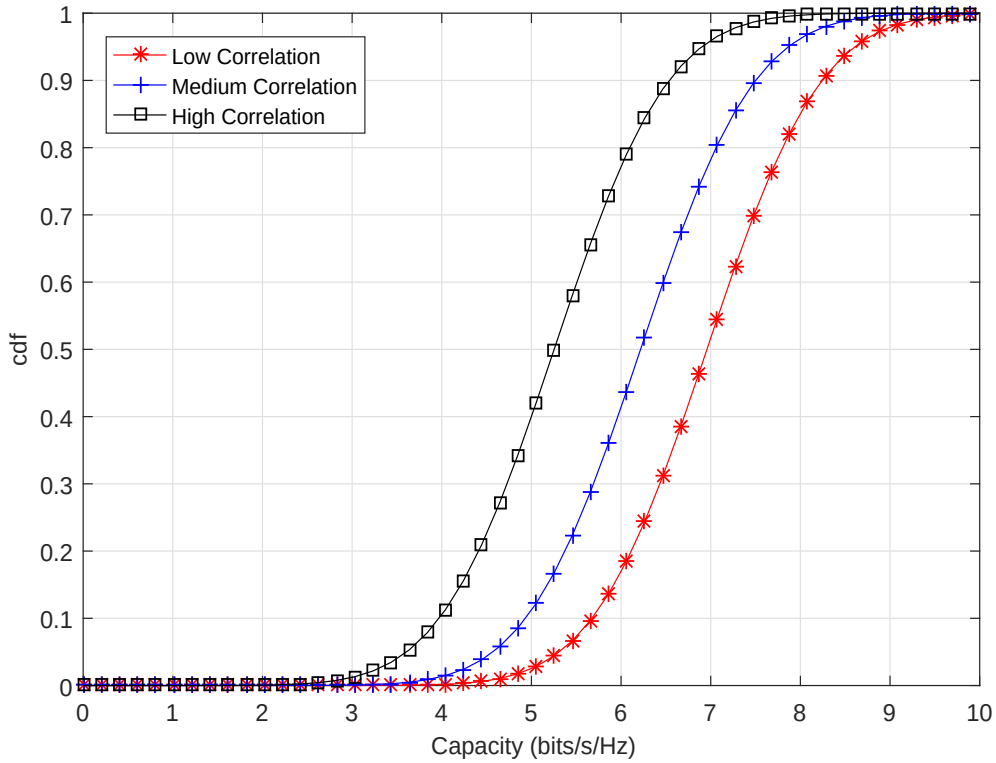

Figure 5.3: CDF for the CN as a function of correlation between the channel coefficients

Figure 5.3 shows the condition number in a MIMO system with low, medium and

high correlation between antenna elements. The lower the correlation between the channel coefficients, the higher the channel capacity will be and vice-versa. Thus, as the correlation increases, the channel capacity decreases. The condition number also represents the spatial selectivity of the channel in terms of the eigenvalue spread. A greater eigenvalue spread provides a larger difference between the maximum and minimum eigenvalues. This results in high condition number.

The relation between channel capacity and condition number with fixed SNR is shown in Figure 5.4. It illustrates that as the condition number increases, the channel capacity decreases. For example, to gain a channel capacity of 8 bits/s/Hz for a condition number of 1 dB, requires a SNR of 10 dB. As the condition number increases to 5 dB, it raises the requirement for the SNR to 20 dB. Thus, it shows that to achieve the same performance with the increase in condition number, the system requires more SNR.

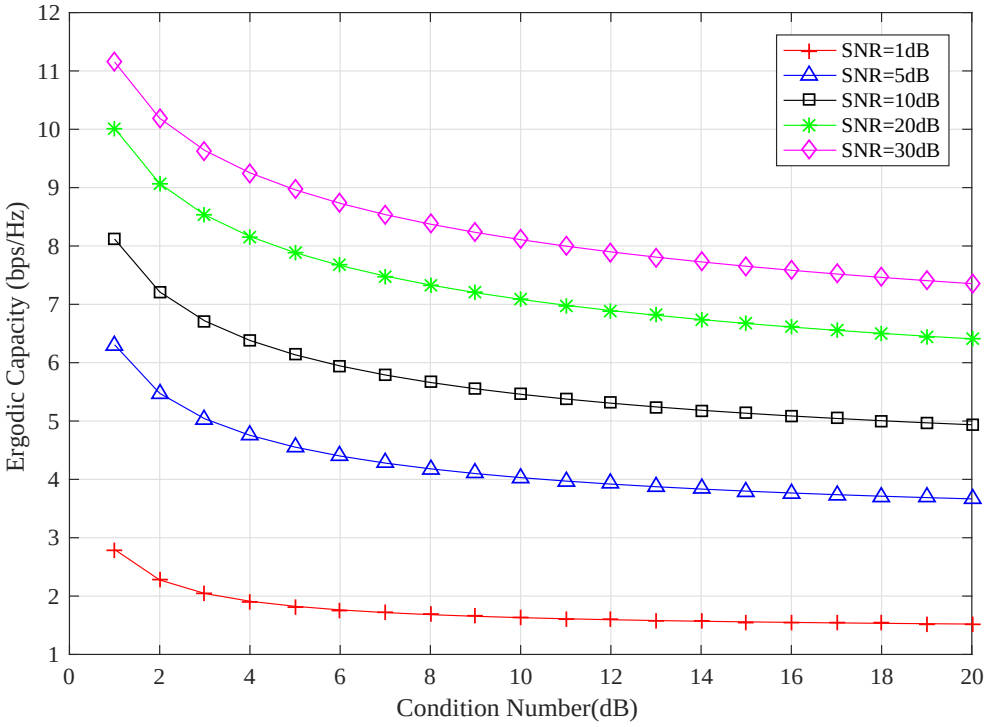

Figure 5.4: Channel capacity with varying SNR

Figure 5.5 depicts the behavior of condition number on the channel capacity with the changing SNR values. It illustrates that at the ergodic capacity of 6 bits/s/Hz, with low correlation or at lowest condition number of 1 dB, it requires SNR around 4 dB. For the highest correlation, with condition number 30 dB, it requires the SNR of 19 dB. It is evident that as the channel condition number increases the MIMO channel capacity decreases. Hence, the channels with low condition number or the highly uncorrelated channels yields high MIMO channel capacity.

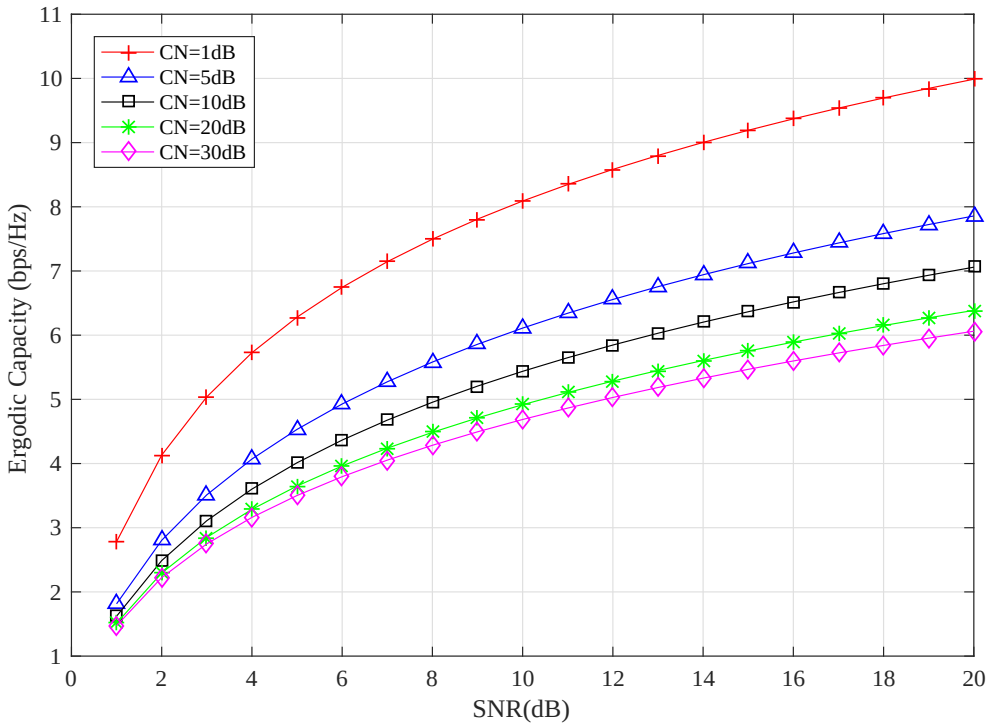

Figure 5.5: Channel capacity with varying Condition Number

5.3 Pattern Configuration Selection using CN

A traditional MIMO system provides the channel matrix with only one channel realization. In MIMO-SPA, the use of parasitic elements samples the electromagnetic field over a much wider space. It provides freedom with the availability of a number

of different channel realizations. Instead of increasing the number of active elements to increase the spatial multiplexing gain, it is possible to achieve this through the use of switching parasitic elements loaded with impedance loads.

MIMO-SPA with a number of switchable parasitic elements provides the structure with different radiation patterns. These parasitic elements acts as scatterers surrounded by the active elements. By changing the switching levels of the impedance loads, in an *on/off* manner, the parasitic elements act *in* and *out* of resonance and can modify the radiation patterns. With the optimal pattern configuration, they can modify the overall radiation pattern of the system [7].

The condition number can be used as the objective function to select the best pattern configuration from all the available pattern configurations. With this optimal selection objective, it is possible to adapt the antenna patterns to the prevailing channel conditions.

Selection criterion using CN

$$\text{Best Pattern Configuration} = min(CN)_P \tag{5.2}$$

where P represents the total number of pattern configurations in MIMO-SPA.

The condition number can be used as the channel quality metric and can be fed back to the transmitter with fewer bits. It gives information on the optimal channel state and can reduce the feedback overhead in MIMO systems.

As discussed in chapter 3 section (3.5.2), three cases with different SPA geometries provide different pattern configurations. To find the optimal pattern configuration, CN is used as the selection criterion for all three cases.

5.3.1 Configuration Selection for MIMO-SPA (2×2) using two Parasitic Elements

MIMO-SPA (2×2) with two parasitic elements at the receiver side provides four different pattern configurations as shown in Figure 3.7. All four pattern configurations with four different channel matrix realizations $(\mathbf{CH}_{00}, \mathbf{CH}_{01}, \mathbf{CH}_{10}, \mathbf{CH}_{11})$ gives different condition numbers. By doing an exhaustive search, selecting the channel matrix with (5.2) gives the minimum value of the condition number.

Table 5.2 shows the simulation results for the uncorrelated scenario. It gives the pattern configuration matrix $\mathbf{CH}_{10}$ with the minimum condition number. This is the optimal pattern configuration with the best channel quality and provides a higher channel capacity than the other configurations.

Table 5.2: Pattern configurations of MIMO-SPA (2×2) using two parasitic elements

No.	**Pattern Configurations**	**Condition Number**	**(dB)**
P1	CH00	2.20	6.84
P2	CH01	3.61	11.14
P3	CH10	1.94	5.78
P4	CH11	3.12	9.88

5.3.2 Configuration Selection for MIMO-SPA (2×2) using four Parasitic Elements

MIMO-SPA (2×2) using four parasitic elements at the receiver side provides sixteen different pattern configurations with different channel realizations as shown in Figure 3.9. All sixteen pattern configurations represent the sixteen different channel matrices $(\mathbf{CH}_{0000}, \mathbf{CH}_{0001}, ..., \mathbf{CH}_{1111})$ with dimensions (2×2) and having different condition numbers. By doing an exhaustive search, the best pattern configuration is selected

with (5.2), which has the minimum condition number.

Table 5.3 shows the simulation results for the uncorrelated scenario. It gives the pattern configuration matrix $\mathbf{CH}_{1000}$ as having the minimum condition number. This is the optimal pattern configuration in this simulation scenario, with the best channel quality, and provides a higher channel capacity than the other pattern configurations.

Table 5.3: Pattern configurations of MIMO-SPA (2×2) using four parasitic elements

No.	**Pattern Configurations**	**Condition Number**	**(dB)**
P1	CH0000	3.97	11.98
P2	CH0001	4.47	13.00
P3	CH0010	4.46	12.99
P4	CH0011	4.95	13.88
P5	CH0100	4.19	12.44
P6	CH0101	4.82	13.66
P7	CH0110	4.60	13.25
P8	CH0111	5.19	14.30
P9	CH1000	3.29	10.34
P10	CH1001	3.53	10.95
P11	CH1010	3.90	11.82
P12	CH1011	4.16	12.38
P13	CH1100	3.47	10.80
P14	CH1101	3.75	11.49
P15	CH1110	4.00	12.05
P16	CH1111	4.29	12.64

5.3.3 Configuration Selection for MIMO-SPA (4×4) using four Parasitic Elements

MIMO-SPA (4×4) using four parasitic elements at the receiver side provides sixteen different pattern configurations with different channel realizations as shown in Figure 3.11. All sixteen pattern configurations represent the sixteen different channel matrices $(\mathbf{CH}_{0000}, \mathbf{CH}_{0001} ... \mathbf{CH}_{1111})$ with dimensions (4×4) and having different condition

numbers. By doing an exhaustive search, the best pattern configuration is selected with (5.2), which has the minimum condition number.

Table 5.4 shows the simulation results for the uncorrelated scenario. It gives the pattern configuration matrix $\mathbf{CH}_{0111}$ as having the minimum condition number. It is the optimal pattern configuration in this simulation scenario, with the best channel quality, and provides a higher channel capacity than the other pattern configurations.

Table 5.4: Pattern configurations of MIMO-SPA (4×4) using four parasitic elements

No.	**Pattern Configurations**	**Condition Number**	**(dB)**
P1	CH0000	3.39	10.60
P2	CH0001	2.78	8.88
P3	CH0010	3.58	11.08
P4	CH0011	3.11	9.86
P5	CH0100	3.95	11.93
P6	CH0101	3.27	10.29
P7	CH0110	2.70	8.61
P8	CH0111	2.49	7.92
P9	CH1000	5.44	14.72
P10	CH1001	3.72	11.42
P11	CH1010	7.10	17.02
P12	CH1011	5.28	14.46
P13	CH1100	4.41	12.89
P14	CH1101	3.41	10.67
P15	CH1110	3.61	11.15
P16	CH1111	2.99	9.50

5.4 Pattern Configuration at Different SNR

According to Shannon's capacity theorem [126], the MIMO channel capacity depends on the SNR values. The pattern configuration performance also changes according to the SNR values. A CN is used as objection function to find the optimal pattern configuration for all the cases mentioned in chapter 3 (section 3.5.2). The performance

of different pattern configurations and channel capacity at different SNRs can also be shown for different three cases.

5.4.1 MIMO-SPA (2×2) using two Parasitic Elements

The behavior of different pattern configuration and channel capacity at different SNRs for MIMO (2×2) using two parasitic elements is shown in Figure 5.6. It shows that at 5 dB, the second pattern configuration ($\mathbf{CH}_{01}$) provides the highest channel capacity. For SNR 10 dB - 25 dB the third pattern configuration ($\mathbf{CH}_{10}$) can be selected as it provides the highest channel capacity.

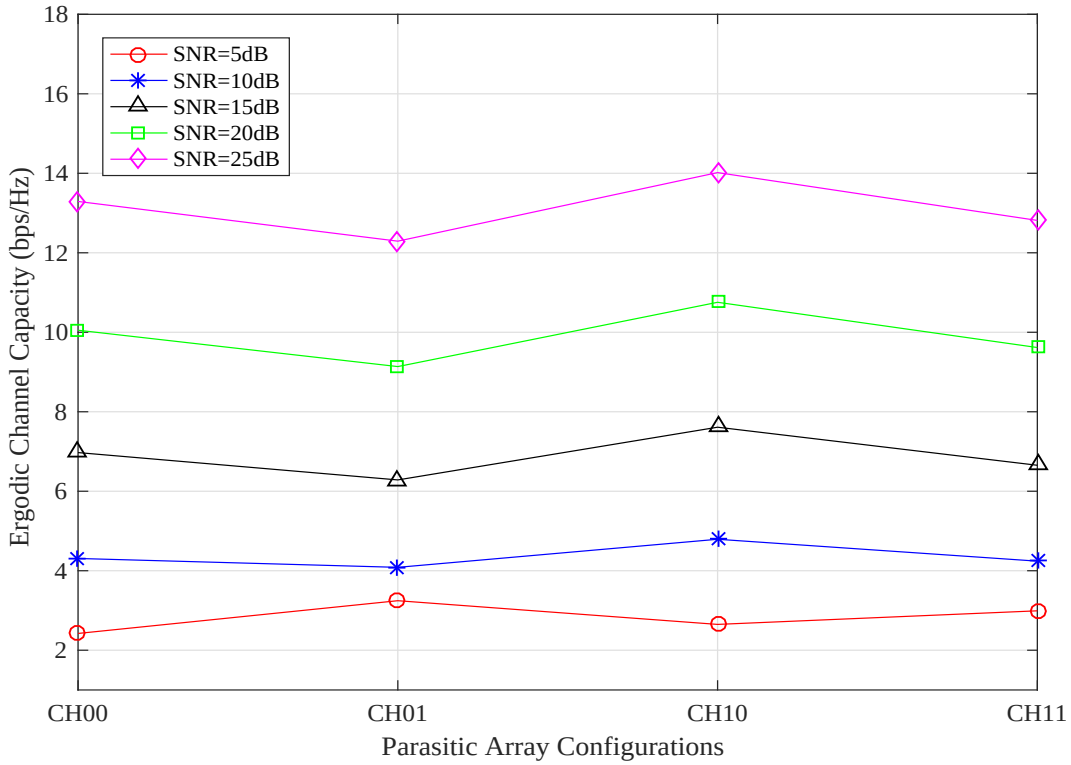

Figure 5.6: Pattern configuration selection for MIMO-SPA (2×2) using two parasitic elements at different SNR values.

5.4.2 MIMO-SPA (2×2) using four Parasitic Elements

The behavior of different pattern configurations and channel capacity at different SNRs for MIMO (2×2) using four parasitic elements is shown in Figure 5.7. It shows that at 5 dB, the pattern configuration ($\mathbf{CH}_{0111}$) provides the highest channel capacity. For SNR 10 dB - 25 dB the pattern configuration ($\mathbf{CH}_{1101}$) can be selected as it provides the highest channel capacity.

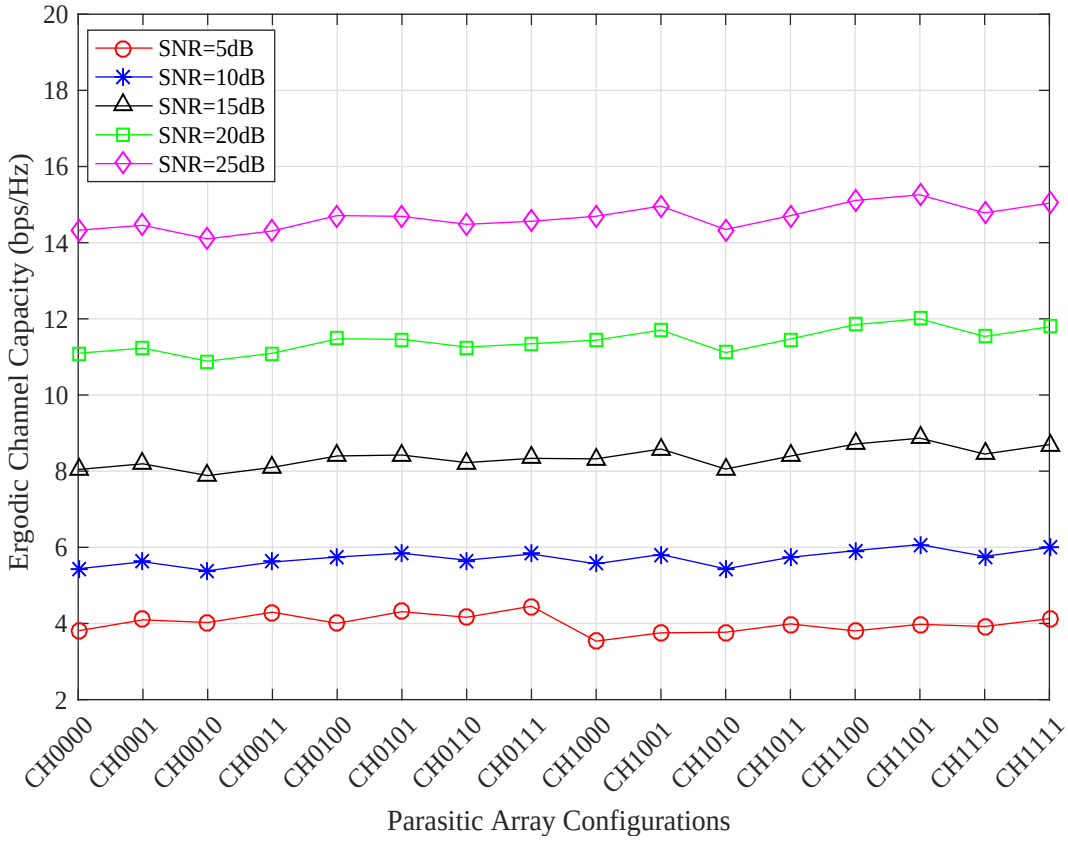

Figure 5.7: Pattern configuration selection for MIMO-SPA (2×2) using four parasitic elements at different SNR values.

5.4.3 MIMO-SPA (4×4) using four Parasitic Elements

The behavior of different pattern configurations and channel capacity at different SNRs for MIMO (4×4) using four parasitic elements is shown in Figure 5.8. It shows that at 5 dB and 10 dB, the pattern configuration ($\mathbf{CH}_{1011}$) provides the highest channel capacity. For SNR 15 dB - 25 dB the fourth pattern configuration ($\mathbf{CH}_{0011}$) can be selected as it provides the highest channel capacity.

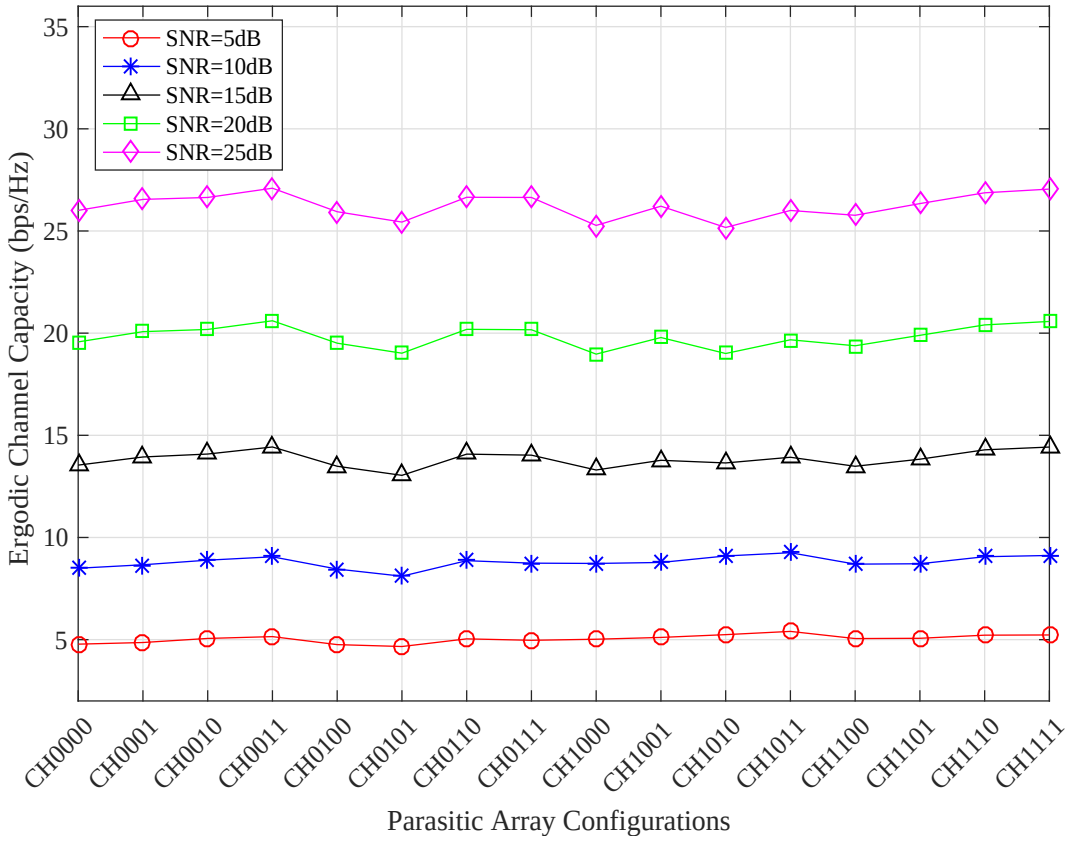

Figure 5.8: Pattern configuration selection for MIMO-SPA (4×4) using four parasitic elements at different SNR values.

5.5 Conclusion

This chapter discussed the importance of channel quality matrices to exploit the requirement of CSI at the transmitter. The relationship between the condition number and the channel capacity is discussed using simulation results. The condition number provides information on the SNR required for acceptable system performance. The distribution of the condition number gives an indication of the prevailing channel conditions and can be used in adaptive MIMO systems. A novel selection criteria selects the optimal pattern configuration depending on the channel conditions. This selection approach can be extended to broad-band channels using MIMO-OFDM technology and can reduce the feedback overhead.

Chapter 6

Conclusions

MIMO technology fulfills the demand of high date transfer rate at the expense of cost, size and hardware complexity by using a number of RF chains. In this thesis, MIMO-SPA systems have been designed with a number of active elements connected to RF chains and several parasitic elements terminated with controllable loads. These parasitic elements do not require extra RF hardware, making MIMO-SPA a viable option for small terminals, where size, cost, and DC power consumption are the main constraints. This structure is intended to reduce the number of costly power amplifiers in the transmit RF chains when compared to conventional MIMO, where each antenna element is connected with an individual RF chain. MIMO-SPA systems require parasitic elements to be placed closer to the active elements to take advantage of the mutual coupling. They can meet the requirements of the small hand-held devices, where the space for placing number of antenna elements is limited.

The potential benefits of MIMO-SPA can be achieved by changing the mutual coupling between the antenna elements. It exploits the pattern diversity and reconfigures the antenna characteristics by altering the radiation patterns in different directions. These parasitic elements need to be placed closer to the active elements for better radiation

pattern control. The change in the mutual coupling redistributes the current on the antenna elements and thus alters the radiation patterns of the antenna array. The radiation pattern control depends on the impedance loading configuration and the relative position of the parasitic elements.

The resolution of the pattern configuration is defined as $360^o/P$. It describes the possible number of directions in which the SPA antennas can direct the main beam with maximum gain. The total number of pattern configurations depends on the levels of the switches and the total number of parasitic elements. Only two states of switches *on/off* have been used in this thesis, to provide a limited level of pattern diversity for simplicity. Variations in the structural parameters of the SPA have been investigated at the operating frequency of 2.4 GHz.

The MIMO-SPA system has been demonstrated through mathematical expressions and electromagnetic theory to achieve the channel performance parameters. The thesis summarizes the research work undertaken as follows:

–*Chapter 3*: This chapter starts with the background of the parasitic array used in Yagi-Uda antennas. The parasitic elements in Yagi-Uda antennas act as reflectors and directors corresponding to the length of the parasitic elements. Use of parasitic elements exploits the pattern diversity by changing the electromagnetic mutual coupling between the antenna elements. The parasitic elements acts as reflectors and directors by switching between the terminated loads. These terminated loads on the parasitic elements has been controlled electronically in a manual way. SPA provides a pre-defined fixed number of radiation patterns.

The effect of mutual coupling on the antenna elements has been evaluated using induced EMF method. The impedance matrices show the effect of mutual coupling between the antenna elements and the loading configurations. The switching between different loading configurations changes the electrical current distribution and

the electromagnetic radiation patterns of the antenna array. The loading configurations have been tested on three testing platforms and then different radiation pattern configurations have been presented for different SPA antenna geometries.

The pattern diversity in MIMO-SPA can be further increased with the number of parasitic elements. But there are some limitations on the number of parasitic elements: too many parasitic elements will produce quite similar radiation patterns without contributing to any performance gain. They will clutter the space and will increase complexity within the communication system.

–*Chapter 4*: In this chapter, conventional MIMO model is converted to MIMO-SPA by replacing the active elements with parasitic elements to reduce the number of RF chains. MIMO-SPA shows the advantage of using parasitic elements which exploits the electromagnetic spectrum over a wider space. The channel matrix of MIMO-SPA includes the effect of the propagation environment as well as the effect of the radiating elements. The effect of SPA on the MIMO channel capacity has been calculated with reference to the impedance matrices using a mathematical model.

The theoretical ergodic capacity analysis for MIMO system is carried out with different numbers of parasitic elements. The average MIMO channel capacity improved in all cases of MIMO-SPA. In the first case, MIMO-SPA (2×2) using only two parasitic elements, the channel capacity improved from 4.1 bit/s/Hz to 5.3 bit/s/Hz compared to a conventional MIMO system using only active elements. In the second case, MIMO-SPA (2×2) using four parasitic elements, the channel capacity improved from 5.3 bit/s/Hz to 5.7 bit/s/Hz as compared to a conventional MIMO. In the last case, MIMO-SPA (4×4) using four parasitic elements, the channel capacity improved from 8.5 bit/s/Hz to 9.2 bit/s/Hz compared to a conventional MIMO system. The results show that the MIMO-SPA channel capacity is improved by using parasitic elements over the conventional MIMO system.

The channel capacity has been analyzed depending on the variation of the covariance matrix as well. In MIMO-SPA (2×2) using 2 parasitic elements an average capacity improvement from 4.9 bit/s/Hz to 5.4 bit/s/Hz has been shown as compared to the conventional MIMO. The average capacity improvement in MIMO-SPA (2×2) using 4 parasitic elements improved from 5.8 bit/s/Hz to 6.2 bit/s/Hz compared to the conventional MIMO. In MIMO-SPA (4×4) using 4 parasitic elements, the capacity improved from 9.1 bit/s/Hz to 9.8 bit/s/Hz compared to the standard MIMO using only active elements. Therefore, the selection of antenna subsets by using IAST with the optimal strategy of power allocation with WPA, provides significant channel capacity improvement over allocating transmit power uniformly across all the antennas.

The covariance matrix has been improved by using IAST and WPA techniques and also showed significant improvement in the MIMO-SPA channel capacity. The covariance matrix has also demonstrated the bounds on the channel capacity.

–*Chapter 5*: This chapter discussed the importance of channel matrices in MIMO and the feed back to the transmitter. With knowledge of the channel matrices, the transmitter can adjust its parameters for the next transmission. Rank is the channel quality metric which only provides information of the number of spatial links to achieve spatial multiplexing gain. A condition number provides the multipath richness available in the propagation channel. It provides information about the quality of channel. It indicates how much SNR is required to properly recover the MIMO transmission.

MIMO-SPA provides a number of pattern configurations according to the number of parasitic elements and the loading configuration. A condition number as a objective function has been used to select the optimal pattern configuration. It can also be sent back to the transmitter with a low-rate feedback channel.

In this thesis, induced EMF method has been proposed to generate the radiation

patterns for MIMO-SPA systems. The parasitic elements in MIMO-SPA do not require any RF hardware and need to be closely-spaced to the active transmit antennas for better control of the radiation patterns. Thus, MIMO-SPA system is an optimal solution to be implemented in portable devices, thus addressing the cost, electrical power and size constraints. According to the results obtained through this work, such antennas can be used to improve the channel capacity compared to the conventional MIMO antenna systems. They can save a considerable amount of size, cost and transmitted power. The novel pattern selection parameter can also reduce the feedback overhead in the future wireless systems.

Chapter 7

Future work

This thesis presented the analysis and practical solutions for MIMO antenna designs where size, cost, space and complexity are the main constraints. Although the use of parasitic elements is discussed with mathematical design in MIMO systems, there are still some aspects that could be further improved in this area. Future work in this research area may address the following topics:

1. Hardware Implementation Issues: In all the simulation scenarios for MIMO-SPA, for the switching purposes between the impedance loads, ideal RF switches properties are assumed as if the switches do not suffer from any insertion or attenuation losses and the switching capability of the switches is very fast without any delay.

   In a practical scenario, the RF switches do not provide instantaneous response without any losses. The selection of RF switches can be done according to the design requirements. Generally, there are two switching technologies: solid-state RF switches and MEMS based switches. Solid-state RF switches include PIN diodes and FET diodes. These diodes can achieve very fast switching speed in the order of 1-100 ns but they provide very high insertion losses. However,

MEMS based switches provides low insertion loss but with very low switching speed in the range of 1-200 μ.

2. Miniaturized designs of MIMO arrays exploiting pattern diversity:

   This thesis used dipole elements for the antenna array design. There are some other possible solution to reduce the size and cost, like patch antennas and planar-inverted F-antennas.

3. Different structures and multi-state controllable impedances:

   The geometric structure used in this work for MIMO-SPA has a small number of active elements surrounded by one ring of parasitic elements arranged in circular fashion. The arrangement with more parasitic elements could be reconfigured in two-rings of parasitic elements. The arrangement of active and parasitic elements could be configured in three dimensional or with other complex geometries as well.

   The impedance loads are terminated with two states *(on/off)* of switches. The number of switches could be controlled in multi-states. By doing this, system performance could be improved with minimum increase in the cost of the structure.

4. Feedback overhead in MIMO-OFDM:

   All the simulation results presented in this thesis are based on the flat-fading correlated Rayleigh channel. However, there are many other interesting channel scenarios, including the Ricean channel and more sophisticated channel models that could be used. Instead of a flat-fading channel, use of MIMO-SPA can be exploited in frequency-selective channels for MIMO-OFDM systems. The channel state information becomes even more relevant in the case of OFDM since there is much more channel information to estimate. Using statistical information can yield significant savings in channel feedback.

As in OFDM, with the number of subcarriers used, there is a need to estimate much more channel state information. It also puts burden on the feedback link to send this information back to the transmitter. The selection criterion with the condition number can be used to reduce the number of bits in the feedback link. Hence, investigating the condition number as a selection criterion can provide low-rate feedback that could be considered as research work in MIMO-OFDM systems.

5. Multiuser MIMO:

   The structure for MIMO systems using SPA presented in this thesis is for point-to-point communication link. The proposed model could be extended to multi-user MIMO, where the parasitic elements can be used at each receiver end.

6. Adaptive MIMO with parasitic array antennas:

   Further investigation could be done on adaptive algorithms with less computational complexity and fast convergence speed for MIMO-SPA systems. The implementation of adaptive MIMO with a parasitic antenna array would also be beneficial in terms of spectral efficiency for wireless communication systems.

References

[1] J. H. Winters, "On the capacity of radio communication systems with diversity in a Rayleigh fading environment," *IEEE Journal on Selected Areas in Communications*, vol. 5, no. 5, pp. 871–878, 1987.

[2] G. Raleigh and J. Cioffi, "Spatio-temporal coding for wireless communication," *IEEE Transactions on Communications*, vol. 46, no. 3, pp. 357–366, 1998.

[3] T. Marzetta and B. Hochwald, "Capacity of a mobile multiple-antenna communication link in Rayleigh flat fading," *IEEE Transactions on Information Theory*, vol. 45, no. 1, pp. 139–157, 1999.

[4] G. J. Foschini and M. J. Gans, "On limits of wireless communications in a fading environment when using multiple antennas," *Wireless Personal Communications*, vol. 6, no. 3, pp. 311–335, 1998.

[5] G. J. Foschini, "Layered space-time architecture for wireless communication in a fading environment when using multi-element antennas," *Bell Labs Technical Journal*, vol. 1, no. 2, pp. 41–59, 2002.

[6] H. Böleskei, D. Gesbert, and A. J. Paulraj, "On the capacity of OFDM-based multi-antenna systems," *IEEE International Conference on Acoustics, Speech and Signal Processing*, vol. 5, no. 650, pp. 2569–2572, 2000.

[7] M. D. Migliore, D. Pinchera, and F. Schettino, "Improving channel capacity using adaptive MIMO antennas," *IEEE Transactions on Antennas and Propagation*, vol. 54, no. 11, pp. 3481–3489, 2006.

[8] S. Vaihunthan, S. Haykin, and M. Sellathurai, "MIMO channel capacity modeling using Markov models," *IEEE 61st Vehicular Technology Conference*, vol. 1, pp. 126–130, 2005.

[9] P. K. Pal and R. S. Sherratt, "MIMO Channel Capacity and Configuration Selection for Switched Parasitic Antennas," *ETRI Journal*, pp. 1–10, 2018.

[10] I. E. Telatar, *Capacity of Multi-antenna Gaussian Channels*. AT&T Bell Laboratories Laboratories, 1995.

[11] R. Murch and K. Letaief, "Antenna systems for broadband wireless access," *IEEE Communications Magazine*, vol. 40, no. 4, pp. 76–83, 2002.

[12] K. Wong, R. Murch, and K. Letaief, "Performance enhancement of multiuser MIMO wireless communication systems," *IEEE Transactions on Communications*, vol. 50, no. 12, pp. 1960–1970, 2002.

[13] D. Gesbert, M. Shafi, D. S. Shiu, P. J. Smith, and A. Naguib, "From theory to practice: An overview of MIMO space-time coded wireless systems," *IEEE Journal on Selected Areas in Communications*, vol. 21, no. 3, pp. 281–302, 2003.

[14] A. J. Paulraj, D. A. Gore, R. U. Nabar, and H. Bolcskei, "An overview of MIMO communications - A key to gigabit wireless," *Proceedings of the IEEE*, vol. 92, no. 2, pp. 198–217, 2004.

[15] H. Jafarkhani, *Space-time Coding : theory and practice*. Cambridge University, 2005.

[16] M. Jankiraman, *Space-time Codes and MIMO Systems*. Artech House, 2004.

[17] T. Brown, E. Carvalho, and P. Kyritsi, *Practical guide to the MIMO radio channel with matlab examples*, 2012.

[18] J. V. Cuan-Cortes, C. Vargas-Rosales, and D. Munoz-Rodriguez, "MIMO channel capacity using antenna selection and water pouring," *EURASIP Journal on Wireless Communications and Networking*, no. 1, pp. 1–11, 2014.

[19] G. H. Golub and C. F. Van Loan, *Matrix Computations*, 3rd ed. The Johns Hopkins University Press, 1996.

[20] J. B. Andersen, "Array gain and capacity for known random channels with multiple element arrays at both ends," *IEEE Journal on Selected Areas in Communications*, vol. 18, no. 11, pp. 2172–2178, 2000.

[21] H. Sampath, P. Stoica, and A. Paulraj, "Generalized linear precoder and decoder design for MIMO channels using the weighted MMSE criterion," *IEEE Transactions on Communications*, vol. 49, no. 12, pp. 2198–2206, 2001.

[22] J. C. Roh and B. D. Rao, "Adaptive modulation for multiple antenna channels," *Proc. Asilomar Conference on Signals, Systems and Computers*, vol. 1, pp. 526–530, 2002.

[23] B. N. Getu, J. B. Andersen, and J. R. Farserotu, "MIMO systems: Optimizing the use of eigenmodes," *IEEE International Symposium on Personal, Indoor and Mobile Radio Communications*, vol. 2, pp. 1129–1133, 2003.

[24] B. M. Hochwald, T. L. Marzetta, and V. Tarokh, "Multiple-antenna channel hardening and its implications for rate feedback and scheduling," *IEEE Transactions on Information Theory*, vol. 50, no. 9, pp. 1893–1909, 2004.

[25] Y. S. Cho, J. Kim, Y. W. Young, and C.-G. Kang, *MIMO-OFDM wireless communications with MATLAB*. John Wiley & Sons (Asia) Pte. Ltd, 2010.

[26] R. K. Mallik, "The pseudo-Wishart distribution and its application to MIMO systems," *IEEE Transactions on Information Theory*, vol. 49, no. 10, pp. 2761–2769, 2003.

[27] S. Jin, M. R. Mckay, X. Gao, and I. B. Collings, "MIMO multichannel beamforming: SER and outage using new eigenvalue distributions of complex noncentral Wishart matrices," *IEEE Transactions on Communications*, vol. 56, no. 3, pp. 424–434, 2008.

[28] L. M. Garth, P. J. Smith, and M. Shafi, "Exact symbol error probabilities for SVD transmission of BPSK data over fading channels," *Proc. IEEE International Conference on Communications*, vol. 4, no. 5, pp. 2271–2276, 2005.

[29] M. Zia, T. Kiani, N. A. Saqib, T. Shah, and H. Mahmood, "Bandwidth-efficient selective retransmission for MIMO-OFDM systems," *ETRI Journal*, vol. 37, no. 1, pp. 66–76, 2015.

[30] R. Heath and D. Love, "Multimode antenna selection for spatial multiplexing systems with linear receivers," *IEEE Transactions on Signal Processing*, vol. 53, no. 8, pp. 3042–3056, 2005.

[31] S. Shim, J. S. Choi, C. Lee, and D. H. Youn, "Rank adaptive transmission to improve the detection performance of the BLAST in spatially correlated MIMO channel," *Proceedings IEEE 56th Vehicular Technology Conference*, pp. 195–198, 2002.

[32] V. Erceg, P. Soma, D. S. Baum, and A. J. Paulraj, "Capacity obtained from Multiple-Input Multiple-Output channel measurements in fixed wireless environments at 2.5 GHz," *International Conference on Communications*, vol. 1, pp. 396–400, 2002.

[33] R. W. Heath and A. J. Paulraj, "Switching between diversity and multiplexing in MIMO systems," *IEEE Transactions on Communications*, vol. 53, no. 6, pp. 962–972, 2005.

[34] D. Piazza, J. Kountouriotis, M. D'Amico, and K. R. Dandekar, "A technique for antenna configuration selection for reconfigurable circular patch arrays," *IEEE Transactions on Wireless Communications*, vol. 8, no. 3, pp. 1456–1467, 2009.

[35] A. Forenza, M. R. McKay, A. Pandharipande, R. W. Heath, and I. B. Collings, "Adaptive MIMO transmission for exploiting the capacity of spatially correlated channels," *IEEE Transactions on Vehicular Technology*, vol. 56, no. 2, pp. 619–630, 2007.

[36] D. Pinchera, S. Member, and M. D. Migliore, "Effectively exploiting parasitic arrays for secret key sharing," *IEEE Transactions on Vehicular Technology*, vol. 65, no. 1, pp. 123–131, 2016.

[37] N. Kita, W. Yamada, A. Sato, D. Mori, and S. Uwano, "Measurement of Demmel condition number for 2x2 MIMO-OFDM broadband channels," *IEEE Vehicular Technology Conference*, vol. 1, pp. 294–298, 2004.

[38] H. Artes, D. Seethaler, and F. Hlawatsch, "Efficient detection algorithms for MIMO channels a geometrical approach to approximate ML detection," *IEEE Transcations on Signal Processing*, vol. 51, no. 11, pp. 1–7, 2003.

[39] M. Matthaiou, D. I. Laurenson, and C. X. Wang, "Reduced complexity detection for Ricean MIMO channels based on condition number thresholding," in *International Wireless Communications and Mobile Computing Conference*, 2008, pp. 988–993.

[40] J. Maurer, G. Matz, and D. Seethaler, "Low-complexity and full diversity MIMO detection based on condition number thresholding," *IEEE International Con-*

ference on Acoustics, Speech and Signal Processing, vol. 3, no. 5, pp. 61–64, 2007.

[41] L. Zhou and M. Shimizu, "A novel condition number-based antenna shuffling scheme for D-STTD OFDM system," *IEEE Vehicular Technology Conference*, pp. 1–5, 2009.

[42] M. Matthaiou, D. I. Laurenson, and C. X. Wang, "On analytical derivations of the condition number distributions of dual non-central Wishart matrices," *IEEE Transactions on Wireless Communications*, vol. 8, no. 3, pp. 1212–1217, 2009.

[43] P. H. Kuo, "Channel Variations in MIMO Wireless Communication Systems : Eigen-Structure Perspectives," Ph.D. dissertation, University of Canterbury, 2007.

[44] P. Almers, E. Bonek, A. Burr, N. Czink, M. Debbah, V. Degli-Esposti, H. Hofstetter, P. Kyölsti, D. Laurenson, G. Matz, A. F. Molisch, C. Oestges, and H. Ozcelik, "Survey of channel and radio propagation models for wireless MIMO systems," *EURASIP Journal on Wireless Communications and Networking*, pp. 1–19, 2007.

[45] J. P. Kermoal, L. Schumacher, K. I. Pedersen, P. E. Mogensen, and F. Frederiksen, "A stochastic MIMO radio channel model with experimental validation," *IEEE Journal on Selected Areas in Communications*, vol. 20, no. 6, pp. 1211–1226, 2002.

[46] D. Chizhik, J. Ling, P. W. Wolniansky, R. A. Valenzuela, N. Costa, and K. Huber, "Multiple-Input-Multiple-Output measurements and modeling in Manhattan," *IEEE Journal on Selected Areas in Communications*, vol. 21, no. 3, pp. 321–331, 2003.

[47] D. Tse, *Fundamentals of Wireless Communications*. Cambridge university press, 2004.

[48] A. Lozano, A. M. Tulino, and S. Verdú, "Multiple-antenna capacity in the low-power regime," *IEEE Transactions on Information Theory*, vol. 49, no. 10, pp. 2527–2544, 2003.

[49] R. Janaswamy, "Effect of element mutual coupling on the capacity of fixed length linear arrays," *IEEE Antennas and Wireless Propagation Letters*, vol. 1, pp. 157–160, 2002.

[50] B. Clerckx, D. Vanhoenacker-Janvier, C. Oestges, and L. Vandendorpe, "Mutual coupling effects on the channel capacity and the space-time processing of MIMO communication systems," *IEEE International Conference on Communications*, vol. 4, pp. 2638–2642, 2003.

[51] H. Shin and J. H. Lee, "Capacity of multiple-antenna fading channels: Spatial fading correlation, double scattering, and keyhole," *IEEE Transactions on Information Theory*, vol. 49, no. 10, pp. 2636–2647, 2003.

[52] C. Waldschmidt, J. Hagen, and W. Wiesbeck, "Influence and modelling of mutual coupling in MIMO and diversity systems," *IEEE Antennas and Propagation Society International Symposium*, no. 3, pp. 190–193, 2002.

[53] O. Oyman, R. Nabar, H. Bolcskei, and A. Paulraj, "Characterizing the statistical properties of mutual information in MIMO channels: insights into diversity-multiplexing tradeoff," *IEEE Transcations on Signal Processing*, vol. 51, no. 11, pp. 2784–2795, 2002.

[54] G. Caire and S. Shamai, "On the achievable throughput of a multi-antenna gaussian broadcast channel," *IEEE Transactions of Information Theory*, vol. 49, no. 7, pp. 1691–1706, 2003.

[55] S. Zhou and G. B. Giannakis, "Optimal transmitter eigen-beamforming and space-time block coding based on channel correlations," *IEEE Transactions on Information Theory*, vol. 49, no. 7, pp. 1673–1690, 2003.

[56] S. Sanayei and A. Nosratinia, "Antenna selection in MIMO systems," *IEEE Communications Magazine*, vol. 42, no. 10, pp. 68–73, 2004.

[57] N. Kong and L. B. Milstein, "Average SNR of a generalized diversity selection combining scheme," *IEEE Communications Letters*, vol. 3, no. 3, pp. 57–79, 1999.

[58] M. Z. Win, N. C. Beaulieu, L. A. Shepp, B. F. Logan, and J. H. Winters, "On the SNR penalty of MPSK with hybrid selection/maximal ratio combining over i.i.d. Rayleigh fading channels," *IEEE Transactions on Communications*, vol. 51, no. 6, pp. 1012–1023, 2003.

[59] M. Z. Win and J. H. Winters, "Analysis of hybrid selection/maximal-ratio combining in rayleigh fading," *IEEE Transactions on Communications*, vol. 47, no. 12, pp. 1773–1776, 1999.

[60] Y. Choi and A. Molisch, "Fast algorithms for antenna selection in MIMO systems," *IEEE Vehicular Technology Conference*, pp. 1733–1737, 2003.

[61] J. S. Park and D. J. Park, "A new antenna selection algorithm with low complexity for MIMO wireless systems," *IEEE International Conference on Communications*, vol. 4, pp. 2308–2312, 2005.

[62] L. Xie and J. Zhan, "A novel antenna selection algorithm for MIMO systems under correlated channels," *6th International Conference on ITS Telecommunications Proceedings*, pp. 461–464, 2006.

[63] M. Gharavi-Alkhansari and A. B. Gershman, "Fast antenna subset selection in MIMO systems," *IEEE Transactions on Signal Processing*, vol. 52, no. 2, pp. 339–347, 2004.

[64] A. Gorokhov, "Antenna selection algorithms for MEA transmission systems," *IEEE International Conference on Acoustics Speech and Signal Processing*, vol. 3, no. 2, pp. 2857–2860, 2002.

[65] A. Gorokhov, D. A. Gore, and A. Paulraj, "Receive antenna selection for MIMO spatial multiplexing: Theory and algorithms," *IEEE Transactions on Signal Processing*, vol. 51, no. 11, pp. 2796–2807, 2003.

[66] M. A. Jensen and M. L. Morris, "Efficient capacity-based antenna selection for MIMO Systems," *IEEE Transactions on Vehicular Technology*, vol. 54, no. 1, pp. 110–116, 2005.

[67] A. Ghrayeb and T. Duman, "Performance analysis of MIMO systems with antenna selection over quasi-static fading channels," *IEEE Transactions on Vehicular Technology*, vol. 52, no. 2, pp. 281–288, 2003.

[68] D. A. Gore and A. J. Paulraj, "MIMO antenna subset selection with space-time coding," *IEEE Transactions on Signal Processing*, vol. 50, no. 10, pp. 2580–2588, 2002.

[69] R. W. Heath, S. Sandhu, and A. Paulraj, "Antenna selection for spatial multiplexing systems with linear receivers," *IEEE Communications Letters*, vol. 5, no. 4, pp. 142–144, 2001.

[70] A. Molisch, M. Win, and J. Winters, "Capacity of MIMO systems with antenna selection," *IEEE Transactions on Wireless Communications*, vol. 4, no. 4, pp. 1759–1772, 2005.

[71] R. S. Blum and J. H. Winters, "On optimum MIMO with antenna selection," *IEEE International Conference on Communications*, vol. 6, pp. 322–324, 2002.

[72] L. Dai, S. Sfar, and K. B. Letaief, "Receive antenna selection for MIMO systems in correlated channels," *IEEE International Conference on Communications*, vol. 5, pp. 2944–2948, 2004.

[73] ——, "Optimal antenna selection based on capacity maximization for MIMO systems in correlated channels," *IEEE Transactions on Communications*, vol. 54, no. 3, pp. 563–573, 2006.

[74] J. Costantine, Y. Tawk, S. E. Barbin, and C. G. Christodoulou, "Reconfigurable antennas: Design and applications," *Proceedings of the IEEE*, vol. 103, no. 3, pp. 424–437, 2015.

[75] R. Goossens and H. Rogier, "Optimal beam forming in the presence of mutual coupling," *Symposium on Communications and Vehicular Technology*, pp. 13–18, 2006.

[76] R. Ramirez and F. D. Flaviis, "A mutual coupling study of linear and circular polarized microstrip antennas for diversity wireless systems," *IEEE Transactions on Antennas and Propagation*, vol. 51, no. 2, pp. 238–248, 2003.

[77] A. Kalis, A. G. Kanatas, and C. B. Papadias, *Parasitic antenna arrays for wireless MIMO systems*. Springer, 2013.

[78] R. Bhagavatula, R. W. Heath, A. Forenza, N. J. Kirsch, and K. R. Dandekar, "Impact of mutual coupling on adaptive switching between MIMO transmission strategies and antenna configurations," *Wireless Personal Communications*, vol. 52, no. 1, pp. 69–87, 2010.

[79] T. Svantesson and A. Ranheim, "Mutual coupling effects on the capacity of multielement antenna systems," *IEEE International Conference on Acoustics, Speech, and Signal Processing*, vol. 4, pp. 2485–2488, 2001.

[80] J. W. Wallace and M. A. Jensen, "Termination-dependent diversity performance of coupled antennas: Network theory analysis," *IEEE Transactions on Antennas and Propagation*, vol. 52, no. 1, pp. 98–105, 2004.

[81] L. Xin and Z. ping Nie, "Effect of mutual coupling on performance of MIMO wireless channels," *IEEE Antennas and Wireless Propagation Letters*, vol. 3, pp. 368–371, 2004.

[82] P. S. Kildal and K. Rosengren, "Electromagnetic analysis of effective and apparent diversity gain of two parallel dipoles," *IEEE Antennas and Wireless Propagation Letters*, vol. 2, pp. 9–13, 2003.

[83] J. B. Andersen and B. K. Lau, "On closely coupled dipoles in a random field," *IEEE Antennas and Wireless Propagation Letters*, vol. 5, no. 1, pp. 73–75, 2006.

[84] R. Vaughan and J. Andersen, "Antenna diversity in mobile communications," *IEEE Transactions on Vehicular Technology*, vol. 36, no. 4, pp. 149–172, 1987.

[85] R. G. Vaughan, "Polarization diversity in mobile communications," *IEEE Trans. Veh. Technol*, vol. 39, no. 3, pp. 177–186, 1990.

[86] Balanis, *Antenna Theory: Analysis and Design*. John Wiley & Sons, 2005.

[87] J. O. Sophocles, *Electromagnetic waves and antennas*, Rutgers University, 2010.

[88] C. G. Christodoulou, Y. Tawk, S. A. Lane, and S. R. Erwin, "Reconfigurable antennas for wireless and space applications," *Proceedings of the IEEE*, vol. 100, no. 7, pp. 2250–2261, 2012.

[89] G. Washington, H. S. Yoon, M. Angelino, and W. H. Theunissen, "Design, modeling and optimization of a mechanically reconfigurable smart reflector antenna system," *IEEE Transactions on Antennas and Propagation*, vol. 50, no. 5, pp. 628–637, 2002.

[90] J. Y. Lee and S. N. Hwang, "A high-gain boost converter using voltage-stacking cell," *Transactions of the Korean Institute of Electrical Engineers*, vol. 57, no. 6, pp. 982–984, 2008.

[91] G. Lovat, P. Burghignoli, and S. Celozzi, "A tunable ferroelectric antenna for fixed-frequency scanning applications," *IEEE Antennas and Wireless Propagation Letters*, vol. 5, no. 1, pp. 353–356, 2006.

[92] Y. Yashchyshyn and J. W. Modelski, "Rigorous analysis and investigations of the scan antennas on a ferroelectric substrate," *IEEE Transactions on Microwave Theory and Techniques*, vol. 53, no. 2, pp. 427–438, 2005.

[93] F. Slab and D. Layer, "Experimental studies of magnetically scannable leaky-wave antennas having a corrugated ferrite slab/dielectric layer structure," *IEEE Transcations on Antennas and Propagation*, vol. 36, no. 7, pp. 911–917, 1988.

[94] D. Theil, S. Smith, *Switched parasitic antennas for cellular communications*. Artech House Publishers, 2001.

[95] L. C. Godara, "Application of antenna arrays to mobile communications, part II: Beam-forming and direction-of-arrival considerations," *Proceedings of the IEEE*, vol. 85, no. 8, pp. 1195–1245, 1997.

[96] R. Harrington, "Reactively controlled directive arrays," *IEEE Transactions on Antennas and Propagation*, vol. 26, no. 3, pp. 390–395, 1978.

[97] D. Thiel, S. O'Keefe, and J. W. Lu, "Electronic beam steering in wire and patch antenna systems using switched parasitic elements," *IEEE Antennas and Propagation Society International Symposium*, vol. 1, pp. 534–537, 1996.

[98] A. Sibille, C. Roblin, and G. Poncelet, "Circular switched monopole arrays for beam steering wireless communications," *Electronics Letters*, vol. 33, no. 7, pp. 551–552, 1997.

[99] S. Preston and D. Thiel, "Electronic beam steering using switched parasitic patch elements," *Electronics Letters*, vol. 33, no. 1, pp. 7–8, 1997.

[100] R. Vaughan, "Switched parasitic elements for antenna diversity," *IEEE Transactions on Antennas and Propagation*, vol. 47, no. 2, pp. 399–405, 1999.

[101] H. Yagi, "Beam transmission of ultra short waves," *Proceedings of the IEEE*, vol. 72, no. 5, pp. 635–645, 1984.

[102] P. Fabre and C. Gueguen, "Improvement of the fast recursive least-squares algorithms via normalization: A comparative study," *IEEE Transactions on Acoustics, Speech, and Signal Processing*, vol. 34, no. 2, pp. 296–308, 1986.

[103] M. Wennstrom and T. Svantesson, "An Antenna Solution For Mimo Channels: The Switched Parasitic Antenna," *IEEE International Symposium on Personal, Indoor and Mobile Radio Communications*, vol. 1, pp. 159–163, 2001.

[104] V. Tarokh, N. Seshadri, and A. R. Calderbank, "Space-time codes for high data rate wireless communication: Performance criterion and code construction," *IEEE Transactions on Information Theory*, vol. 44, no. 2, pp. 744–765, 1998.

[105] R. Bains and R. R. Müller, "Using parasitic elements for implementing the rotating antenna for MIMO receivers," *IEEE Transactions on Wireless Communications*, vol. 7, no. 11, pp. 4522–4533, 2008.

[106] I. Sohn and D. Gwak, "Single-RF MIMO-OFDM system with beam switching antenna," *EURASIP Journal on Wireless Communications and Networking*, no. 1, p. 37, 2016.

[107] M. Yoshida, K. Sakaguchi, and K. Araki, "Single front-end MIMO architecture with parasitic antenna elements," *IEICE Transactions on Communications*, vol. E95-B, no. 3, pp. 882–888, 2012.

[108] G. Jo, J. N. Lee, H. O. Bae, Y. H. Lee, D. Gwak, and J. H. Oh, "LTE based Spatial Multiplexing MIMO with Single Radio," in *Proceedings of the 46th European Microwave Conference*, 2016, pp. 1319–1322.

[109] G. Jo, H. O. Bae, D. Gwak, and J. H. Oh, "Demodulation of 4x4 MIMO Signal using Single RF," in *19th International Conference on Advanced Communications Technology*, 2016, pp. 390–393.

[110] K. Gyoda and T. Ohira, "Design of Electronically Steerable Passive Array Radiator (ESPAR) Antennas," *Antennas and Propagation Society International Symposium*, vol. 2, pp. 922–925, 2000.

[111] T. Ohira and K. Iigusa, "Electronically steerable parasitic array radiator antenna," *Electronics and Communications in Japan Part II-Electronics*, vol. 87, no. 10, pp. 25–45, 2004.

[112] C. Sun, A. Hirata, T. Ohira, and N. C. Karmakar, "Fast beamforming of electronically steerable parasitic array radiator antennas: Theory and experiment," *IEEE Transactions on Antennas and Propagation*, vol. 52, no. 7, pp. 1819–1832, 2004.

[113] R. Milne, "A small adaptive array antenna for mobile communications," *Antennas and Propagation Society International Symposium*, vol. 23, pp. 797–800, 1985.

[114] H. Singh, H. L. Sneha, and R. M. Jha, "Mutual coupling in phased arrays: A review," *International Journal of Antennas and Propagation*, pp. 1–23, 2013.

[115] R. W. Schlub, "Practical Realization of Switched and Adaptive Parasitic Monopole Radiating Structures," Ph.D. dissertation, Griffith University, 2004.

[116] Kyeong-Sik Min, Dong-Jin Kim, and Young-Min Moon, "Improved MIMO antenna by mutual coupling suppression between elements," *The European Conference on Wireless Technology*, pp. 135–138, 2005.

[117] H. Wang, D. G. Fang, and X. L. Wang, "Mutual coupling reduction between two microstrip patch antennas by using the parasitic elements," *Proceedings of Asia Pacific Microwave Conference*, pp. 10–13, 2008.

[118] E. D. Tapia, "Design of isofrequency reconfigurable repeaters," Ph.D. dissertation, Polytechnic University of Catalonia, 2013.

[119] J. R. Mautz and R. F. Harrington, "Modal analysis of loaded N-port scatterers," *IEEE Transactions on Antennas and Propagation*, vol. 21, no. 2, pp. 188–199, 1973.

[120] R. J. Dinger, "Reactively steered adaptive array using microstrip patch elements at 4GHz," *IEEE Transactions on Antennas and Propagation*, vol. 32, no. 8, pp. 848–856, 1984.

[121] M. R. Mofolo, A. A. Lysko, T. O. Olwal, and W. A. Clarke, "Beam steering for circular switched parasitic arrays using a combinational approach," *IEEE AFRICON Conference*, pp. 13–15, 2011.

[122] B. Schaer, K. Rambabu, J. Bornemann, and R. Vahldieck, "A simple algorithm for the control of reactances in beam steering applications with parasitic elements," *IEEE Topical Conference on Wireless Communication Technology*, pp. 394–395, 2003.

[123] S. C. Panagiotou, T. D. Dimousios, C. I. Tsitouri, and C. N. Capsalis, "A simple switched parasitic array with a fixed active element for WiFi and WLAN applications at 2.4 GHz," *Loughborough Antennas and Propagation Conference*, pp. 257–260, 2008.

[124] J. C. Ke, C. W. Ling, and S. J. Chung, "Implementation of a multi-beam switched parasitic antenna for wireless applications," *Antennas and Propagation Society International Symposium*, pp. 3368–3371, 2007.

[125] P. K. Varlamos, P. J. Papakanellos, and C. N. Capsalis, "Design of circular switched parasitic dipole arrays using a genetic algorithm," *International Journal of Wireless Information Networks*, vol. 11, no. 4, pp. 201–206, 2004.

[126] C. E. Shannon, "A mathematical theory of communication," *The Bell System Technical Journal*, vol. 27, pp. 379–423, 1948.

[127] P. J. Voltz, "Characterization of the optimum transmitter correlation matrix for MIMO with antenna subset selection," *IEEE Transactions on Communications*, vol. 51, no. 11, pp. 1779–1782, 2003.

[128] G. Tsoulos, *MIMO System Technology for Wireless Communications*. Taylor & Francis, 2006.

[129] C. Moler, "Eigenvalues and Singular Values," in *Numerical computing with MATLAB*. Society for Industrial and Applied Mathematics, 2008.

[130] R. Strang, *Introduction to Linear Algebra*. Cambridge University, 1946.

[131] J. Zik, "Maximizing LTE performance through MIMO optimization," *PCTEL Inc.,Germantown, PA, USA*, pp. 1–14, 2011.

[132] S. Schindler, "Assessing a MIMO channel," *Rhode&Schwarz*, pp. 1–18, 2011.

Appendix-A

MIMO Channel Capacity and Configuration Selection for Switched Parasitic Antennas

Paramvir Kaur Pal and Robert Simon Sherratt

Multiple-input multiple-output (MIMO) systems offer significant enhancements in terms of their data rate and channel capacity compared to traditional systems. However, correlation degrades the system performance and imposes practical limits on the number of antennas that can be incorporated into portable wireless devices. The use of switched parasitic antennas (SPAs) is a possible solution, especially where it is difficult to obtain sufficient signal decorrelation by conventional means. The covariance matrix represents the correlation present in the propagation channel, and has significant impact on the MIMO channel capacity. The results of this work demonstrate a significant improvement in the MIMO channel capacity by using SPA with the knowledge of the covariance matrix for all pattern configurations. By employing the "water-pouring algorithm" to modify the covariance matrix, the channel capacity is significantly improved compared to traditional systems, which spread transmit power uniformly across all the antennas. A condition number is also proposed as a selection metric to select the optimal pattern configuration for MIMO-SPAs.

Keywords: Condition number, Eigenvalue spread, MIMO, Switched parasitic antennas.

I. Introduction

Multiple-input multiple-output (MIMO) systems employ multiple transmit and receive antennas to improve the channel capacity and data rates using multiplexing, without increasing the transmit power or bandwidth [1], [2]. The performance enhancements obtained through MIMO techniques come at the expense of implementing multiple antennas, which occupy more space and have higher power requirements. It also increases the hardware complexity for multi-dimensional signal processing. Although MIMO systems are capable of providing the expected data rates theoretically, it is often not possible in practice owing to the spatial correlation between antennas [2]. Generating multiple spatial streams requires uncorrelated paths for each stream through the propagation medium, such that the individual streams arrive at the receiver with sufficiently distinct spatial signatures. A solution to all of these problems is to employ antennas with different radiation patterns by using switched parasitic antennas (SPAs) [3]–[5], which makes pattern diversity attractive in the design of small user terminals for MIMO communication systems. In portable communication devices, the use of SPAs reduces cost, power consumption, and hardware complexity.

The working principle of MIMO using SPA is based on electromagnetic coupling between all of the elements, and the beam-pattern is controlled by switching the loads of parasitic elements. In MIMO-SPA, few active elements are connected to the RF chains, and they are surrounded by some parasitic elements terminated with impedances loads. By modifying the controllable impedance loads, parasitic elements can be set in and out of resonance. These antennas are capable of dynamically changing their radiation properties by means of RF switches used to vary the current distribution on the antenna array structure.

Manuscript received June 6, 2017; revised Nov. 8, 2017; accepted Jan. 18, 2018.

Paramvir Kaur Pal (paramvir.kaur@pgr.reading.ac.uk) and Robert Simon Sherratt (corresponding author, r.s.sherratt@reading.ac.uk) are with the Department of Biomedical Engineering, The University of Reading, UK.

Appendix-A

Thus, it is possible to improve the received signal power, in a similar manner to beamforming arrays. In MIMO-SPAs, the parasitic elements are able to sample the electromagnetic field in a much wider space compared to the conventional MIMO systems made of active elements only. This technique helps to achieve independent fading by transmitting/receiving different signal paths at each antenna.

The pattern diversity antennas allow a number of uncorrelated patterns per antenna element, to optimally tune the wireless channel for the highest spectral efficiency [6], [7]. By choosing the antennas patterns carefully, it is possible to achieve significantly improved performance by orienting the antennas such that they have diverse radiation patterns with appropriate angles [8]–[10]. Several studies of MIMO systems have shown the benefits of pattern diversity through practical measurements with array designs that employ SPAs [11], [12]. On the other hand, carefully adjusting the radiation patterns of different antennas has the potential to reduce channel correlation and improve multiplexing gain. By properly selecting the array configuration using SPAs, it is possible to choose the channel scenario that allows for the highest throughput in MIMO wireless communication systems [13].

The MIMO channel generally includes the propagation environment, as well as the physical transmit and receive antenna array designs. Changes to any of these sub-systems can significantly impact the channel capacity. MIMO systems allow a growth in transmission rate that is linear in terms of the minimum number of antennas at each end of the wireless link [14]. This performance enhancement strongly depends on the quality of the channel state information (CSI) which is available at the transmitter and the receiver links. The best performance can be achieved when such CSI is complete and perfect at both ends of the communication link. However, this is not practically feasible, especially at the transmitter side owing to feedback overhead and bandwidth requirements. However, this can be achieved with the knowledge of the covariance matrix, and can be fed back to the transmitter [15].

The eigenvalue spread (EVS) of the covariance matrix is the most widely used indicator of spatial selectivity to estimate the effective spatial links that are possible within a MIMO system [16]. The two important MIMO channel metrics based on eigenvalues are the rank and condition number (CN), and they reveal important MIMO system characteristics in the spatial domain. The rank of the transmission matrix indicates the number of data streams that can be spatially multiplexed on a MIMO link. However, it does not give any indication about the quality of the channel matrix, whether it is a well-conditioned or ill-conditioned channel. CN indicates the channel quality [17], [18], and is related to the EVS of the channel matrix. A high EVS indicates that the channel is correlated with a high condition number, and this is referred to as an ill-conditioned channel matrix. Thus, small variations in the channel coefficients will result in drastic variations at the receiver side, making the system unstable. Most of the research work uses the CN as a selection criterion for several purposes. Heath and Paulraj [19] used a CN of the MIMO channel to perform switching between diversity and multiplexing gain purposes. In a similar way, Piazza et al. [20] used a CN to switch between different modes of circular patch reconfigurable antennas. For the adaptive modulation scheme, CN was used by Forenza et al. to obtain the spatial selectivity of the channel [21]. In other studies [22], [23], the regular CN (or its reciprocal) was used to evaluate the quality of the channel matrix as it provides some intuition on channel quality. Thus, the CN can indicate the quality of the MIMO channel to the transmitter using fewer bits, and can overcome the feedback bandwidth requirements.

The feedback mechanism can be more rigorously designed and is more feasible in practice if the dynamic behaviour of the eigenvalues is known statistically. In the absence of the CSI at the transmitter, the best strategy for power allocation is to distribute the power evenly across the antennas. In a high signal-to-noise ratio (SNR) regime, greater capacity can be achieved if the eigenvalues are less spread out. However, in a low-SNR regime, the optimal policy is to inject power into the strongest eigenvalue only, as in the case of beamforming. By using the 'water-pouring algorithm (WPA), the channel capacity can be achieved if the transmission power distributed on the eigenvalues is based on the quality of the channel [24].

The focus of this paper is to propose the use of SPAs in MIMO systems with the knowledge of channel correlation in the form of the covariance matrix. In comparison to conventional MIMO, MIMO-SPAs need a smaller number of RF chains, which reduces cost, space, and hardware complexity. Using parasitic elements, it is possible to perform switching between different radiation patterns by changing the terminated impedance loads separately without affecting the transceiver design. This paper uses the increment antenna selection technique (I-AST) with WPA for proper power allocation in order to achieve the MIMO channel capacity. A CN is also proposed as a selection criterion to select the optimal pattern configuration at the receiver side by using the exhaustive search method. The results show that the channel capacity has been improved by using a covariance matrix for

https://doi.org/10.4218/etrij.2017-0071

optimal power allocation compared to the conventional means with equal power allocated across all the transmit antennas.

This paper is organized as follows: Section II describes the overall MIMO system model, Section III presents details of parasitic antenna theory with different pattern configurations, and Section IV shows simulation results of the MIMO channel capacity with the knowledge of different covariance matrices. Finally, Section V concludes the paper.

II. MIMO System Model

A typical MIMO communication link consists of M_T transmit and N_R receive antennas, and the resulting MIMO channel can be described by an $M_T \times N_R$ channel matrix $\mathbf{H}$, whose $(i;j)$th entry characterizes the path between the jth transmit and the ith receive antenna. $\mathbf{Z_{Tx}}$ and $\mathbf{Z_{Rx}}$ represent the impedance matrices on the transmitter and receiver sides, respectively [25]. Using Thevenin's theorem, the M_T sources at the transmitter side can be represented as an ideal voltage in series with lumped impedance $\mathbf{Z_S}$. The input current can be found as [7]:

$$\widetilde{\mathbf{I}}_\mathbf{S} = (\mathbf{Z_{Tx}} + \mathbf{Z_S})^{-1}\widetilde{\mathbf{V}}_\mathbf{S}, \tag{1}$$

where $\widetilde{\mathbf{I}}_\mathbf{S} = [I_{S1}, I_{S2}, \ldots, I_{SM_T}]^T$, $\widetilde{\mathbf{V}}_\mathbf{S} = [V_{S1}, V_{S2}, \ldots, V_{SM_T}]^T$, and $\mathbf{Z_S} = \mathrm{diag}(Z_{S1}, Z_{S2}, \ldots, Z_{SM_T})$.

As previously shown [7], assume an operator $\mathbf{G}$ that relates the gap current vector $\widetilde{\mathbf{I}}_\mathbf{S}$ to the vector $\widetilde{\mathbf{V}}_\mathbf{O} = [V_{O1}, V_{O2}, \ldots, V_{ON_R}]^T$. Thus, the voltage at the N_R receiving antennas is:

$$\widetilde{\mathbf{V}}_\mathbf{O} = \mathbf{G}\widetilde{\mathbf{I}}_\mathbf{S}. \tag{2}$$

At the receiver side, the open-circuit voltage vector $\widetilde{\mathbf{V}}_\mathbf{O}$ is related to the voltages $\mathbf{V_R}$ with the receiver impedances $\mathbf{Z_L}$ as follows:

$$\widetilde{\mathbf{V}}_\mathbf{R} = \mathbf{Z_{Rx}}(\mathbf{Z_{Rx}} + \mathbf{Z_L})^{-1}\widetilde{\mathbf{V}}_\mathbf{O}, \tag{3}$$

where $\widetilde{\mathbf{V}}_\mathbf{R} = [V_{R1}, V_{R2}, \ldots, V_{RN_R}]^T$, $\mathbf{Z_L} = \mathrm{diag}(Z_{L1}, Z_{L2}, \ldots, Z_{LN_R})$, and $\mathbf{Z_{Rx}}$ is the impedance matrix of the receiving array.

A direct relation between the transmitting and receiving voltages can be obtained as [7]:

$$\widetilde{\mathbf{V}}_\mathbf{R} = \mathbf{Z_{Rx}}(\mathbf{Z_{Rx}} + \mathbf{Z_L})^{-1}\mathbf{G}(\mathbf{Z_{Tx}} + \mathbf{Z_S})^{-1}\widetilde{\mathbf{V}}_\mathbf{S} = \widetilde{\mathbf{H}}\widetilde{\mathbf{V}}_\mathbf{S}, \tag{4}$$

where $\mathbf{Z_S}$ and $\mathbf{Z_L}$ are the controlling load impedances at the transmitter and receiver sides, respectively. Thus, if the number of parasitic elements changes, there will only be a change in the impedance matrices in the design. It is not possible to calculate voltages across parasitic elements directly, and it can thus be calculated as:

$$\mathbf{V_R} = \mathbf{S_R}\widetilde{\mathbf{H}}\widetilde{\mathbf{V}}_\mathbf{S}, \tag{5}$$

where $\mathbf{S_R}$ is a permutation matrix. Further the values of $\widetilde{\mathbf{H}}$ that are relative to active elements at the receiver side are extracted. If the parasitic elements are connected to the transmitting side, then Z_{S_i} is the variable impedance that controls the elements, and $V_{S_i} = 0$. The voltage at the receiver side can thus be described as:

$$\mathbf{V_R} = \mathbf{S_R}\widetilde{\mathbf{H}}\mathbf{S_T}\mathbf{V_S} = \mathbf{H}\mathbf{V_S}, \tag{6}$$

where $\mathbf{S_T}$ is a permutation matrix, and extract the values of $\widetilde{\mathbf{H}}$ that are relative to active elements at the transmitter side, and $\mathbf{V_S}$ is the vector of the voltages at the transmitter. In (6), $\mathbf{H}$ corresponds to the channel matrix of the suggested MIMO system. As the parasitic elements are not connected to any RF source, the output cannot be observed directly on the parasitic elements, but can be collected at the active elements owing to the strong electromagnetic coupling effect. The MIMO system using SPA will provide different channel matrices $\mathbf{H}$ depending on the number of parasitic elements and the number of states of parasitic loads at the transmitter and receiver sides.

In this paper, parasitic elements are used only at the receiver side for simplicity, thus changing the loads of impedance matrix $\mathbf{Z_L}$. It is also possible to change the parasitic controlling impedances at the transmitter side, such as at a base station, but it will significantly impact all of the users at the receiver side.

When communicating over MIMO fading channels, $\mathbf{H}$ is a random matrix that depends on the specific system architecture and the specific propagation conditions. Hence, $\mathbf{H}$ is considered to be obtained from a certain probability distribution, which characterizes the system and scenario of interest, and is known as the MIMO channel matrix. In MIMO wireless communications, the large number of scatterers in the channel, which contribute to the signal at the receiver, results in zero-mean Gaussian distributed channel matrix coefficients. The highest channel capacity in the ideal case is possible with a rich scattering environment, where it ensures that all of the channel coefficients of the channel matrix are uncorrelated.

The transmitted symbol vector $\mathbf{s}$, which is composed of M_T independent input symbols $s_1, s_2, \ldots, s_{M_T}$, is transmitted from M_T active transmit antennas. Then, the received signal can be written as follows:

$$\mathbf{y} = \sqrt{\frac{E_s}{M_T}}\mathbf{H}\mathbf{s} + \mathbf{n}, \tag{7}$$

Appendix-A

where $\mathbf{n} = (n_1, n_2, \ldots, n_{N_R})^T$ is a noise vector, which is assumed to be a zero-mean circular symmetric complex Gaussian. The autocorrelation of the transmitted signal vector is defined as: $\mathbf{R_{ss}} = \mathrm{E}\{ss^H\}$. The total transmission power for each transmit antenna is assumed to be 1, such as $\mathrm{Tr}(\mathbf{R_{ss}}) = M_T$.

When the CSI is available at the transmitter side, singular value decomposition (SVD) can be performed to identify the number of independent equations out of multiple equations of the MIMO system. Accordingly, the transmitted signal can be pre-processed with $\mathbf{V}$ in the transmitter, and then the received signal can be post-processed with $\mathbf{U}^H$. The output of the MIMO system can be described as:

$$\tilde{\mathbf{y}} = \sqrt{\frac{E_s}{M_T}}\mathbf{U}^H\mathbf{H}\mathbf{V}\tilde{\mathbf{s}} + \tilde{\mathbf{n}}. \tag{8}$$

Using the SVD model, the number of MIMO channels is divided into a number of independent SISO channels. The channel matrix $\mathbf{H} \in \mathbb{C}^{M_T \times N_R}$ with SVD can be represented as:

$$\mathbf{H} = \mathbf{U}\Sigma\mathbf{V}^H, \tag{9}$$

where $\mathbf{U} \in \mathbb{C}^{N_R \times N_R}$ and $\mathbf{V} \in \mathbb{C}^{M_T \times M_T}$ are unitary matrices, and $\mathbf{\Sigma} \in \mathbb{C}^{M_T \times N_R}$ is a rectangular matrix whose diagonal elements are non-negative real numbers, and whose off-diagonal elements are zero. The diagonal elements of $\mathbf{\Sigma}$ are the singular values of the matrix $\mathbf{H}$, and are denoted by $\sigma_1, \sigma_2, \ldots, \sigma_{\min}$, where $N_{\min} \triangleq \min(M_T, N_R)$. In fact, $\sigma_1 \geq \sigma_2 \geq \cdots \geq \sigma_{\min}$, that is, the diagonal elements of $\mathbf{\Sigma}$, are the ordered singular values of the matrix $\mathbf{H}$. The rank of $\mathbf{H}$ corresponds to the number of non-zero singular values, such that $\mathrm{rank}(\mathbf{H}) \leq N_{\min}$.

The MIMO channel capacity is evaluated using Shannon's theory as follows [26]:

$$C = \mathrm{E}\left\{\max_{\mathrm{Tr}(\mathbf{R_{ss}})=M_T} \log_2 \det\left(\mathbf{I}_{N_R} + \frac{E_S}{M_T N_0}\mathbf{H}\mathbf{R_{ss}}\mathbf{H}^H\right)\right\}, \tag{10}$$

where E_S is the total transmitted power, and N_0 is the variance of the additive white Gaussian noise at the receiver. In a flat-fading MIMO system, channel matrix $\mathbf{H}$ is a Rayleigh fading model with independent distribution. The covariance matrix $\mathbf{R_{ss}}$ should be determined in order to satisfy the transmitter power constraints. If the CSI is known at the transmitter, then WPA can be used by employing the increment antenna selection technique (I-AST) to improve the channel capacity.

III. Parasitic Array Theory

The Yagi-Uda antenna is a linear multi-element array [27], and consists of one active dipole and a number of parasitic dipoles. The parasitic dipoles are placed close to the active element, so that strong currents are induced in them. The SPA concept originates from the Yagi-Uda dipole array. Electromagnetic mutual coupling has been used as a design tool in order to meet the antenna requirements. The distribution of the currents on the parasitic elements of the array can be carefully designed by adjusting the spacing between the elements and the length of the parasitic dipoles. In the case of the Yagi-Uda antennas, the lengths of all elements are mechanically fixed with different sizes. However, in SPA, the variation of the parasitic elements' electrical equivalent lengths enables the parasitic elements to be switched between the reflector and director state by using the switches [28].

When the RF switch is in the OFF state, the corresponding parasitic element is open-circuited and acts as a director. Therefore, the parasitic element does not have a resonant length, and a minimal amount of current is induced into it. When the switch is in the ON state, the corresponding parasitic element is short-circuited and acts as a reflector. Therefore, the parasitic element acquires a resonant length and strong currents are induced in it. By simply changing the position of the ON/OFF switches, a number of diverse radiation patterns can therefore be created in different angular directions. The most common antenna structure used for this purpose is the circular array [29]. In this case, active elements are placed at the center, and a number of parasitic elements are evenly spaced on the periphery of a circle with radius d, around the active elements. Parasitic arrays also have symmetrical properties if there is an even number of parasitic elements.

In this paper, the total number of the parasitic elements is assumed to be P, and the number of possible states of the impedance load on the parasitic elements is denoted by L_S. The total number of combinations that can be attained by changing the load states of the parasitic elements are [28]:

$$\text{Total combinations} = (L_S)^P. \tag{11}$$

With $P = 2$ and $L = 2$, there are total four combinations, as shown in Fig. 1. These combinations are achieved by changing the impedance loads of parasitic elements between Z_{ON} and Z_{OFF}. The ON state is represented by binary "1," and the OFF state is represented by binary "0."

The active elements are driven by voltages V_1 and V_2. I_1 and I_2 represent the current across the two elements, and are calculated by solving the network equations:

Appendix-A

$$\begin{aligned} V_1 &= Z_{11}I_1 + Z_{12}I_2 + \cdots + Z_{1N}I_N \\ V_2 &= Z_{21}I_1 + Z_{22}I_2 + \cdots + Z_{2N}I_N \\ &= \quad \vdots \\ V_N &= Z_{N1}I_1 + Z_{N2}I_2 + \cdots + Z_{NN}I_N. \end{aligned} \tag{12}$$

Alternatively, (12) can be written in matrix form, which is normally referred to as the impedance matrix equation:

$$\begin{bmatrix} V_1 \\ V_2 \\ \vdots \\ V_N \end{bmatrix} = \begin{bmatrix} Z_{11} & Z_{12} & \cdots & Z_{1N} \\ Z_{21} & Z_{22} & \cdots & Z_{2N} \\ \vdots & & \ddots & \vdots \\ Z_{N1} & Z_{N2} & \cdots & Z_{NN} \end{bmatrix} \begin{bmatrix} I_1 \\ I_2 \\ \vdots \\ I_N \end{bmatrix}, \tag{13}$$

which can also be represented as:

$$\mathbf{V} = \mathbf{ZI}, \tag{14}$$

where $\mathbf{V}$ is the column vector of the excitation voltages $\mathbf{V_i}$, for $n = 1, 2, \ldots, N$. $\mathbf{Z}$ is the square impedance matrix, which is formed by the self and mutual impedances of the elements of the array. $\mathbf{I}$ is the column vector of the complex currents along the array elements. In this paper, there are two active elements present at the receiver side. The active elements are typically terminated with 50-Ω loads, and parasitic elements are terminated with the impedance loads:

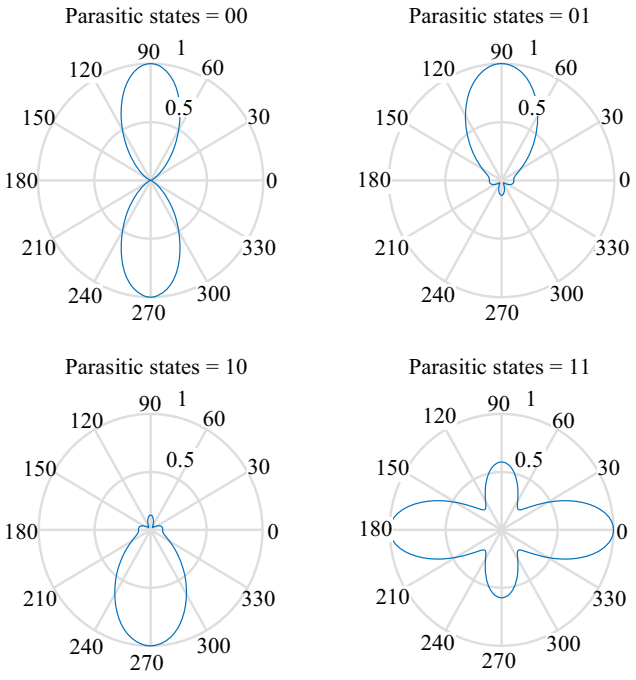

Fig. 1. Typical radiation patterns for load configurations.

$$\begin{bmatrix} V_1 \\ V_2 \\ 0 \\ \vdots \\ V_N \end{bmatrix} = \begin{bmatrix} Z_{11} & Z_{12} & Z_{13} & \cdots & Z_{1N} \\ Z_{21} & Z_{22} & Z_{23} & \cdots & Z_{2N} \\ Z_{31} & Z_{32} & Z_{33}+Z_{L3} & \cdots & Z_{3N} \\ \vdots & \vdots & \vdots & \ddots & \vdots \\ Z_{N1} & Z_{N2} & Z_{N3} & \cdots & Z_{NN}+Z_{LN} \end{bmatrix} \begin{bmatrix} I_1 \\ I_2 \\ I_3 \\ \vdots \\ I_N \end{bmatrix} \tag{15}$$

or can be written as [28]:

$$\mathbf{V} = [\mathbf{Z} + \mathbf{Z_L}]\mathbf{I}, \tag{16}$$

where $\mathbf{Z_L}$ is the diagonal matrix consisting of the impedance loads across the terminal of each passive element:

$$\mathbf{Z_L} = \begin{bmatrix} 0 & 0 & 0 & \cdots & 0 \\ 0 & 0 & 0 & \cdots & 0 \\ 0 & 0 & Z_{L_3} & \cdots & 0 \\ \vdots & \vdots & \vdots & \ddots & \vdots \\ 0 & 0 & 0 & \cdots & Z_{L_P} \end{bmatrix}, \tag{17}$$

where Z_{L_P} is the impedance load connected to the pth parasitic element in the array. In the load matrix $\mathbf{Z_L}$, all the diagonal entries except the first two are non-zero. The first two entries are zero because the active elements are not connected to any controllable impedance loads. This load matrix can be computed separately from the impedance matrix. This feature is beneficial because the impedance loads of the individual parasitic elements can be changed separately. The new impedance matrix is computed using the induced electromagnetic force (EMF) method [27] by adding the initial impedance matrix and the load matrix. Once the impedance matrix is computed, the individual element's current excitations can be calculated easily.

The dipole antennas are used as antenna array elements to generate different radiation patterns using the EMF method [27], as shown in Fig. 1. The structural parameters were calculated based on the array theory [28]. Here, the variable impedances have only two different levels (Z_{ON}, Z_{OFF}), which give $(L_S)^P$ different pattern configurations. Thereafter, all of the antenna attributes, including radiation patterns, can be calculated.

IV. Results

In this work, MIMO systems have two transmitting and two receiving antennas with the channel matrix $\mathbf{H}$ (2×2), but using switched parasitic elements ($P = 2$) at the receiver side only.

http://onlinelibrary.wiley.com/journal/10.4218/(ISSN)2233-7326

Appendix-A

The simulation scenario for a MIMO system (2 × 2) using two parasitic elements at the receiver side only is given as follows:

- Number of active elements on the transmitter side $M_{\text{ta}} = 2$
- Number of active elements on the receiver side $N_{\text{ra}} = 2$
- Number of parasitic elements on the transmitter side $M_{\text{tp}} = 0$
- Number of parasitic elements on the receiver side $N_{\text{rp}} = 2$
- Total number of elements on the transmitter side $M_{\text{T}} = M_{\text{ta}} + M_{\text{tp}} = 2$
- Total number of elements on the receiver side $N_{\text{R}} = N_{\text{ra}} + N_{\text{rp}} = 4$

Two parasitic antennas with ON/OFF states give four different pattern configurations on the receiver side. In MIMO-SPAs, there are four different channel matrices ($\mathbf{CH_{00}}, \mathbf{CH_{01}}, \mathbf{CH_{10}}, \mathbf{CH_{11}}$), according to the state of the switches (ON/OFF). The channel matrix ($\mathbf{CH_{00}}$), when both of the parasitic elements switches are in the OFF state, is similar to the conventional MIMO (without using any parasitic elements).

With the knowledge of these matrices, it is possible to evaluate the Shannon's channel capacity as follows [24]:

$$C = \log_2\left(\left|I_{N_{\text{R}}} + \frac{E_S}{M_{\text{T}} N_0}\mathbf{H}\mathbf{R}_{\mathbf{ss}}\mathbf{H}^H\right|\right). \tag{18}$$

The covariance matrix $\mathbf{R_{ss}}$ should be determined to satisfy the transmitter power constraints. With four different channel matrices, the MIMO channel capacity will be different across each pattern configuration. The more the channel is correlated, the lower will be the channel capacity.

1. Influence of Covariance Matrix

It is well known that the covariance matrix can change the channel capacity mainly according to the power allocation at the transmitter side by using SVD [24].

To determine the effect of the covariance matrix on the MIMO channel capacity, two different propagation medium cases can be analyzed:

i Uncorrelated

ii Correlated.

In the uncorrelated case, the covariance matrix is an identity matrix. The diagonal elements of the matrix $\mathbf{R_{ss}}$ are 1's and all other elements are zeros. This means that all of the channel coefficients are uncorrelated. Thus, equal power is allocated to all of the transmit antennas. Figure 2 shows that the ergodic channel capacity increases with respect to SNR in the uncorrelated case.

In the correlated case, all the elements of the covariance matrix are set to 1. This means that all of the channel coefficients are correlated. The channel capacity decreases with respect to SNR owing to the correlation effect, as shown in Fig. 3. The high correlation provided by the matrix $\mathbf{R_{ss}}$, represents a negative influence on the channel capacity.

If the channel conditions are known to the transmitter, then the incremental/decremental antenna-selection techniques can be applied with the WPA for proper power

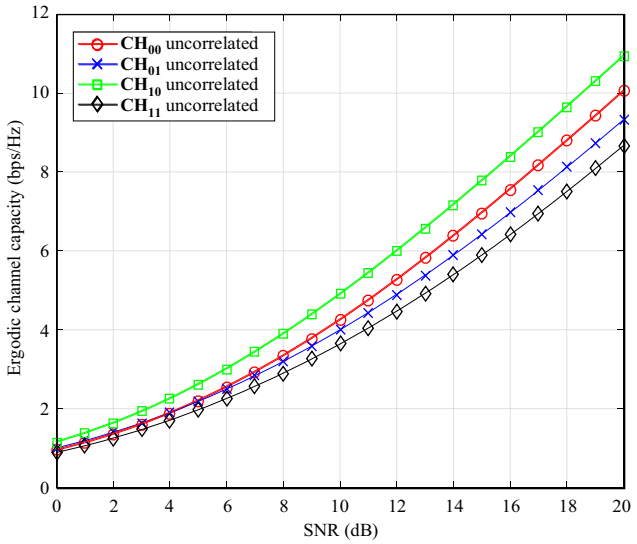

Fig. 2. Channel capacity using identity matrix as covariance matrix.

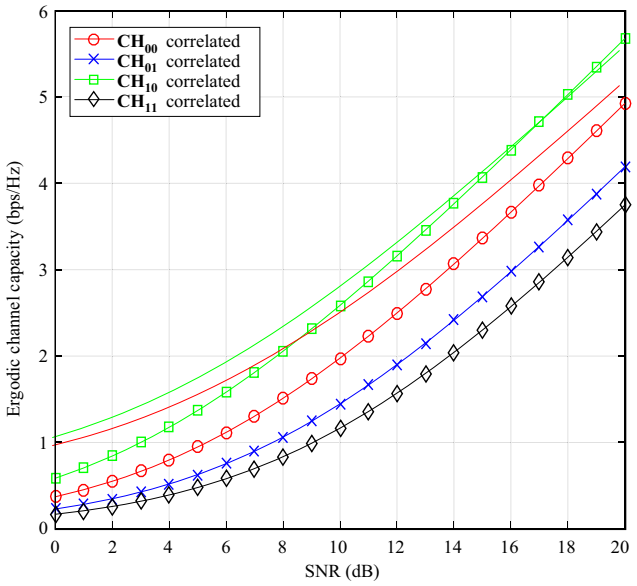

Fig. 3. Channel capacity using matrix of all ones as covariance matrix.

https://doi.org/10.4218/etrij.2017-0071

Appendix-A

allocation at the transmitter side. The knowledge of the channel conditions can be fed back to the transmitter in the form of a covariance matrix. The covariance matrix represents the correlation present in the channel, and with WPA, more power can be distributed to the best channel, and less power to channels that contribute less to the channel capacity.

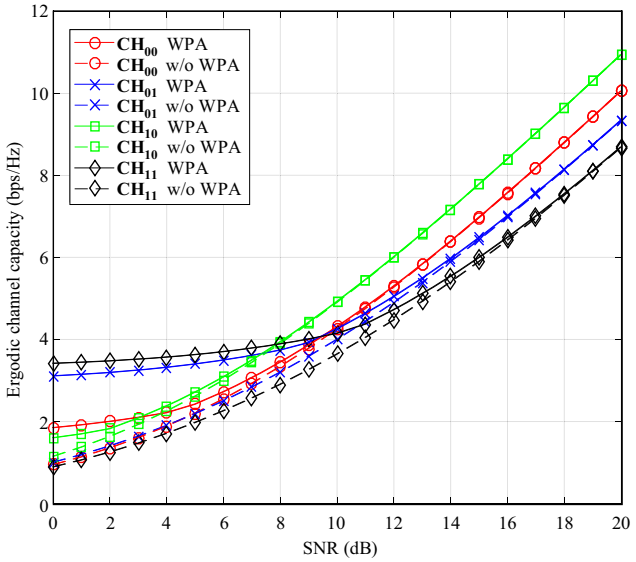

Fig. 4. Comparison of all pattern configuration matrices with and without WPA.

A comparison of four different configurations for the uncorrelated case with and without WPA is shown in Fig. 4. For all of the parasitic configurations, the MIMO channel capacity is improved with the power allocation using WPA as compared to the equal power distribution across all the eigenvalues.

2. Comparison of Different Covariance Matrices

In this section, the I-AST is used to select the best set of antennas, and then allocates power by carrying out WPA.

The comparison between covariance matrices across all the pattern configurations is shown in Fig. 5. The comparison is discussed with three different covariance matrices as follows:

- I-AST with correlated covariance matrix- $[\mathbf{R}_{ss}]_{corr}$
- I-AST with uncorrelated covariance matrix- $[\mathbf{R}_{ss}]_{uncorr}$
- I-AST with improved covariance matrix WPA-$[\mathbf{R}_{ss}]_{WPA}$

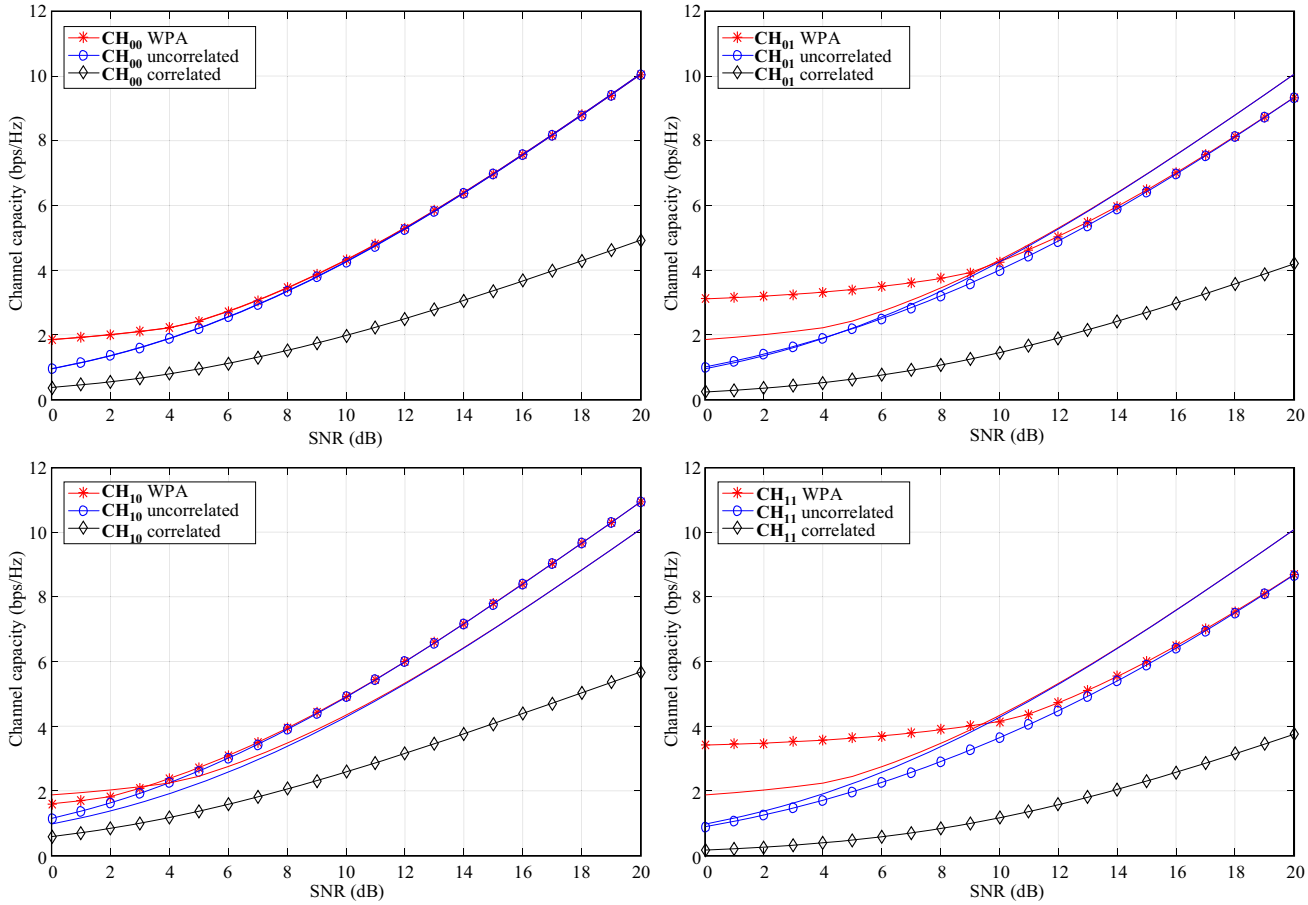

Fig. 5. Comparison of channel capacity with three different forms of covariance matrices across all pattern configurations.

http://onlinelibrary.wiley.com/journal/10.4218/(ISSN)2233-7326

In this comparison, when the channel matrix is correlated, it gives the lower bounds for the MIMO channel capacity for all of the pattern configurations. When the channel matrix is uncorrelated with I-AST, the channel capacity is improved compared to the correlated case. Figure 5 shows that when the covariance matrix is improved with WPA, in all different configuration matrices, the channel capacity provides the upper bounds. These are the bounds according to the influence of the covariance matrix in three different cases.

3. Pattern Configuration Selection

CN is known as the channel quality indicator and used to obtain the best pattern configuration. It represents the EVS of the channel as [15]:

$$\mathrm{CN} = \frac{\lambda_{\max}}{\lambda_{\min}}, \tag{19}$$

where $\lambda_{\max}$ and $\lambda_{\min}$ are the maximum and minimum eigenvalues of the covariance matrix, respectively.

If eigenvalues of the covariance matrix are less spread out, it provides a small CN value. In MIMO-SPAs, there are four different pattern configurations. All four pattern configurations represent the four different channel matrices $(\mathbf{CH_{00}}, \mathbf{CH_{01}}, \mathbf{CH_{10}}, \mathbf{CH_{11}})$, and have different CNs. By performing the exhaustive search, the channel matrix or pattern that has a low CN is selected. For the selection purpose in the uncorrelated case, as shown in Fig. 5, the pattern configuration $\mathbf{CH_{10}}$ matrix with the lowest CN is selected. This is the optimal pattern configuration with the best channel quality, and provides the greatest channel capacity compared with other configurations.

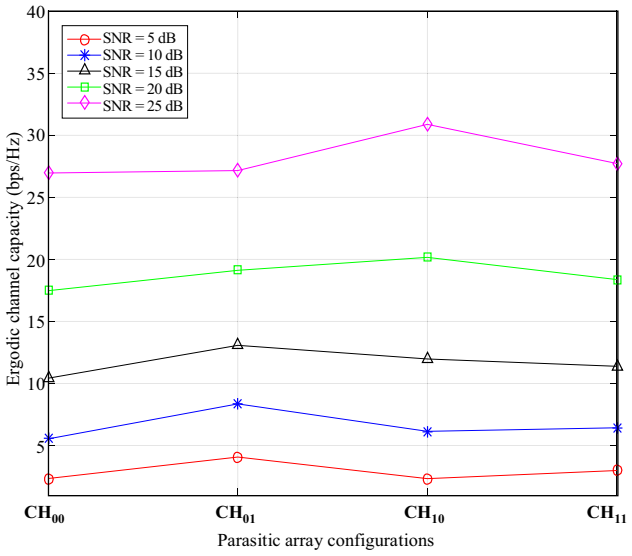

Fig. 6. Pattern configuration selection at different SNR values.

4. Pattern Configuration for Different SNR Values

The MIMO channel capacity also depends on the SNR values. The behavior of four pattern configurations at different SNRs levels are shown in Fig. 6. It can be seen that at 5 dB–15 dB, the second pattern configuration $\mathbf{CH_{01}}$ provides the highest channel capacity.

At 20 dB and 25 dB, the third configuration $\mathbf{CH_{10}}$ can be selected as it provides the highest channel capacity.

V. Conclusion

SPAs offer a significant advantage in terms of the use of handheld devices, where space, cost, and hardware complexity are the primary constraints. The main advantages of SPAs are their ability to change their radiation pattern and to operate within a specific changing environment, while maintaining good electromagnetic characteristics. For simplicity, and to provide a limited level of pattern diversity, only two switch positions (ON/OFF) were used in this study.

Based on the knowledge of the channel statistics, a decomposition model decouples the transmit signal into orthogonal eigenbeams. The power distribution assigned to these eigenvalues is according to the WPA, which means that there is a greater power in directions where the channel is strong, but reduced or no power in directions with weak channels. Using the I-AST technique with WPA, the MIMO-SPAs channel capacity is significantly improved for all the pattern configurations. A comparison of three covariance matrices showed that the improved power allocation of the covariance matrix with WPA has a higher channel capacity than others.

The novel contribution of this paper is the use of the CN as a selection criterion to determine the optimal pattern configuration for the receiver antenna array. The behavior of the CN of the covariance matrix represents the EVS of the channel. Using a good-quality channel, a high multiplexing gain can be achieved with proper transmission. Thus, the CN is an excellent indicator of channel quality, and is a very useful metric in link adaptation schemes.

In the future, this work will be extended for application to multicarrier systems such as orthogonal frequency-division multiplexing (OFDM), where it is possible to select the pattern selection using the CN across a number of subcarriers. It also has the advantage of feedback and bandwidth reduction in future wireless communication systems.

https://doi.org/10.4218/etrij.2017-0071

References

[1] E. Telatar, "Capacity of Multi-antenna Gaussian Channel," *Trans. Emerg. Telecommun. Technol.*, vol. 10, no. 6, Nov. 1999, pp. 585–595.

[2] G.J. Foschini and M.J. Gans, "On Limits of Wireless Communications in a Fading Environment when Using Multiple Antennas," *Wireless Personal Commun.*, vol. 6, no. 3, Mar. 1998, pp. 311–335.

[3] R. Vaughan, "Switched Parasitic Elements for Antenna Diversity," *IEEE Trans. Antennas Propag.*, vol. 47, no. 2, Feb. 1999, pp. 399–405.

[4] M. Wennstrom and T. Svantesson, "An Antenna Solution for MIMO Channels: The Switched Parasitic Antenna," *IEEE Int. Symp. Personal, Indoor Mobile Radio Commun.*, San Diego, CA, USA, Sept. 2001, pp. 159–163.

[5] A. Kalis, A.G. Kanatas, and C.B. Papadias, "A Novel Approach to MIMO Transmission Using a Single RF Front End," *IEEE J. Sel. Areas Commun.*, vol. 26, no. 6, Aug. 2008, pp. 972–980.

[6] A. Kalis, A.G. Kanatas, and C.B. Papadias, *Parasitic Antenna Arrays for Wireless MIMO Systems*, New York, USA: Springer, 2014.

[7] M.D. Migliore, D. Pinchera, and F. Schettino, "Improving Channel Capacity Using Adaptive MIMO Antennas," *IEEE Trans. Antennas Propag.*, vol. 54, no. 11, Nov. 2006, pp. 3481–3489.

[8] O.N. Alrabadi, C. Divarathne, P. Tragas, A. Kalis, N. Marchetti, C.B. Papadias, and R. Prasad, "Spatial Multiplexing with a Single Radio: Proof-of-Concept Experiments in an Indoor Environment with a 2.6 GHz Prototype," *IEEE Commun. Lett.*, vol. 15, no. 2, Feb. 2011, pp. 178–180.

[9] O.N. Alrabadi, J. Perruisseau-Carrier, and A. Kalis, "MIMO Transmission Using a Single RF Source: Theory and Antenna Design," *IEEE Trans. Antennas Propag.*, vol. 60, no. 2, Feb. 2012, pp. 654–664.

[10] D. Gwak, I. Sohn, and S.H. Lee, "Analysis of Single-RF MIMO Receiver with Beam-Switching Antenna," *ETRI J.*, vol. 37, no. 4, Aug. 2015, pp. 647–656.

[11] R. Bains and R. Muller, "Using Parasitic Elements for Implementing the Rotating Antenna for MIMO Receivers," *IEEE Trans. Wireless Commun.*, vol. 7, no. 11, Nov. 2008, pp. 4522–4533.

[12] M. DiZazzo, M.D. Migliore, F. Schettino, V. Patriarca, and D. Pinchera, "A Novel Parasitic-MIMO Antenna," *IEEE Antennas Propag. Soc. Inter. Symp*., Albuquerque, NM, USA, July 2006, pp. 4447–4450.

[13] M. Yoshida, K. Sakaguchi, and K. Araki, "Single Front-End MIMO Architecture with Parasitic Antenna Elements," *IEICE Trans. Commun.*, vol. E95-B, no. 3, Mar. 2012, pp. 882–888.

[14] M. Vu and A. Paulraj, "MIMO Wireless Linear Precoding," *IEEE Signal Process. Mag.*, vol. 24, no. 5, Sept. 2007, pp. 86–105.

[15] D. Sacristán-Murga and A. Pascual-Iserte, "Differential Feedback of MIMO Channel Gram Matrices Based on Geodesic Curves," *IEEE Trans. Wireless Commun.*, vol. 9, no. 12, Dec. 2010, pp. 3714–3727.

[16] D. Tse and P. Viswanath, *Fundamentals of Wireless Communication*, Cambridge, UK: Cambridge University Press, 2005.

[17] J. Zik, *Maximizing LTE Performance through MIMO Optimization*, Germantown, PA, USA: PCTEL Inc., Apr. 2011.

[18] M. Zia, T. Kiani, H. Mahmood, T. Shah, and N.A. Saqib, "Bandwidth-Efficient Selective Retransmission for MIMO-OFDM Systems," *ETRI J.*, vol. 37, no. 1, Feb. 2015, pp. 66–76.

[19] R.W. Heath and A.J. Paulraj, "Switching Between Diversity and Multiplexing in MIMO Systems," *IEEE Trans. Commun.*, vol. 53, no. 6, 2005, pp. 962–968.

[20] D. Piazza, J. Kountouriotis, M. D'Amico, and K.R. Dandekar, "A Technique for Antenna Configuration Selection for Reconfigurable Circular Patch Arrays," *IEEE Trans. Antennas Propag.*, vol. 8, no. 3, Mar. 2009, pp. 1456–1467.

[21] A. Forenza, A. Pandharipande, H. Kim, and R.W. Heath, "Adaptive MIMO Transmission Scheme: Exploiting the Spatial Selectivity of Wireless Channels," *IEEE Veh. Technol. Conf.*, Stockholm, Sweden, May 30–June 1, 2005, pp. 3188–3192.

[22] D. Pinchera and M.D. Migliore, "Effectively Exploiting Parasitic Arrays for Secret Key Sharing," *IEEE Trans. Veh. Tech.*, vol. 65, no. 1, Jan. 2016, pp. 123–131.

[23] R.W. Heath and D.J. Love, "Multimode Antenna Selection for Spatial Multiplexing Systems with Linear Receivers," *IEEE Trans. Signal Process.*, vol. 53, no. 8, Aug. 2005, pp. 3042–3056.

[24] J.V. Cuan-Cortes, C. Vargas-Rosales, and D. Munoz-Rodriguez, "MIMO Channel Capacity Using Antenna Selection and Water Pouring," *EURASIP J. Wireless Commun. Netw.*, vol. 2014, Dec. 2014, pp. 1–10.

[25] C.A. Balanis, *Antenna Theory*, New York, USA: Wiley, 2005.

[26] C.E. Shannon, "A Mathematical Theory of Communication," *Bell Syst. Tech. J.*, vol. 27, no. 3, 1948, pp. 379–423.

[27] S.J. Orfanidis, "Electromagnetic Waves and Antennas," Rutgers University, 2002, pp. 702–733, Accessed 2017. http://www.ece.rutgers.edu/~orfanidi/ewa/

[28] M.R.O. Mofolo, A.A. Lysko, T.O. Olwal, and W.A. Clarke, "Beam Steering for Circular Switched Parasitic Arrays Using a Combinational Approach," *IEEE AFRICON*, Livingstone, Zambia, Sept. 13–15, 2011, pp. 1–6.

[29] K. Gyoda and T. Ohira, "Design of Electronically Steerable Passive Array Radiator (ESPAR) Antennas," *IEEE Antennas Propag. Soc. Int. Symp.*, Salt Lake City, UT, USA, July 16–21, 2000, pp. 922–925.

Paramvir Kaur Pal received her BEng degree in electronics engineering from Nagpur University, India, in 2001, and her MEng degree in electronics from Punjab Engineering College, Chandigarh, India in 2004. From 2004 to 2006, she worked as a lecturer at the Shaheed Udham Singh College of Engineering and Technology, Mohali, India. She is currently pursuing her PhD degree at the University of Reading, UK. Her research interests are in the area of MIMO wireless communication for closely spaced antennas and spatial multiplexing.

Robert Simon Sherratt received his BEng degree in electronic systems and control engineering from Sheffield City Polytechnic, UK, in 1992, and his MSc and PhD degrees in electronic engineering from the University of Salford, UK, in 1994 and 1996, respectively. From 1996, he has been with the University of Reading, UK, where he is now a full professor. His research areas are signal processing and personal communications in consumer devices, focusing on wearable devices for healthcare applications.

https://doi.org/10.4218/etrij.2017-0071

MATLAB Code

```
clear all;
clc;

%Antenna Specifications to generate radiation patterns
N=4;        % Active Element=2 + Parasitic Element=2 --- at Rx side
M=2;        % Active Element=2 + Parasitic Element=0--- at Tx side
c=3e8;      %speed of light in m/s
f=2.4e9;    %operational frequency
lambda=(c/f); %lambda=c/f
phi=((0:2*pi/359:2*pi));
L = [0.5, 0.5,0.5,0.5]; % lengths of the antenna elements
a = [0.001, 0.001,0.001,0.001]; % radii of the antenna elements
d = [0.125,0; -0.125,0; 0,0.125;0,-0.125]; % xy locations
%%%%%%%%%%%%%%%%%%%%%%%%%%%%%%%%%%%%%%%%%%%%%%%%%%%%%%%%%%%%%%%%

V=[1 1 0 0]';  %Driving voltages
Z = impedmat(L,a,d); % impedance matrix

%Combinations of the parasitic load values

Zload1 = [50      0      0      0;
          0      50      0      0;
          0      0      10000      0;
          0      0      0      10000];

Zload2 = [50      0      0      0;
          0      50      0      0;
          0      0      10000      0;
          0      0      0      1];

Zload3 = [50      0      0      0;
          0      50      0      0;
          0      0      1      0;
          0      0      0      10000];

Zload4 = [50      0      0      0;
          0      50      0      0;
          0      0      1      0;
          0      0      0      1];

% Calculate impedance matrix with parasitic load values

Z_r=Z;
Z_Rx1=Z_r+Zload1;
```

```
Inv_Z_Rx1=inv(Z_Rx1);
Z_Rx11=Z_r*(Inv_Z_Rx1);
I1=Z_Rx1\V;
[ge1,gh1,gt1]=gain2(L,d,I1,359);

Z_Rx2=Z_r+Zload2;
Inv_Z_Rx2=inv(Z_Rx2);
Z_Rx22=Z_r*(Inv_Z_Rx2);
I2=Z_Rx2\V;
[ge2,gh2,gt2]=gain2(L,d,I2,359);

Z_Rx3=Z_r+Zload3;
Inv_Z_Rx3=inv(Z_Rx3);
Z_Rx33=Z_r*(Inv_Z_Rx3);
I3=Z_Rx3\V;
[ge3,gh3,gt3]=gain2(L,d,I3,359);

Z_Rx4=Z_r+Zload4;
Inv_Z_Rx4=inv(Z_Rx4);
Z_Rx44=Z_r*(Inv_Z_Rx4);
I4=Z_Rx4\V;
[ge4,gh4,gt4]=gain2(L,d,I4,359);

Z_Tx1=Z_Rx1;
Z_Tx2=Z_Rx2;
Z_Tx3=Z_Rx3;
Z_Tx4=Z_Rx4;

MaxIter=100;      % Maximum Iterations
SNRdBs=[0:20];

for i=1:length(SNRdBs)
    SNRdB = SNRdBs(i);

    cum00_corr=0;
    cum00_uncorr=0;
    cum00_WPA=0;
    cum01_corr=0;
    cum01_uncorr=0;
    cum01_WPA=0;
    cum10_corr=0;
    cum10_uncorr=0;
    cum10_WPA=0;
    cum11_corr=0;
    cum11_uncorr=0;
    cum11_WPA=0;
    cumAE=0;
```

```
    for n=1:MaxIter

    rand('seed',1);
    randn('seed',1);

  G=sqrt(0.5)*(randn(N,M)+1j*randn(N,M));
  H_hat1=Z_Rx11*G*eye(2);
  H_hat2=Z_Rx22*G*eye(2);
  H_hat3=Z_Rx33*G*eye(2);
  H_hat4=Z_Rx44*G*eye(2);

S_r=zeros(2,4);
S_t=zeros(4,2);
S_r(1,1)=1;
S_r(2,2)=1;
S_t=eye(2);

 H1=S_r*H_hat1*S_t;
 H2=S_r*H_hat2*S_t;
 H3=S_r*H_hat3*S_t;
 H4=S_r*H_hat4*S_t;

 I=eye(2,2);
 I_corr=ones(2,2);
 %%%%%%%%%%%%%%%%%%%%%%%%%%%%%%%%%%%%%%%%%%%%%%%%%%%%%%%%%%%%

 %H00-H1--2X2%%%%%%%%%%%%%%%%%%%%%%%%%%%%%%%%%%%%%%%%%%%%%%%%
 H00_1=H1(:,1);
 H00_2=H1(:,2);

 sel_ant1=1;
 SNR_sel_ant1 = 10.^(SNRdB/10)/sel_ant1;
 log_SH00_1 = log2(real(det(I+SNR_sel_ant1*H00_1*H00_1')));
 log_SH00_2 = log2(real(det(I+SNR_sel_ant1*H00_2*H00_2')));
 log_SH00=[log_SH00_1 log_SH00_2 ];

  c00=sort(log_SH00,'descend');
  node00_1=find(c00(1)==log_SH00);
  node00_2=find(c00(2)==log_SH00);

  node00=[node00_1 node00_2 ];

  newH00_1=H1(:,node00_1);
  newH00_2=H1(:,node00_2);
  %%%%%%%%%%%%%%%%%%%%%%%%%%%%%%%%%%%%%%%%%%%%%%%%%%%%%%%%%%%%
```

```
newH00=[newH00_1 newH00_2];
SV00 = svd(newH00'*newH00);
Gamma00 = Water_Pouring(SV00,SNR_sel_ant1,2);

maximum_capacity00_WPA = log2(det(I+SNR_sel_ant1/2*diag(Gamma00)*diag(SV00)));
maximum_capacity_00_uncorr = log2(real(det(I+SNR_sel_ant1/2*H1'*H1)));
maximum_capacity_00_corr = log2(real(det(I+SNR_sel_ant1/2*I_corr*H1'*H1)));
%%%%%%%%%%%%%%%%%%%%%%%%%%%%%%%%%%%%%%%%%%%%%%%%

cum00_uncorr = cum00_uncorr + maximum_capacity_00_uncorr;      % uncorrelated
cum00_WPA = cum00_WPA + maximum_capacity00_WPA;                % WPA
cum00_corr=cum00_corr + maximum_capacity_00_corr;              % correlated
%%%%%%%%%%%%%%%%%%%%%%%%%%%%%%%%%%%%%%%%%%%%%%%%

%H01----H2---2X2%%%%%%%%%%%%%%%%%%%%%%%%%%%%%%%%%%%

H01_1=H2(:,1);
H01_2=H2(:,2);

sel_ant1=1;
SNR_sel_ant1 = 10.^(SNRdB/10)/sel_ant1;
log_SH01_1 = log2(real(det(I+SNR_sel_ant1*H01_1*H01_1')));
log_SH01_2 = log2(real(det(I+SNR_sel_ant1*H01_2*H01_2')));
log_SH01=[log_SH01_1 log_SH01_2 ];

c01=sort(log_SH01,'descend');
node01_1=find(c01(1)==log_SH01);
node01_2=find(c01(2)==log_SH01);

node01=[node01_1 node01_2];

newH01_1=H2(:,node01_1);
newH01_2=H2(:,node01_2);
%%%%%%%%%%%%%%%%%%%%%%%%%%%%%%%%%%%%%%%%%%%%%%%%

newH01=[newH01_1 newH01_2];
SV01 = svd(newH01'*newH01);
Gamma01 = Water_Pouring(SV01,SNR_sel_ant1,2);

maximum_capacity01_WPA = log2(det(I+SNR_sel_ant1/2*diag(Gamma01)*diag(SV01)));
maximum_capacity_01_uncorr = log2(real(det(I+SNR_sel_ant1/2*H2'*H2)));
maximum_capacity_01_corr = log2(real(det(I+SNR_sel_ant1/2*I_corr*H2'*H2)));
%%%%%%%%%%%%%%%%%%%%%%%%%%%%%%%%%%%%%%%%%%%%%%%%

cum01_uncorr = cum01_uncorr + maximum_capacity_01_uncorr;      % uncorrelated
cum01_WPA = cum01_WPA + maximum_capacity01_WPA;                % WPA
cum01_corr=cum01_corr + maximum_capacity_01_corr;              % correlated
```

```
%%%%%%%%%%%%%%%%%%%%%%%%%%%%%%%%%%%%%%%%%%%%%%%%%%%%%%%%%%%
%%H10----H3---2X2%%%%%%%%%%%%%%%%%%%%%%%%%%%%%%%%%%%%%%
H10_1=H3(:,1);
H10_2=H3(:,2);

sel_ant1=1;
SNR_sel_ant1 = 10.^(SNRdB/10)/sel_ant1;
 log_SH10_1 = log2(real(det(I+SNR_sel_ant1*H10_1*H10_1')));
 log_SH10_2 = log2(real(det(I+SNR_sel_ant1*H10_2*H10_2')));
 log_SH10=[log_SH10_1 log_SH10_2 ];

 c10=sort(log_SH10,'descend');

 node10_1=find(c10(1)==log_SH10);
 node10_2=find(c10(2)==log_SH10);

 node10=[node10_1 node10_2];
 newH10_1=H3(:,node10_1);
 newH10_2=H3(:,node10_2);
 %%%%%%%%%%%%%%%%%%%%%%%%%%%%%%%%%%%%%%%%%%%%%%%%%%%%%%%%%%

newH10=[newH10_1 newH10_2 ];
SV10 = svd(newH10'*newH10);
Gamma10 = Water_Pouring(SV10,SNR_sel_ant1,2);

maximum_capacity10_WPA = log2(det(I+SNR_sel_ant1/2*diag(Gamma10)*diag(SV10)));
maximum_capacity_10_uncorr = log2(real(det(I+SNR_sel_ant1/2*H3'*H3)));
maximum_capacity_10_corr = log2(real(det(I+SNR_sel_ant1/2*I_corr*H3'*H3)));
%%%%%%%%%%%%%%%%%%%%%%%%%%%%%%%%%%%%%%%%%%%%%%%%%%%%%%%%%%

cum10_uncorr = cum10_uncorr + maximum_capacity_10_uncorr;        % uncorrelated
cum10_WPA = cum10_WPA + maximum_capacity10_WPA;                  % WPA
cum10_corr=cum10_corr + maximum_capacity_10_corr;                %  correlated
%%%%%%%%%%%%%%%%%%%%%%%%%%%%%%%%%%%%%%%%%%%%%%%%%%%%%%%%%%%%

%H11----H4---2X2%%%%%%%%%%%%%%%%%%%%%%%%%%%%%%%%%%%%%%%%
 H11_1=H4(:,1);
 H11_2=H4(:,2);

 sel_ant1=1;

 SNR_sel_ant1 = 10.^(SNRdB/10)/sel_ant1;
 log_SH11_1 = log2(real(det(I+SNR_sel_ant1*H11_1*H11_1')));
 log_SH11_2 = log2(real(det(I+SNR_sel_ant1*H11_2*H11_2')));
 log_SH11=[log_SH11_1 log_SH11_2 ];
```

```
 c11=sort(log_SH11,'descend');

 node11_1=find(c11(1)==log_SH11);
 node11_2=find(c11(2)==log_SH11);
 node11=[node11_1 node11_2];

 newH11_1=H4(:,node11_1);
 newH11_2=H4(:,node11_2);
 %%%%%%%%%%%%%%%%%%%%%%%%%%%%%%%%%%%%%%%%%%%%%%%%%%%%%%%%%%%%

newH11=[newH11_1 newH11_2 ];
SV11 = svd(newH11'*newH11);
Gamma11 = Water_Pouring(SV11,SNR_sel_ant1,2);

maximum_capacity11_WPA = log2(det(I+SNR_sel_ant1/2*diag(Gamma11)*diag(SV11)));
maximum_capacity_11_uncorr = log2(real(det(I+SNR_sel_ant1/2*H4'*H4)));
maximum_capacity_11_corr = log2(real(det(I+SNR_sel_ant1/2*I_corr*H4'*H4)));
%%%%%%%%%%%%%%%%%%%%%%%%%%%%%%%%%%%%%%%%%%%%%%%%%%%%%%%%%%%%

cum11_uncorr = cum11_uncorr + maximum_capacity_11_uncorr;          % uncorrelated
cum11_WPA = cum11_WPA + maximum_capacity11_WPA;                    % WPA
cum11_corr=cum11_corr + maximum_capacity_11_corr;                  % correlated
%%%%%%%%%%%%%%%%%%%%%%%%%%%%%%%%%%%%%%%%%%%%%%%%%%%%%%%%%%%%

%Without Parasitic elements---only Active Elements
%Impedance Matrix with only Active Elements
  L1 = [0.5, 0.5];                 % lengths
  a1 = [0.001, 0.001];             % radii
 d1 = [0.125,0; -0.125,0];         % xy locations
 phi1=((0:2*pi/359:2*pi));
 V1=[1 1]';                        %Driving voltages
 Z1 = impedmat(L1,a1,d1);          % impedance matrix
 Z_AE=Z1;

 Zload_AE = [50         0;
                0         50];

 Z_Rx_AE=Z_AE+Zload_AE;
 Inv_Z_Rx_AE=inv(Z_Rx_AE);
 Z_Rx_AAEE=Z_AE*(Inv_Z_Rx_AE);
 I_AE=Z_Rx_AE\V1;
 [ge5,gh5,gt5]=gain2(L1,d1,I_AE,359);
%%%%%%%%%%%%%%%%%%%%%%%%%%%%%%%%%%%%%%%%%%%%%%%%%%%%%%%%%%%%

 H_AE=G(1:2,1:2);
H_hat_AE=Z_Rx_AAEE*H_AE*eye(2);
```

```
cumAE=cumAE+log2(real(det(I+(SNR_sel_ant1/2)*H_hat_AE'*H_hat_AE)));

 end
%%%%%%%%%%%%%%%%%%%%%%%%%%%%%%%%%%%%%%%%%%%%%%%%%%%%%%%%%%%%%%%%

  sel_capacity00_uncorr(i) = cum00_uncorr/MaxIter;
  sel_capacity00_corr(i) = cum00_corr/MaxIter;
  sel_capacity00_WPA(i) = cum00_WPA/MaxIter;
  sel_capacity01_uncorr(i) = cum01_uncorr/MaxIter;
  sel_capacity01_corr(i) = cum01_corr/MaxIter;
  sel_capacity01_WPA(i) = cum01_WPA/MaxIter;
  sel_capacity10_uncorr(i) = cum10_uncorr/MaxIter;
  sel_capacity10_corr(i) = cum10_corr/MaxIter;
  sel_capacity10_WPA(i) = cum10_WPA/MaxIter;
  sel_capacity11_uncorr(i) = cum11_uncorr/MaxIter;
  sel_capacity11_corr(i) = cum11_corr/MaxIter;
  sel_capacity11_WPA(i) = cum11_WPA/MaxIter;
  sel_capacityAE(i) = cumAE/MaxIter;

 end
sel_capacity = [sel_capacity00_uncorr' sel_capacity01_uncorr' sel_capacity10_uncorr'
                sel_capacity11_uncorr'];
sel_capacity_AS = [sel_capacity00_WPA' sel_capacity01_WPA' sel_capacity10_WPA'
                   sel_capacity11_WPA'];
 %%%%%%%%%%%%%%%%%%%%%%%%%%%%%%%%%%%%%%%%%%%%%%%%%%%%%%%%%%%%%%%%

 %Condition Number (CN)

 CN1=cond(H1);
 CN2=cond(H2);
 CN3=cond(H3);
 CN4=cond(H4);

 CN=[CN1 CN2 CN3 CN4];

%Optimal CN

 CN_lowest=sort(CN,'ascend');
 BEST=find(CN_lowest(1)==CN);

 %Condition Number (CN) in dB

 CN_dB1=20.*log10(CN1);
 CN_dB2=20.*log10(CN2);
 CN_dB3=20.*log10(CN3);
 CN_dB4=20.*log10(CN4);
 CN_dB=[CN_dB1 CN_dB2 CN_dB3 CN_dB4];
```

```
 CN_dB_lowest=sort(CN_dB,'ascend');
 BEST_dB=find(CN_dB_lowest(1)==CN_dB)
%%%%%%%%%%%%%%%%%%%%%%%%%%%%%%%%%%%%%%%%%%%%%

figure(1);

plot(SNRdBs,sel_capacity00_WPA,'-ro',SNRdBs,sel_capacity00_uncorr,'--ro',
     SNRdBs, sel_capacity00_corr,':ro',SNRdBs,sel_capacity01_WPA,'-bx',
     SNRdBs,sel_capacity01_uncorr,'--bx',SNRdBs,sel_capacity01_corr,':bx',
     SNRdBs,sel_capacity10_WPA,'-gs',SNRdBs,sel_capacity10_uncorr,'--gs',
     SNRdBs,sel_capacity10_corr,':gs',SNRdBs,sel_capacity11_WPA,'-kd',
     SNRdBs,sel_capacity11_uncorr,'--kd',SNRdBs,sel_capacity11_corr,':kd');

xlabel('SNR [dB]');
ylabel('Ergodic Channel Capacity (bps/Hz)');

set(0,'DefaultAxesFontName', 'Times New Roman');
set(0,'DefaultAxesFontSize', 10);

grid on;
legend('CH00 WPA','CH00 Uncorrelated','CH00 Correlated',...
        'CH01 WPA','CH01 Uncorrelated','CH01 Correlated',...
        'CH10 WPA','CH10 Uncorrelated','CH10 Correlated',...
        'CH11 WPA','CH11 Uncorrelated','CH11 Correlated');
legend('Location','Northwest');
%%%%%%%%%%%%%%%%%%%%%%%%%%%%%%%%%%%%%%%%%%%%%%

figure(2);

plot(SNRdBs,sel_capacity00_WPA,'-ko',SNRdBs,sel_capacity00_uncorr,'--ko',
     SNRdBs, sel_capacity00_corr,':ko',SNRdBs,sel_capacity01_WPA,'-kx',
     SNRdBs,sel_capacity01_uncorr,'--kx', SNRdBs,sel_capacity01_corr,':kx',
     SNRdBs,sel_capacity10_WPA,'-ks',SNRdBs,sel_capacity10_uncorr,'--ks',
     SNRdBs,sel_capacity10_corr,':ks',SNRdBs,sel_capacity11_WPA,'-kd',
     SNRdBs,sel_capacity11_uncorr,'--kd',SNRdBs,sel_capacity11_corr,':kd');

xlabel('SNR [dB]');
ylabel('Ergodic Channel Capacity (bps/Hz)');

set(0,'DefaultAxesFontName', 'Times New Roman');
set(0,'DefaultAxesFontSize', 10);

grid on;
legend('CH00 WPA','CH00 Uncorrelated','CH00 Correlated',...
        'CH01 WPA','CH01 Uncorrelated','CH01 Correlated',...
        'CH10 WPA','CH10 Uncorrelated','CH10 Correlated',...
```

```
        'CH11 WPA','CH11 Uncorrelated','CH11 Correlated');
legend('Location','Northwest');
%%%%%%%%%%%%%%%%%%%%%%%%%%%%%%%%%%%%%%%%%%%%%

figure(3);

h = subplot(2,2,1)
plot( SNRdBs,sel_capacity00_WPA,'-k*',SNRdBs,sel_capacity00_uncorr,'-ko',
        SNRdBs,sel_capacity00_corr,'-kd');
xlabel('SNR[dB]');
ylabel('Channel Capacity (bps/Hz)');
set(0,'DefaultAxesFontName', 'Times New Roman')
set(0,'DefaultAxesFontSize', 8)
grid on;
legend('CH00 WPA','CH00 Uncorrelated','CH00 Correlated');
legend('Location','Northwest');
xlim([0 20]);
ylim([0 12]);

h = subplot(2,2,2);
plot(SNRdBs,sel_capacity01_WPA,'-k*',SNRdBs,sel_capacity01_uncorr,'-ko',
      SNRdBs,sel_capacity01_corr,'-kd')
xlabel('SNR[dB]');
ylabel('Channel Capacity (bps/Hz)');
set(0,'DefaultAxesFontName', 'Times New Roman');
set(0,'DefaultAxesFontSize', 8);
grid on;
legend('CH01 WPA','CH01 Uncorrelated','CH01 Correlated');
legend('Location','Northwest');
xlim([0 20]);
ylim([0 12]);

h = subplot(2,2,3);
plot( SNRdBs,sel_capacity10_WPA,'-k*',SNRdBs,sel_capacity10_uncorr,'-ko',
       SNRdBs,sel_capacity10_corr,'-kd')
xlabel('SNR[dB]');
ylabel('Channel Capacity (bps/Hz)');
set(0,'DefaultAxesFontName', 'Times New Roman');
set(0,'DefaultAxesFontSize', 8);
grid on;
legend('CH10 WPA','CH10 Uncorrelated','CH10 Correlated');
legend('Location','Northwest');
xlim([0 20]);
ylim([0 12]);

h = subplot(2,2,4);
plot(SNRdBs,sel_capacity11_WPA,'-k*',SNRdBs,sel_capacity11_uncorr,'-ko',
```

```
    SNRdBs,sel_capacity11_corr,'-kd')
xlabel('SNR[dB]');
ylabel('Channel Capacity (bps/Hz)');
set(0,'DefaultAxesFontName', 'Times New Roman');
set(0,'DefaultAxesFontSize', 8);
grid on;
legend('CH11 WPA','CH11 Uncorrelated','CH11 Correlated');
legend('Location','Northwest');
xlim([0 20]);
ylim([0 12]);
subplotsqueeze(gcf, 1.2);
%%%%%%%%%%%%%%%%%%%%%%%%%%%%%%%%%%%%%%%%%%%%%%%%%%%%%%

figure(4);

plot(SNRdBs,sel_capacity00_uncorr,'-ro',SNRdBs,sel_capacity01_uncorr,'--bx',
    SNRdBs,sel_capacity10_uncorr,'--gs',SNRdBs,sel_capacity11_uncorr,'--kd')
xlabel('SNR [dB]');
ylabel('Ergodic Channel Capacity (bps/Hz)');
set(0,'DefaultAxesFontName', 'Times New Roman');
set(0,'DefaultAxesFontSize', 10);
grid on;
legend('CH00','CH01','CH10','CH11');
legend('Location','Northwest');
%%%%%%%%%%%%%%%%%%%%%%%%%%%%%%%%%%%%%%%%%%%%%%%%%%%%%%%

figure(5);

plot(SNRdBs,sel_capacity00_uncorr,'-ko',SNRdBs,sel_capacity01_uncorr,'-kx',
    SNRdBs,sel_capacity10_uncorr,'-ks',SNRdBs,sel_capacity11_uncorr,'-kd')
xlabel('SNR [dB]');
ylabel('Ergodic Channel Capacity (bps/Hz)');
set(0,'DefaultAxesFontName', 'Times New Roman');
set(0,'DefaultAxesFontSize', 10);
grid on;
legend('CH00 Uncorrelated','CH01 Uncorrelated','CH10 Uncorrelated','CH11 Uncorrelated');
legend('Location','Northwest');
%%%%%%%%%%%%%%%%%%%%%%%%%%%%%%%%%%%%%%%%%%%%%%%%%%%%%%

figure(6);

plot(SNRdBs, sel_capacity00_corr,':ro',SNRdBs,sel_capacity01_corr,':bx',
    SNRdBs,sel_capacity10_corr,':gs',SNRdBs,sel_capacity11_corr,':kd')
xlabel('SNR [dB]');
ylabel('Ergodic Channel Capacity (bps/Hz)');
set(0,'DefaultAxesFontName', 'Times New Roman');
set(0,'DefaultAxesFontSize', 10);
```

```
grid on;
legend('CH00','CH01','CH10','CH11');
legend('Location','Northwest');
%%%%%%%%%%%%%%%%%%%%%%%%%%%%%%%%%%%%%%%%%%%%%%%%%%%

figure(7);

plot(SNRdBs, sel_capacity00_corr,'-ko',SNRdBs,sel_capacity01_corr,'-kx',
     SNRdBs,sel_capacity10_corr,'-ks',SNRdBs,sel_capacity11_corr,'-kd')
xlabel('SNR [dB]');
ylabel('Ergodic Channel Capacity (bps/Hz)');
set(0,'DefaultAxesFontName', 'Times New Roman');
set(0,'DefaultAxesFontSize', 10);
grid on;
legend('CH00 Correlated','CH01 Correlated','CH10 Correlated','CH11 Correlated');
legend('Location','Northwest');
%%%%%%%%%%%%%%%%%%%%%%%%%%%%%%%%%%%%%%%%%%%%%%%%%%%

figure(8);

plot(SNRdBs,sel_capacity00_WPA,'-ko',SNRdBs,sel_capacity00_uncorr,'--ko',...
     SNRdBs,sel_capacity01_WPA,'-kx',SNRdBs,sel_capacity01_uncorr,'--kx',...
     SNRdBs,sel_capacity10_WPA,'-ks',SNRdBs,sel_capacity10_uncorr,'--ks',...
     SNRdBs,sel_capacity11_WPA,'-kd', SNRdBs,sel_capacity11_uncorr,'--kd');
xlabel('SNR [dB]');
ylabel('Ergodic Channel Capacity (bps/Hz)');
set(0,'DefaultAxesFontName', 'Times New Roman');
set(0,'DefaultAxesFontSize', 10);
grid on;
legend('CH00 WPA','CH00 w/o WPA',...
       'CH01 WPA','CH01 w/o WPA',...
       'CH10 WPA','CH10 w/o WPA',...
       'CH11 WPA','CH11 w/o WPA');
legend('Location','Northwest');
%%%%%%%%%%%%%%%%%%%%%%%%%%%%%%%%%%%%%%%%%%%%%%%%%%%

figure(9);

plot(SNRdBs,sel_capacity00_uncorr,'-ko',SNRdBs,sel_capacity01_uncorr,'-
kx',SNRdBs,sel_capacity10_uncorr,'-ks',SNRdBs,sel_capacity11_uncorr,'-
kd',SNRdBs,sel_capacityAE,'-r+')
xlabel('SNR [dB]');
ylabel('Ergodic Channel Capacity (bps/Hz)');
set(0,'DefaultAxesFontName', 'Times New Roman');
set(0,'DefaultAxesFontSize', 10);
grid on;
legend('CH00','CH01','CH10','CH11','AE');
```

```
legend('Location','Northwest');
%%%%%%%%%%%%%%%%%%%%%%%%%%%%%%%%%%%%%%%%%%%%%%%

figure(10);

h1=figure(10);
set(h1,'DefaultAxesFontSize',8);
subplot(2,2,1);polar(phi,gh1); title('States=00' );
subplot(2,2,2);polar(phi,gh2); title('States=01' );
subplot(2,2,3);polar(phi,gh3); title('States=10' );
subplot(2,2,4);polar(phi,gh4); title('States=11' );
 %%%%%%%%%%%%%%%%%%%%%%%%%%%%%%%%%%%%%%%%%%%%%%%
```